# Adipocyte Lipolysis and Acute Insulin Resistance

Katelyn Wellcome Ahern

Jacksonville, Florida
Norfolk, Virginia
Whidbey Island, Washington
Corpus Christi, Texas

M.S. Biological and Physical Sciences, University of Virginia, 2017
B.S. Biochemistry, Auburn University, 2015

A Dissertation presented to the Graduate Faculty
of the University of Virginia in Candidacy for the Degree of
Doctor of Philosophy

Department of Pharmacology

University of Virginia
December 2020

# ABSTRACT

Acute hyperglycemia and systemic insulin resistance often develop after trauma, but the underlying mechanisms remain unknown. It is, however, known that surgical animal models rapidly develop adipose insulin resistance, and impaired insulin action in adipose tissue alone can result in whole body insulin resistance. Therefore, we studied the contributions of adipocyte lipolysis to the metabolic response to acute stress and the release of two signaling molecules: oxidized fatty acids (oxFA) and resistin.

To better study the potential role of oxFA, we developed a novel high-performance liquid chromatography-tandem mass spectrometry (HPLC-MS/MS) method that employed positive-ion ionization in conjunction with differential energy (DiffE) qualifier ion monitoring (QIM) to measure full-length oxidation products of linoleic acid (LA) and arachidonic acid (AA). Using this method, we demonstrated levels of oxFA increased in response to lipolysis both *in vitro* and *in vivo*. In addition, we showed that reactive oxygen species (ROS) are critical for lipolysis-dependent inhibition of the mammalian target of rapamycin (mTOR) complexes and provided preliminary data that an oxFA is responsible.

We demonstrated *in vivo* that resistin is released in a stress- and lipolysis-dependent manner during hemorrhagic shock (HS) and cardiovascular stress. When we further investigated this mechanism *in vitro*, we observed a significant, lipolysis-dependent release of resistin from adipocytes into the media. In addition, overnight pretreatment with the antioxidant EUK prevented lipolysis-dependent resistin secretion, suggesting a potential role for oxidized lipid signaling in the acute release of resistin.

# ACKNOWLEDGEMENTS

It's hard to believe we finally made it to the end. And I say we purposefully, as I know full well that there is no way I could've made it without the help of some extremely important people. You all were in the trenches with me either physically or vicariously. I was only able to succeed because of your help and will never be able to thank you enough. But alas, I will try a bit here.

I would like to thank my mentor, Dr. Thurl Harris. He has taught me lessons about science, but even more about myself and the importance of resiliency. I want to thank all members of the Harris Lab, both past and present who have been my collaborators and friends. I would like to particularly thank my undergraduates, The Dream Team. Working with each of you was the best part of my days in the lab. Catherine Wingrove, as an undergraduate, you were already a better graduate student than me. You pushed me to be a better scientist and mentor. Hannah Chung, I couldn't have asked for a more amazing first undergraduate. You spoiled me. I could always rely on you. Even when I was in Germany, I knew I could pass the reins of the project and the Dream Team to you and that they were in capable hands. Zach Palas, you were never afraid to call me out, and you somehow always found a way to make me laugh, despite my broken sense of humor. Arad Jain, you amaze me with your science skills, even despite starting in the lab when I was in Germany and the fact that I am frequently running around like a crazy person. Much of the research in this thesis reflects each of my undergraduate's hard work. I very literally could not have done this without you.

I would like to thank the Pharmacology Department, particularly my committee: Dr. Kevin Lynch, Dr. Norbert Leitinger, Dr. Michelle Bland, and Dr. Ku-Lung Hsu. Thank you for your advice and teaching me how to stand up for my science. I would also like to thank the Pharmacology Department administration: Tammy Snow, Jolene Kidd, Deborah Steele, and Antoinette Reid. Thank you for helping me with every problem I brought to you from fellowship applications to double paychecks to international FedEx fiascos.

I would like to thank my fellow Pharmacology students, particularly the older students who always were there for advice and a beer. I would especially like to thank Dr. Vlad Serbulea. First and foremost, you taught me how to run the mass spectrometer and helped me plan out my first author paper (which turned out to be the golden ticket out of graduate school). You were in a different lab with your own project and trainees, but you never complained about taking the time to teach me and having me cut into your instrument time. Most importantly, thank you for introducing me to your girlfriend, now wife, Anne Serbulea. Spending time with the two of you outside of the lab was always the stress-relief I needed. I would be remiss if I did not mention my classmate Dr. Brittany Martinez. You were the best foxhole buddy a person could ask for. I always knew you were in my corner, and you always let me know that I wasn't alone when I was struggling. There were many days that I couldn't have gotten through without you. Thank you for always being my biggest advocate.

I would like to thank the Robert M. Berne Cardiovascular Research Center for providing me with invaluable training, professional development, and scientific opportunities. It is due to the training I received in the CVRC that I was able to get my

American Heart Association Pre-Doctoral Fellowship. I would also like to thank the Basic Cardiovascular Research Training Grant for providing funding for my time in graduate school when I was not on my AHA fellowship.

One of those CVRC opportunities was to take part in the International Research Training Group with Heinrich Heine University in Düsseldorf, Germany. These interactions, and particularly my time in Germany, were unquestionably the best part of graduate school. I would like to thank the members of the IRTG, particularly the students, for all of the great times both in Charlottesville and in Germany. Our annual visits were something I always looked forward to. I would like to thank the entire Gödecke lab for making my stay in Germany the best two months of graduate school and making it so hard to go home. You made me feel like part of the team from the very first day. While everyone I met through the program was wonderful, I would particularly like to thank a couple of Germans (one of which being an honorary German). Dr. Katharina Bottermann, having you in the lab for a year was a gift. You brought so much life and laughter to the lab. Getting to spend time with you again during my stay in Düsseldorf was a blessing that occurred only with of unintentionally perfect timing. You and Sepp always made sure I had plenty of food (and even more beer. I would like to thank Dr. Philipp Jakobs for always making me laugh with your dry sense of humor. Thank you for having the extreme patience to teach me how to speak German, throw darts, and brake while rollerblading. Dr. Lisa Kalfhues, one of my regrets in graduate school is that our exchanges overlapped, and we missed out on extra time together. But we certainly made the most of the time we did have. Thank you for somehow managing to make me feel welcome in Germany despite the fact that you were in America at the time. You left me

samples, equipment, and a desk all set up and ready for me to arrive. I will always cherish our trip to Croatia with Vici. Whether we were exploring somewhere new or simply sitting on the balcony with a bottle of wine, I will fondly remember every minute. Which brings me to the honorary German, Dr. Vici Oenarto. I say that my trip to Germany was the best part of graduate school, but it was arguably the best two months of my life thus far. I feel confident in saying that is in large part because of you. You made my time in the Gödecke lab and exploring Düsseldorf such a joy, but it is our adventures that I will always be most grateful for. I wanted to cram as much into my two months as possible, and you were always right there by my side ready to go. Thank you for being my perfect travel companion. I look forward to even more adventures together.

Despite all of the gratitude that I've already expressed to various people at UVA, I have yet to thank the two most important people: Marissa Gonzales and Beth Wagner. They really should put out a disclaimer to the first years letting them know how important their choice of Core Course table will be to their graduate school experience. As it turns out, I got unbelievably lucky that I happened to sit down at your table. I know without a doubt that I could not have done this without the two of you here with me. We celebrated each other's accomplishments over almond champagne. Whether we were watching Grey's, playing trivia, or having game night, these are the little moments that made the tough times bearable. You are two of the best friends a person could ask for. I know we will be friends long after graduate school, and I will always strive to be as thoughtful of a friend to the two of you as you have been for me.

There are a few people outside of UVA who contributed to my success and deserve recognition. First, I would like to thank all of the members of Team Pete. Being

part of the movement taught me how to be a leader and the impact of standing up for issues you are passionate about. In particular, I would like to thank Lauren Boggs Meslar. We accomplished so much together, in part because of our perfect mind meld. It was a busy few months, but I couldn't and wouldn't have done it with anybody else. To my Auburn friends, I know we were spread out across the country, but you were always a source of joy. When we are together, you always have a way of reminding me who I truly am, which I sometimes started to lose while in graduate school. I would especially like to thank Nicholas Pannell. Thank you for helping keep the Auburn group together. I also need to thank my oldest friend, Kaitlyn Parkman. Whether we hadn't talked in months or we were talking every week, I have always known that you are just one phone call away. I know we will always be the best of friends.

Most importantly, I must thank my family. Growing up in a military family and moving every couple of years, my family has always been my most important source of friends and adventure partners. Sarah Ahern, you started out as my rascally younger sister and now you are my inspiration. You do things that I could never do, whether you are saving a patient or climbing a volcano with a broken foot. While I have had great friends in Charlottesville, it has been such a blessing to have my sister so close by. That being said, I was also privileged enough to have Meghan Ahern just a short drive away. Growing up you were always my partner in crime, and I know that will never change. Thank you for always making me laugh and being my actual longest friend. Last but not least, I need to thank my parents. Mom, growing up you taught me the importance of venting and boy did I put that to good use in graduate school. Thank you for always picking up the phone to listen to me complain for an hour straight without me ever asking

about your day. Thank you for always going above and beyond to help me succeed and make my life easierTo my Dad, quite simply, you are my hero. I work every day to be just a little bit more like you. I know I may not have been grateful at the time, but I wouldn't trade growing up as a Navy Brat for anything. It is because of you and our Navy life that I am who I am today and not afraid to seek out the next opportunity or adventure.

Again, thank you all. While I have done my best, I will never be able to put into words the impact each of you has had on my success. I look forward to sharing life's next adventure together.

# TABLE OF CONTENTS

Abstract ..... ii
Acknowledgements ..... iii
Table of Contents ..... ix
Summary of Figures ..... xi
Summary of Tables ..... xii
Summary of Acronyms ..... xiii
1 Chapter 1: General Introduction ..... 1
1.1 Acute Stress ..... 1
1.2 Obesity ..... 3
1.3 Anabolic and Catabolic Signaling ..... 6
1.4 Oxidative Stress ..... 13
1.5 Adipose Tissue as an Endocrine Organ ..... 18
2 Chapter 2: Experimental Methods ..... 21
2.1 Air Oxidation of NEFA ..... 21
2.2 Animals ..... 21
2.3 Cell Culture ..... 22
2.4 Gene Expression Analysis ..... 24
2.5 Glucose Uptake and Turnover ..... 25
2.6 Hemorrhagic Shock Model ..... 26
2.7 Hyperinsulinemic-Euglycemic Clamps ..... 27
2.8 LAD Artery Ligation Model of Myocardial Infarction ..... 27
2.9 Lipid Extraction ..... 28
2.10 Metabolite Measurements ..... 29
2.11 mTOR Complex Activity ..... 30
2.12 Pressure Overload-Induced Heart Failure Model ..... 32
2.13 Regioisomer-Independent Analysis of OxFA by HPLC-Electrospray (ESI)-MS/MS ..... 33
2.14 Serum Collection for OxFA Measurement ..... 36
2.15 Western Blot and Quantitative Analysis ..... 37
3 Chapter 3: Adipocyte Lipolysis Drives Adrenergic Stress-Induced Insulin Resistance and mTOR Complex Dissociation ..... 40
3.1 Abstract ..... 40
3.2 Introduction ..... 41
3.3 Results ..... 43
3.4 Discussion and Conclusions ..... 73
4 Chapter 4: Regioisomer-Independent Quantification of Fatty Acid Oxidation Products by HPLC-ESI-MS/MS Analysis of Sodium Adducts ..... 80
4.1 Abstract ..... 80
4.2 Introduction ..... 81
4.3 Results ..... 83
4.4 Discussion and Conclusions ..... 121
5 Chapter 5: OxFA Serve a Critical Role in Pathologies Characterized by Insulin Resistance ..... 124
5.1 Abstract ..... 124
5.2 Introduction ..... 125

5.3 Results ..... 126
5.4 Discussion and Conclusions ..... 140
6 Chapter 6: The Adipokine Resistin is Acutely Released During Catecholamine-Induced Lipolysis ..... 145
6.1 Abstract ..... 145
6.2 Introduction ..... 146
6.3 Results ..... 148
6.4 Discussion and Conclusions ..... 167
7 Conclusions and Future Directions ..... 172
7.1 Summary ..... 172
7.2 Conclusions and Significance ..... 173
7.3 Future Directions ..... 176
8 Appendix: Characterization of Adipose-Derived Signaling Molecules in COVID-19 Patients ..... 182
8.1 Abstract ..... 182
8.2 Introduction ..... 183
8.3 Methods ..... 185
8.4 Results ..... 185
8.5 Discussion and Conclusions ..... 192
9 Publications ..... 195
9.1 Publications Resulting from this Work ..... 195
9.2 Additional Publications ..... 195
10 References ..... 196

## SUMMARY OF FIGURES

Figure 1-1: Insulin signaling cascade ..... 9
Figure 1-2: β-adrenergic and lipolysis pathway ..... 11
Figure 1-3: Full-length and truncated categories of oxidized lipids ..... 16
Figure 3-1: Acute inhibition of lipolysis improves metabolic impairments in HS ..... 46
Figure 3-2: Genetic deletion of adipocyte *Atgl* improves metabolic impairments in HS ..... 48
Figure 3-3: Inhibition of lipolysis abolishes epinephrine-induced impairments in glucose uptake during hyperinsulinemic-euglycemic clamps ..... 52
Figure 3-4: Glycerol release contributes to hyperglycemia but not insulin resistance ..... 56
Figure 3-5: Resistin levels correlate with lipolysis during adrenergic-stress ..... 59
Figure 3-6: Catecholamine-induced insulin resistance *in vitro* requires lipolysis ..... 63
Figure 3-7: β-adrenergic pathway-stimulated lipolysis disrupts insulin signaling by inhibiting the mTOR complexes ..... 65
Figure 3-8: Lipolytic products inhibit mTOR complex activity *in vitro* ..... 68
Figure 3-9: Lipolytic products dissociate the mTOR complexes ..... 71
Figure 4-1: Chemical structures for the sodium adducts of LA and AA and their full-length oxidation products ..... 86
Figure 4-2: Direct infusion-MS/MS detection and fragmentation of oxFA sodium adducts with positive-ion ionization ..... 90
Figure 4-3: Direct infusion-MS/MS detection and fragmentation of unoxidized LA and AA sodium adducts with positive-ion ionization ..... 92
Figure 4-4: DiffE transition intensity curves for oxFA and NEFA species ..... 96
Figure 4-5: HPLC-MS/MS approach to quantification of oxFA sodium adducts with positive-ion ionization ..... 103
Figure 4-6: Alternate, compatible HPLC methods ..... 105
Figure 4-7: HPLC-MS/MS calibration curves for oxFA and unoxidized NEFA species ..... 107
Figure 4-8: Method validation with a complex mixture of species and isoforms ..... 111
Figure 4-9: Quantification validation with a complex mixture of species and isoforms ..... 113
Figure 4-10: Internal standard conditions and validation ..... 117
Figure 4-11: Quantification of oxFA species in biological sample ..... 119
Figure 5-1: Adrenergic-stimulated lipolysis in adipocytes produces oxFA ..... 129
Figure 5-2: Adipocyte lipolysis increases levels of oxFA in circulation *in vivo* ..... 131
Figure 5-3: OxFA inhibit mTOR complex activity through complex dissociation ..... 135
Figure 5-4: OxFA increase with HFD and affect macrophage gene expression ..... 138
Figure 6-1: Catecholamines stimulate lipolysis and acute release of resistin ..... 151
Figure 6-2: Lipolysis is necessary for adrenergic-stimulated release of resistin ..... 153
Figure 6-3: Antioxidants reduce resistin expression and lipolysis-dependent release ..... 156
Figure 6-4: Inhibiting lipolysis reduces circulating resistin during heart failure ..... 163
Figure 6-5: Lean and obese mice exhibit unique resistin release and mRNA expression profiles during myocardial infarction ..... 165
Figure 8-1: Circulating levels of adipose-derived signaling molecules in ICU patients ..... 188
Figure 8-2: Correlations between adipose-derived signaling molecules in ICU patients ..... 190

## SUMMARY OF TABLES

Table 4-1: Optimized MS/MS conditions for oxFA detection and quantification ..... 88
Table 4-2: Method validation parameters..... 101

## SUMMARY OF ACRONYMS

| | |
|---|---|
| AA | Arachidonic Acid |
| AngII | Angiotensin II |
| ANOVA | Analysis of Variance |
| AQP7 | Aquaporin 7 |
| ATGL | Adipose Triglyceride Lipase |
| ATM | Adipose Tissue Macrophage |
| ATP | Adenosine Triphosphate |
| BSA | Bovine Serum Albumin |
| C17:0 | Heptadecanoic Acid |
| cAMP | Cyclic Adenosine Monophosphate |
| DAG | Diacylglycerol |
| DiffE | Differential Energy |
| DMEM | Dulbecco's Modified Eagle's Medium |
| DTT | Dithiothreitol |
| EDTA | Ethylene Diamine Tetraacetic Acid |
| EGTA | Ethylene Glycol Tetraacetic Acid |
| ELISA | Enzyme-Linked Immunosorbent Assay |
| ESI | Electrospray Ionization |
| FSK | Forskolin |

| | |
|---|---|
| GIR | Glucose Infusion Rate |
| HETE | Hydroxy-Eicosatetraenoic Acid |
| HFD | High-Fat Diet |
| HODE | Hydroxy-Octadecadienoic Acid |
| HPETE | Hydroperoxy-Eicosatetraenoic Acid |
| HPLC | High Performance Liquid Chromatography |
| HPODE | Hydroperoxy-Octadecadienoic Acid |
| HS | Hemorrhagic Shock |
| HSL | Hormone Sensitive Lipase |
| ICU | Intensive Care Unit |
| INS | Insulin |
| i.p. | Intraperitoneal |
| IR | Insulin Receptor |
| ISO | Isoproterenol |
| KETE | Keto-Eicosatetraenoic Acid |
| KODE | Keto-Octadecadienoic Acid |
| LA | Linoleic Acid |
| LAD | Left Anterior Descending |
| LOQ | Limit of Quantification |
| m/z | Mass to Charge Ratio |

| | |
|---|---|
| MS | Mass Spectrometry |
| MS/MS | Tandem Mass Spectrometry |
| mTOR | Mammalian Target of Rapamycin |
| NEFA | Non-Esterified Fatty Acid |
| OxAA | Oxidized Arachidonic Acid |
| OxFA | Oxidized Fatty Acid |
| OxLA | Oxidized Linoleic Acid |
| OxPL | Oxidized Phospholipid |
| PAI-1 | Plasminogen Activator Inhibitor-1 |
| PKA | Protein Kinase A |
| QIM | Qualifier Ion Monitoring |
| QIR | Qualifier Ion Ratio |
| ROS | Reactive Oxygen Species |
| SEM | Standard Error of the Mean |
| SKM | Skeletal Muscle |
| TAG | Triacylglycerol |
| WAT | White Adipose Tissue |
| WT | Wild-Type |

# 1 CHAPTER 1: GENERAL INTRODUCTION

## 1.1 ACUTE STRESS

### 1.1.1 Significance

Severe trauma, such as severe illness and surgery, activates an acute stress response that results in systemic insulin resistance and hyperglycemia, appropriately known as critical illness diabetes (1). Of concern, hyperglycemia has been shown to be an independent risk factor for increased mortality and morbidity after major surgery, in patients with and without diabetes (2–4). As a result, the maintenance of euglycemia is a major therapeutic target in the intensive care unit (ICU) after injury or critical illness (5). Intensive insulin therapy to maintain blood glucose levels at approximately 80-110 mg/dL reduces mortality by 34-50%, and reduces complications such as infection, acute renal failure, and liver dysfunction while also shortening hospital stays (6, 7). However, intensive insulin therapy is only effective in some patients and requires careful monitoring and individualization, as it increases hypoglycemic incidents which often negate the positive effects of tight glucose control (1). Furthermore, this treatment does not correct the underlying insulin resistance, the mechanism of which remains unknown. Elucidating this mechanism is critical as each 1 mg/kg/min decrease in insulin sensitivity (as measured by hyperinsulinemic-euglycemic clamp) correlates to a two-fold increase in major complications (4).

### 1.1.2 Cardiovascular Disease

While a variety of trauma and critical illness can stimulate the acute stress response, cardiovascular events and surgery have been well-documented to cause

metabolic impairments in humans (2–4). Previous studies have shown that hyperglycemia during cardiopulmonary bypass surgery is an independent risk factor for death and complications, even in patients without history of diabetes (3). In addition, a 50% decrease in insulin sensitivity after cardiac surgery increased the risk of major complications by more than 5-fold and the risk of severe infection by more than 10-fold (2, 4). This is particularly worrisome because nondiabetic patients can lose up to 90% of insulin sensitivity during major surgery (2).

The acute stress response can be activated by cardiovascular events such as myocardial infarction. During myocardial infarction, sympathetic nervous system activity increases in response to pain, anxiety, and a fall in cardiac output. This leads to an increase in plasma norepinephrine and epinephrine levels which activate lipolysis (8). After myocardial infarction, the recovery process is categorized into three stages: inflammation, healing, and remodeling (9). During the inflammation phase, inflammatory cells, such as macrophages and neutrophils, are recruited to the injured myocardium to digest the damaged tissue and prepare the tissue for regeneration. During the healing phase, fibroblasts in the border zone of the infarct proliferate producing fibrotic scar tissue in the infarct, and immune cells become polarized towards an anti-inflammatory state (9, 10). During the remodeling phase, infarcts can exhibit persistent inflammation and progress to ventricular dilation (10). Numerous studies have shown that suppressing lipolysis during myocardial infarction leads to smaller infarcts, less ventricular tachycardia and fibrillation, and reduced myocardial ischemia in angina (11, 12). While most work has focused on the effect of non-esterified fatty acids (NEFA) from lipolysis, much less attention has been dedicated toward the release and effect of adipokines on

myocardial infarction. Furthermore, lipids and adipokines could be playing varying roles during the myocardial infarction and recovery process.

Both myocardial infarction and chronic hypertension can lead to the development of heart failure (13). Heart failure affects 1% of people in their 50s, with prevalence increasing progressively with age, eventually afflicting 10% of people in their 80s. In addition to its high prevalence, heart failure is lethal, with one-third of patients dying within two years of diagnosis (14). The 6-year mortality rate is 82% for men and 67% for women (13, 14). Hypertension is the single most important risk factor in the development of heart failure in the United States (15). It increases the chances of developing congestive heart failure 2-fold in men and 3-fold in women (13). Left ventricular hypertrophy is an adaptive response to increased cardiac workload meant to preserve systolic function against increased resistance. If the increased resistance is temporary, such as in athletes performing isometric exercise, the hypertrophy regresses spontaneously after return to normal cardiac workload. However, if the stimulus is prolonged, such as with chronic hypertension, left ventricular hypertrophy can become pathological. In this case, the prolonged stress leads to the development of myocardial fibrosis which leads to dilation of the heart and decreased heart function (15).

## 1.2 OBESITY

### 1.2.1 Significance

Obesity affects more than 1 in 3 adults and 1 in 6 children in the United States (16, 17). The rapidly increasing prevalence of obesity worldwide has infection and undernutrition as the highest contributor to poor health. Furthermore, the obesity epidemic increases the risk of the current leading causes of death, including stroke,

cardiovascular disease, and diabetes (18, 19). Type 2 diabetes alone is expected to affect 366 million people by 2030 (20). Despite the healthcare costs of obesity being as high as $147 billion per year (nearly 10% of annual medical expenses), there are very few reliable, long-term treatment options (21, 22). The most common course of treatment is weight loss, however, after an initial weight loss, most patients regain weight. Maintaining weight loss requires lifelong lifestyle changes that can hindered by time constraints, socioeconomic status, obesity-related comorbidities, and mental health status (22). Medications can counter neurobiological and endocrine changes that promote regaining weight (22, 23). Unfortunately, long-term compliance with obesity medications is poor, with a 1-year compliance rate of less than 10% (22, 24). Currently, the only effective treatment for sustainable weight loss and resolution of obesity-related comorbidities is bariatric surgery. However, in most cases, this treatment is only an option for extreme obesity (22, 25).

### 1.2.2 Disease Hallmarks

White adipose tissue (WAT) is the primary adipose tissue associated with obesity. Adipocytes in WAT contain a single, large lipid droplet and are held together in the adipose tissue by connective tissue. WAT is poorly vascularized with sympathetic innervation (26, 27). WAT is distributed over the entire body and these depots vary in metabolic activity and their potential role in insulin resistance (27–29). As compared to subcutaneous fat, expansion of visceral fat in obesity correlates with increased development of comorbidities. This is likely because visceral fat is more lipolytic, less insulin sensitive, and in closer proximity to portal vasculature, allowing for increased and easier delivery of NEFA into circulation (27, 30, 31). In addition, adipocytes in

individuals with obesity receive exposure to increased levels of catecholamines and exhibit increased basal lipolysis, resulting in increased circulation of NEFA (32). Many consider the release of these NEFA to be the most important factor in modulating insulin signaling. Furthermore, increased levels of NEFA correlate with the development of insulin resistance in both obesity and type 2 diabetes (33). On a cellular level, obesity is associated with impaired glucose uptake by adipocytes and increased basal lipolysis due to elevated levels of catecholamines, which induce whole body insulin resistance and hyperglycemia (32, 34). While hyperglycemia contributes to the comorbidities listed above, treatment for the underlying cause, insulin resistance, is lacking, prompting the need for novel therapeutic targets.

In addition to adipocytes, WAT also contains ATM, leukocytes, fibroblasts, and endothelial cells (27). During obesity, there is a significant accumulation of macrophages within adipose tissue which can increase to be up to 50% of stromal cells (35–39). In addition, the localization of adipose tissue macrophages (ATM) changes from interstitially spaced in lean WAT to clustered in crown-like structures in obese WAT (35, 40, 41). Furthermore, recent studies have demonstrated that macrophages also change phenotype with obesity. The traditional paradigm claimed that ATM in lean mice have an anti-inflammatory M2 phenotype, while in obesity this switches to a pro-inflammatory M1 phenotype (42). This switch to M1 mirrors the increased level of basal inflammation observed in obese individuals (43). Recent work from our collaborators demonstrated a third, Mox phenotype (44). This work showed that ATM macrophages are primarily Mox with M1 and M2 macrophages infiltrating WAT during obesity (45). Furthermore, this work demonstrated that various macrophage polarizations could be induced by different

categories of oxidized lipids (44, 45). It is thought that an increased pro-inflammatory state in obesity contributes to the induction of local and systemic insulin resistance (46). As such, adipocyte-derived factors, such as oxidized lipids that can alter macrophage function, are of interest and potential therapeutic importance.

## 1.3 ANABOLIC AND CATABOLIC SIGNALING

### 1.3.1 Insulin Pathway

The acute stress response is characterized by inhibition of anabolic signaling and activation of catabolic signaling to provide substrates for tissue healing (47). Insulin is a key anabolic hormone, and its signaling is potently inhibited during acute stress (47). Insulin resistance is the inability of insulin to adequately stimulate glucose uptake or inhibit gluconeogenesis in the liver (1). The mechanism by which insulin resistance develops in chronic or acute conditions in various tissues is still largely unknown (1). Insulin signals through the insulin receptor and the downstream insulin receptor substrates/phosphatidylinositol 3-kinase/Akt pathway, leading to many intracellular changes such as the synthesis of lipids, proteins, and glycogen, as well as increased glucose uptake by translocation of GLUT4-containing vesicles to the membrane in adipose tissue and striated muscle **(Figure 1-1)** (48).

Integral steps in this pathway are the mTOR complexes **(Figure 1-1)**. The mTOR complexes are serine/threonine kinases that function as key regulators of cell growth and metabolism. mTOR is found in two unique protein complexes: mTORC1, in which mTOR interacts with raptor and PRAS40; and mTORC2, in which it interacts with rictor and mSin (49). Association of mTOR with raptor or rictor is required for mTORC1 and mTORC2 kinase activity, respectively (50). Both mTOR complexes phosphorylate and

activate a subgroup of the AGC family of protein kinases (those in the protein kinase A, G, and C families), including the mTORC1 substrates S6K1 and 4E-BP1 and the mTORC2 substrate Akt (50). Of note, inhibition of these complexes has been strongly associated with the onset of insulin resistance.

### 1.3.2 Adrenergic Signaling and Lipolysis

In addition to inhibiting insulin signaling, acute stress induces a sympathetic nervous system response and the rapid release of catecholamines, which are major catabolic hormones. Catecholamines, such as epinephrine, activate adrenergic receptors which are comprised of two groups, α and β. All β-receptors, including the $\beta_3$-receptor which is expressed predominantly in adipose tissue in mice, are $G\alpha_s$-coupled G protein-coupled receptors **(Figure 1-2)**. Their activation by epinephrine leads to the breakdown of glycogen, production of glucose, and the induction of lipolysis (47, 51, 52). Lipolysis is the breakdown of stored fats in the form of triacylglycerol (TAG) from lipid droplets. The first and rate-limiting step of this process, the removal of a single fatty acid from a TAG to produce diacylglycerol (DAG), is catalyzed by adipose triglyceride lipase (ATGL) (53). Mice lacking ATGL, such as our fat-specific knockout ($FATA^{-/-}$) mice, exhibit drastic reductions in their ability to begin the breakdown of TAG and undergo lipolysis (54). The final products of the breakdown of TAG are glycerol and FA. Glycerol serves as a gluconeogenic substrate for the liver, and its increased abundance could contribute to hyperglycemia during critical illness diabetes. NEFA can undergo beta-oxidation to serve as a source of energy, be used as precursors for other lipids, or act as signaling molecules (51, 52).

### 1.3.3 Anabolic and Catabolic Crosstalk

To prevent futile cycling and conserve cellular adenosine triphosphate (ATP), both anabolic and catabolic signaling pathways have mechanisms to oppose one another. The mechanism by which the anabolic pathway inhibits the catabolic pathway is fairly well-defined. In hepatocytes, insulin decreases the expression of gluconeogenesis genes (55). In adipocytes, insulin inhibits lipolysis through activation of phosphodiesterase 3B, a substrate of Akt. Phosphodiesterase 3B degrades cyclic adenosine monophosphate (cAMP), leading to inhibition of catabolic signaling by decreasing protein kinase A (PKA) and lipase activity (56). However, the mechanism by which catabolic signaling inhibits anabolic processes is largely unknown. It has long been established that catecholamines inhibit insulin-stimulated glucose uptake in adipocytes through stimulation of β-adrenergic receptors (32, 57). Despite the fact that inhibition of insulin signaling by catecholamines in adipocytes has been demonstrated repeatedly for decades, the mechanistic details of this crosstalk have remained unclear. Furthermore, how this crosstalk may be functioning *in vivo* between multiple different tissues is increasingly more complicated.

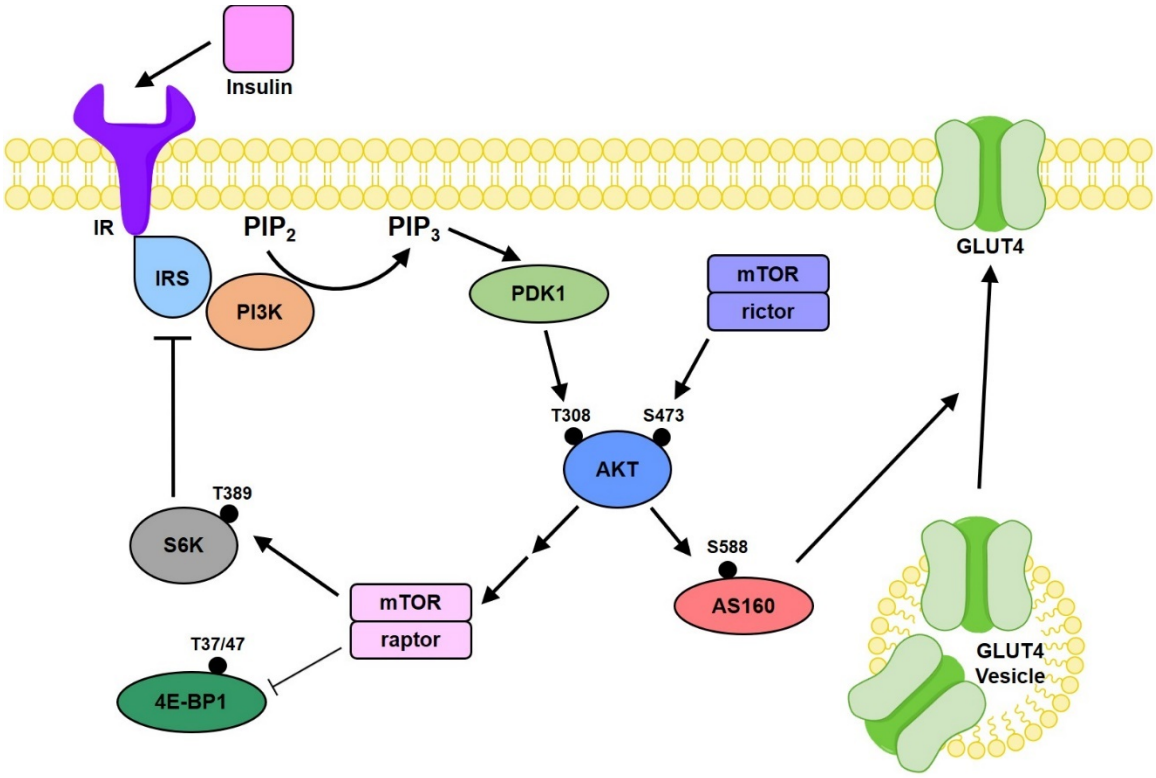


**Figure 1-1: Insulin signaling cascade**

**Figure 1-1 Legend**

Insulin binds to insulin receptor (IR), causing the activation of insulin receptor substrate (IRS). IRS activates phosphoinositide 3-kinase (PI3K) which catalyzes the conversion of phosphatidylinositol 4,5-bisphosphate ($PIP_2$) to phosphatidylinositol 3,4,5-trisphosphate ($PIP_3$). Increased levels of $PIP_3$ activate phosphoinositide-dependent kinase 1 (PDK1). AKT is fully activated when phosphorylated by PDK1 and mTORC2. Once active, AKT phosphorylates AS160, leading to GLUT4 translocation to the membrane and subsequent glucose uptake. AKT can also phosphorylate mTORC1 which can inhibit eukaryotic translation initiation factor 4E-binding protein 1 (4E-BP1) or activate p70-S6 Kinase 1 (S6K). S6K exerts negative feedback on IRS to inhibit insulin signaling.

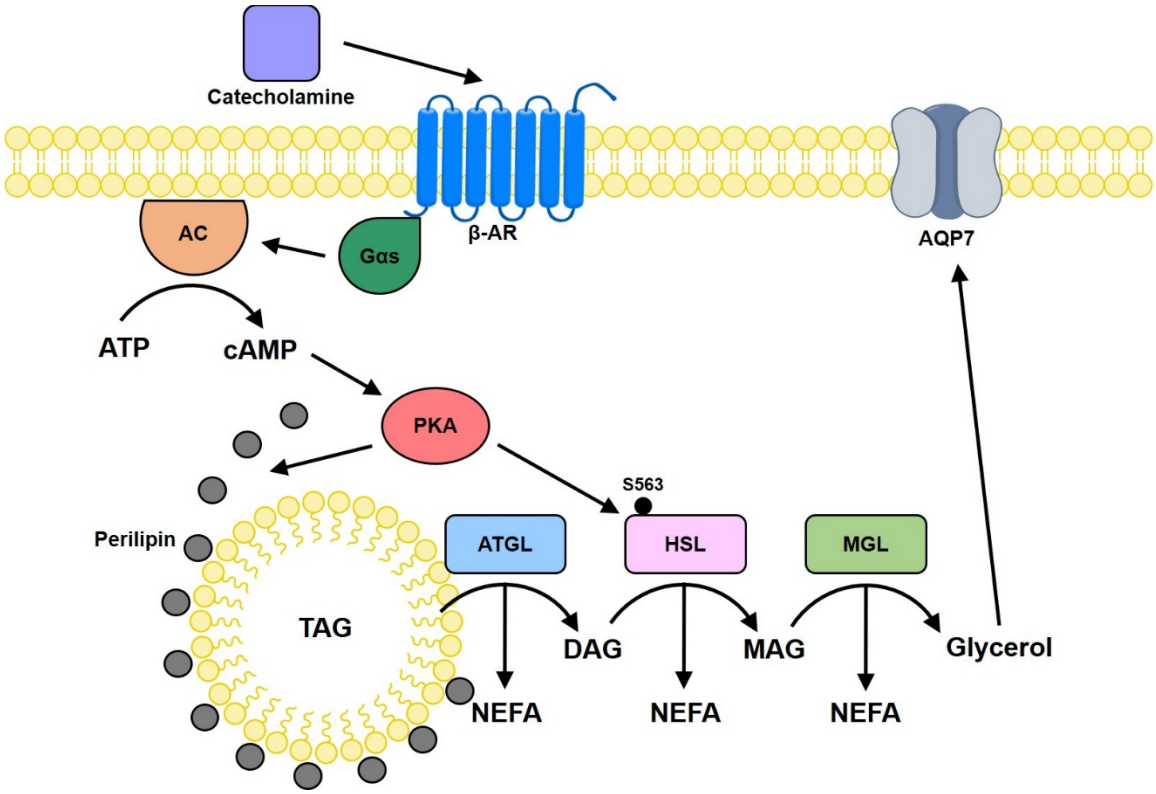


**Figure 1-2: β-adrenergic and lipolysis pathway**

**Figure 1-2 Legend**

Catecholamines activate β-adrenergic receptors on the surface of adipocytes. β-adrenergic receptors are coupled to $G\alpha_s$ protein which activates adenylyl cyclase (AC). AC converts adenosine triphosphate (ATP) to cyclic adenosine monophosphate (cAMP). Increased levels of cAMP lead to the activation of protein kinase A (PKA). PKA phosphorylates perilipin and hormone-sensitive lipase (HSL) to initiate lipolysis. Perilipin coats lipid droplets to protect triglyceride (TAG) from lipase activity. Once acted on by PKA, perilipin moves off the lipid droplet and releases CGI-58 allowing it to associate with and activate adipose triacylglycerol lipase (ATGL). ATGL hydrolyzes TAG to diacylglycerol (DAG) and non-esterified fatty acid (NEFA). HSL hydrolyzes DAG to monoacylglycerol (MAG) and FA. Monoacylglycerol lipase (MGL) hydrolyzes MAG to NEFA and glycerol. Glycerol is released from adipocytes through aquaporin 7 (AQP7).

## 1.4 OXIDATIVE STRESS

### 1.4.1 Redox Imbalance During Acute Stress

Under homeostatic conditions, cells carefully regulate redox reactions to accomplish important biological functions. For example, oxygen accepts free electrons (forming ROS) from the mitochondrial electron transport chain which establishes the pH gradient within mitochondria that is necessary for the production of ATP (58). However, ROS can arise from a number of sources including nicotinamide adenine dinucleotide phosphate (NADPH) oxidase and xanthine oxidase (5). Cellular ROS levels result from a careful balance between ROS production and elimination to prevent dangerous nonspecific reactions. Important antioxidant enzymes responsible for minimizing ROS levels are the superoxide dismutase enzymes, including the mitochondrial isoform superoxide dismutase 2, which catalyze the reaction converting ROS species, such as superoxide and peroxide ions, to oxygen and hydrogen peroxide (5). Hydrogen peroxide can be further reduced to water by the enzyme catalase. Cells also produce antioxidant compounds that act as ROS scavengers; the most abundant antioxidant compound *in vivo* is Vitamin E (59).

During acute stress, catecholamines induce vasoconstriction in peripheral tissues, including liver and adipose tissue (47). This vasoconstriction leads to a hypoxic environment, which is compounded by hypoxic conditions created by the initiating trauma, such as hemorrhage or surgical injury (5). During hypoxia, cells are in a more reductive state, as there is insufficient oxygen available for the electron transport chain. As a result, there is a buildup of reducing equivalents in the mitochondria, such as nicotinamide adenine dinucleotide (NADH) and flavin adenine dinucleotide ($FADH_2$).

This buildup of reducing equivalents makes electrons more available for reduction reactions, such as the reduction of oxygen to superoxide (60). As such, the major cellular source of ROS is the electron transport chain of the mitochondria, specifically complex I and III (5, 61). Additionally, increased lipolysis during acute stress can result in increased production of ROS (62). During oxidative stress, ROS production surpasses cellular control, and ROS can then nonspecifically react with molecules within nanometers of their generation. This leads to destructive biological processes, such as membrane damage, protein modification, DNA oxidation, deposition of atherogenic plaque, and tissue inflammation (45, 63–65). In an adipocyte where the intracellular volume is dominated by a large lipid droplet, it is likely that ROS species will come into contact and react with TAG (66).

### 1.4.2 Oxidized Lipids

While oxidized lipids can be produced enzymatically in a tightly regulated fashion by lipoxygenases and cyclooxygenases to form signaling molecules, such as leukotrienes and prostaglandins (67, 68), non-enzymatic lipid oxidation during oxidative stress may surpass cellular control. ROS can react with polyunsaturated FA, free or esterified in TAG, resulting in lipid peroxidation and the formation of biologically active compounds (69). The double bonds of polyunsaturated fatty acids are subject to abstraction of a proton by ROS. This leads to the addition of an oxygen to the polyunsaturated fatty acid and the formation of full-length oxFA, including hydroperoxides, hydroxides, and ketones **(Figure 1-3)**. The generation of lipid radicals allows for a further series of reactions resulting in the fragmentation of the acyl chain and formation of truncated oxFA (70). Only in recent years have scientists begun to appreciate the diverse structures

of the oxidized lipidome and focused on investigating their unique signaling activities and pathological consequences.

When produced in an unregulated manner, oxidized lipids can cause destructive biological processes, such as membrane damage, protein modification, DNA oxidation, deposition of atherogenic plaque, and tissue inflammation (45, 63–65). However, these processes also allow oxidized lipids to act as signaling molecules within a cell. For example, various oxFAs dissociate protein complexes by post-translational modifications. In particular, oxidized n-3 NEFA can react with cysteine in Keap1, causing a change in its secondary structure and dissociation from Cullin3, leading to activation of the redox regulatory transcription factor, Nrf2 (64, 69, 71). Recent studies have demonstrated that the signaling mechanisms of oxFA are highly selective and can be reversible, providing evidence for oxFA as the link between redox and metabolic status (69).

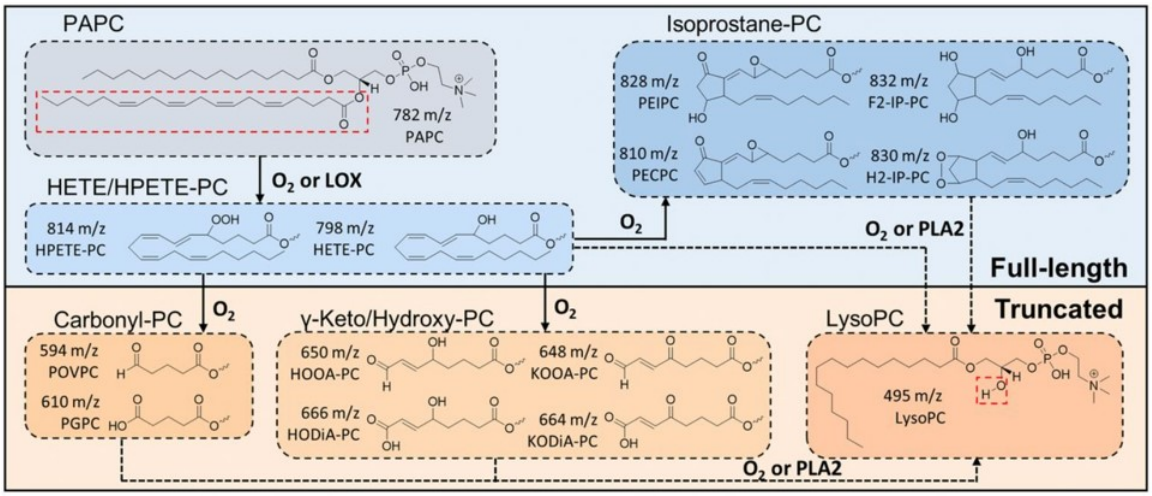


**Figure 1-3: Full-length and truncated categories of oxidized lipids**

Published in Serbulea V, Upchurch CM, Schappe MS, Voigt P, DeWeese DE, Desai BN, Meher AK, Leitinger N. Macrophage phenotype and bioenergetics are controlled by oxidized phospholipids identified in lean and obese adipose tissue. *PNAS*. 2018 July 3. PMCID: PMC6142199.

**Figure 1-3 Legend**

Schematic outlining oxidation products of AA (in red, dotted-line box). As an example, AA is incorporated into a phospholipid (oxPAPC), but the same products can be formed from non-esterified AA. Oxidation products can be assigned into two broad categories: full-length which have an intact acyl chain and a higher molecular weight than AA and truncated which have a cleaved acyl chain and lower molecular weight than AA. Oxidized lipids can be further split into smaller categories based on chemical moieties and biological activity.

## 1.5 ADIPOSE TISSUE AS AN ENDOCRINE ORGAN

### 1.5.1 Adipose Tissue and Whole-Body Metabolism

Even though insulin resistance depends on insulin action in various tissues, multiple studies have supported adipose tissue as a central player in controlling peripheral insulin signaling. For example, adipose-specific loss of GLUT4 (encoded by *Slc2a4*) caused mice to develop hyperglycemia and peripheral insulin resistance, whereas adipose-specific overexpression of GLUT4 enhanced insulin sensitivity (72, 73). Previous work from our laboratory demonstrated that decreased rictor expression in adipose tissue led to hyperglycemia and systemic insulin resistance (50). This indicates that impaired insulin action in adipose tissue alone is sufficient to drive hyperglycemia and whole-body insulin resistance. Despite these findings, how adipose tissue is signaling and driving insulin resistance in these peripheral tissues is still unknown.

### 1.5.2 Adipokines

In addition to storing and mobilizing TAG, adipose tissue has been increasingly appreciated for its role in endocrine signaling, such as through the release of cytokines and adipokines. In lean individuals, adipose tissue secretes primarily anti-inflammatory cytokines, such as TGFβ, IL-10, IL-4, IL-1Ra, and IL-12. However, during obesity, adipocytes release primarily pro-inflammatory cytokines, such as TNF-α and IL-6 (74–76). Adipocytes can also secrete adipokines such as adiponectin, leptin, plasminogen activator inhibitor-1 (PAI-1), and resistin. Adiponectin improves whole-body insulin sensitivity, stimulates appetite, and reduces energy expenditure. During obesity, levels of adiponectin decrease and correlate with loss of insulin sensitivity (75, 77, 78). On a cellular level, adiponectin stimulates glucose uptake and NEFA oxidation (76, 79). Leptin

signals to the brain about body fat stores and regulates appetite and energy expenditure. As such, leptin increases with obesity and overfeeding. It also can affect cellular functions such as glucose metabolism, lipid oxidation, and adipocyte apoptosis (76, 79–81). PAI-1 is primarily produced by vascular endothelial and smooth muscle cells, but can also be produced by adipocytes (76, 82). The contribution of adipocytes to circulating PAI-1 levels increases with obesity. PAI-1 alters the balance of fibrinolysis and fibrinogenesis and may serve as a connection between obesity and cardiovascular disease (76, 83).

### 1.5.3 Resistin

Resistin is an adipokine that is released by adipocytes in rodents (84–88). Resistin acquired its name due to its initial association with the development of insulin resistance (84, 87). Initial characterization of resistin showed that circulating levels were increased in mouse models of obesity. Manipulating levels of resistin altered blood glucose and insulin function (84). For example, administration of recombinant resistin impaired glucose tolerance and led to insulin resistance while treatment with an anti-resistin antibody improved blood glucose and insulin sensitivity. Interestingly, while circulating levels of resistin have been shown to also increase in obesity in humans, resistin was found to be secreted by macrophages in humans as opposed to adipocytes (86–88). In humans, resistin is associated with inflammation rather than adiposity (87). However, a characteristic of obesity is increased basal inflammation and infiltration of macrophages into adipose tissue. Furthermore, inflammatory cytokines have previously been linked to the development of insulin resistance (89). As such, it is possible that, despite differences in tissue secretion, resistin still affects insulin sensitivity in humans. Of note, despite

being discovered two decades ago, the regulation, mechanism, and receptor of resistin remain unknown.

Due to its initial characterization in chronic conditions such as obesity and type 2 diabetes, little attention has been focused to the potential acute role for resistin. However, recent studies on the acute stress response in humans have demonstrated a correlation between circulating resistin and trauma or critical illness, with higher levels of resistin associated with worse outcomes (90–97). Prolonged elevation of resistin levels was an independent predictor of illness severity and mortality, independent of body mass index (BMI) (90, 93, 94). As such, studies have increasingly investigated resistin as a potential therapeutic target for critical illness (98, 99).

# 2 CHAPTER 2: EXPERIMENTAL METHODS

## 2.1 AIR OXIDATION OF NEFA

OxFA mixtures were prepared by auto-oxidation of either LA or AA (Cayman Chemicals) following a protocol adapted from phospholipid auto-oxidation (100). From stock solutions in methanol, 1 mg of LA or AA was transferred to a glass test tube and dried down under a stream of nitrogen. The tube was loosely covered with foil to deter the introduction of contaminants and exposed to atmospheric oxygen for up to 96 h. The progression of oxidation was assessed by both direct infusion-MS/MS and HPLC-MS/MS analysis.

## 2.2 ANIMALS

### 2.2.1 Colony Maintenance

All animals were bred and housed in accordance with Institutional Animal Care and Use Committee regulations. Animals were maintained on 12 h light/12 h dark cycle and had ad libitum access to food and water. Unless otherwise indicated, 8- to 12-week old male and female mice were used for studies. All used mice were of an inbred C57BL/6J mouse line background. For all studies, control mice were age and sex-matched litter mates.

### 2.2.2 Transgenic Animals

*Atgl*$^{flox/flox}$ (B6N.129S-*Pnpla2*$^{tm1Eek}$/J, Jax #024278), AdipoQ-cre (B6;FVB-Tg(Adipoq-cre)$^{1Evdr/J}$, Jax #010803), and C57BL/6J (WT, Jax #000664) were from the Jackson Laboratory. *Aqp7*$^{-/-}$ (*Aqp7*$^{Gt(NAISTrap\_TPM2\text{-}118)Yais}$) sperm was obtained from Riken Resource Center and used to re-derive mice at the University of Virginia's Genetically

Engineered Murine Model Core (101). Adipocyte-specific ATGL knockout ($FATA^{-/-}$) mice were generated by crossing $Atgl^{flox/flox}$ with AdipoQ-Cre mice. Successful adipose tissue-specific loss of ATGL was demonstrated by immunoblot. The functional consequences of this deletion were confirmed by fasting mice 4 h before intraperitoneal (i.p.) injection of 2 mg/kg epinephrine and measuring the release of glycerol and NEFA after 30 min. Inducible, cardiomyocyte-specific loss of p38 MAPKα in mice (iCMp38KO) was generated by crossing mice homozygous floxed *Mapk14* with a mouse line expressing tamoxifen-inducible Cre-recombinase (merCremer) specifically in cardiomyocytes under the control of α-MHC promotor (102). To induce *Mapk14* gene deletion and loss of p38 MAPKα, iCMp38KO mice were injected i.p. with 500 µg OH-Tamoxifen (5 mg/mL in peanut oil) with a 23 G needle followed by a defined recovery time, to ensure a successful knockout and to exclude side effects of OH-Tamoxifen injections.

## 2.3 CELL CULTURE

### 2.3.1 Primary Adipocyte Isolation

Primary adipocytes were isolated as previously described (103). Briefly, mice were anesthetized by i.p. injection of 5 mL/kg body weight of a ketamine/xylazine/acepromazine mixture in saline and euthanized by cervical dislocation before epididymal fat pads were harvested. Fat pads were added to Krebs Ringer HEPES-bovine serum albumin (BSA) buffer containing 1 mg/mL collagenase type I (Worthington Biochemical) used at 2 mg/g tissue. The fat pads were minced with scissors while in the collagenase solution and incubated for 70 min at 37 °C in a water bath shaking at 100 rpm. The fat cells were separated from nonfat cells and undigested debris

by filtration through a 0.4-mm Nitex nylon mesh (Tetko) and then washed four times by flotation with Krebs Ringer HEPES-BSA.

### 2.3.2 Culture of 3T3-L1 Cells

3T3-L1 mouse preadipocytes (Zen-Bio) were cultured as previously described (52, 104). Namely, preadipocytes were grown in Dulbecco's Modified Eagle's Medium (DMEM, Gibco) containing 10% newborn calf serum (Gibco), 1% fetal bovine serum, and 1% antibiotics (Gibco). Preadipocytes were differentiated into adipocytes by addition of 100 U/mL insulin (Humulin R, Eli Lilly), 0.5 mM 3-isobutyl-1-methylxanthine, and 0.25 μM dexamethasone to DMEM containing 10% fetal bovine serum and 1% antibiotics. Adipocytes were fed 4 days after differentiation and every other day thereafter with DMEM containing 10% fetal bovine serum and 1% antibiotics. Adipocytes were used 7-12 days after differentiation and fed the day before the experiment.

### 2.3.3 Adipocyte Treatments

Isolated adipocytes or 3T3-L1 adipocytes were treated in serum-starved or low-serum media, as specified in each figure legend. Lipolysis was induced by treating with 10 μM forskolin (FSK) or 1 μM isoproterenol (ISO, Sigma-Aldrich) for the time specified in each figure legend. Insulin signaling was induced by treatment for 15 min with 70 nM. For inhibitor studies, cells were treated with 150 μM E600 or 10 μM atglistatin (Cayman Chemicals) for 1 h prior to lipolysis stimulation. For antioxidant studies, cells were treated with 100 μM TmPyP, 100 μM TBAP, or 100 μM EUK (Cayman Chemicals) overnight prior to lipolysis stimulation. Oxidative stress was increased by treating with TBH (Sigma-Aldrich) overnight at the noted concentration

before lipolysis stimulation. Media samples were collected in tubes and centrifuged at 2,500 x g for 10 min. Media supernatant was used for further analysis when specified.

### 2.3.4 Bone Marrow-Derived Macrophage Isolation, Culture, and Treatment

The bone marrow from the hind legs of mice was isolated and cleared of erythrocyte progenitors by incubation with 0.83% $NH_4Cl$. The bone marrow was then cultured with RPMI media (Gibco) containing 10% FDA, 2% HEPES, 1% antibiotic, and 10% L929-conditioned media. Bone marrow was cultured for 7 days, with media changed every 3 days with media lacking L929-conditioned media. On day 7, bone marrow-derived macrophages were separated from the Petri dish using 0.25% trypsin, centrifuged, had media refreshed, and re-plated before treatment with vehicle, 6.4 μM oxPAPC, 6.4 μM oxPAPE, or 6.4 μM oxidized arachidonic acid (oxAA) for 4 h.

## 2.4 Gene Expression Analysis

### 2.4.1 RNA Isolation

RNA was isolated using TRIzol reagent. For tissues, 1 mL of TRIzol (Invitrogen) was added to 50-100 mg of tissue before homogenization with a Potter-Elvehjem homogenizer. For cells, 1 mL of TRIzol was added to a cell pellet from a 6-cm plate. Cells were homogenized by pipetting. To the TRIzol mixture, 200-250 μL of chloroform was added before being vortexed. Tubes were then centrifuged at 16,000 x g for 10 min at 4 °C. Supernatant was discarded, and 500 μL of isopropanol was added to each tube. For cell samples, the isopropanol mixture was stored overnight at -20 °C. Tubes were centrifuged at 16,000 x g for 10 min at 4 °C. Supernatant was discarded, and 500 μL of 70% ethanol was added to each tube. Tubes were centrifuged at 16,000 x g for 10 min at 4 °C. Ethanol was carefully pipetted without disturbing the pellet. The pellet was then air

dried for 20 min before resuspension in 20 μL of nuclease-free water and heated at 55 °C for 10 min. For tissue samples, mixture was treated with DNase I (Promega) at 37 °C for 10 min. To stop the DNase I reaction, 0.5 μL of 500 mM ethylene diamine tetraacetic acid (EDTA) was added to each tube.

### 2.4.2 Real-Time qPCR Analysis

cDNA was reverse transcribed from 1 μg of RNA using the High Capacity cDNA Reverse Transcription Kit (Applied Biosystems) and amplified by PCR. Analysis by real-time qPCR was set up using 1 μg of cDNA, 10 pmol of each primer (forward and reverse), and iQ SYBR Green Supermix (BioRad). Primers were designed and validated for mouse *B2m*, *Csnk2b*, *Cxcl1*, *Cxcl2*, *G6pdx*, *Gclm*, *Slc2a1* (GLUT1), *Hmox1*, *Il1β*, *Il6*, *Pgd*, *Retn*, *Rn18S*, *Srxn1*, and *Taldo*.

## 2.5 GLUCOSE UPTAKE AND TURNOVER

Glucose uptake was measured in isolated adipocytes, as previously described (105). Briefly, isolated adipocytes were diluted 10-fold in Krebs Ringer HEPES buffer with 0.5% BSA to produce a cell suspension. Cell suspension aliquots of 100 μL were mixed with 350 μL of Krebs Ringer HEPES-BSA buffer with or without treatments for 30 min in a 37 °C shaking water bath. To each cellular suspension, 1.25 μCi of [U-$^{14}$C]-D-glucose (PerkinElmer) in Krebs Ringer HEPES-BSA buffer was added. Samples were incubated an additional 20 min in the water bath. Glucose uptake was terminated by centrifuging each cellular suspension through 150 μL of dinonyl phthalate to separate the cells from the assay media. The radioactivity of the cellular fraction was determined by liquid scintillation counting. Nonspecific cellular radioactivity was determined by performing the assay with 20 μM cytochalasin B. Results were expressed as attomoles

per minute per cell. The number of cells was calculated from lipid weights and adipocyte size (105).

## 2.6 HEMORRHAGIC SHOCK MODEL

Surgical trauma and HS were induced as previously described with minor modifications (5). Briefly, 10- to 12-week old mice were fasted 4 h before experiments. For inhibitor studies, atglistatin and GS-9667 (Gilead Sciences) in dimethyl sulfoxide were diluted in vehicle (1% Cremophor-EL in saline) and administered i.p. 4 h and 1 h prior to the start of experiment, respectively. For vehicle treatments in atglistatin and GS-9667 studies, animals received matched volumes of dimethyl sulfoxide in 1% Cremophor-EL. For glycerol treatments, a bolus of 3 mg/g glycerol was administered i.p. immediately before the start of the HS protocol. Mice were then anesthetized with isoflurane inhalation. Mice were kept anesthetized throughout the surgical procedure by continuous inhalation of 1.5% isoflurane and 98.5% air. Mice were then shaved and restrained in a supine position. Soft tissue trauma was represented by a 2-cm ventral midline laparotomy in the abdomen that was closed with 6-0 Ethilon sutures. Mean arterial pressure was monitored by a polyethylene-10 catheter placed in the right femoral artery. Within 10 min, mice were bled to a mean arterial pressure of 35-40 mm Hg and maintained at this pressure. At the end of 30 min, saline or 0.5 U insulin was injected into the inferior vena cava. After 4 min, tissues were harvested. Blood glucose and lactate levels were measured at the tail vein by a handheld glucometer (One-touch Ultra) and lactate monitor (Nova Biomedical), respectively.

## 2.7 HYPERINSULINEMIC-EUGLYCEMIC CLAMPS

Hyperinsulinemic-euglycemic clamps were conducted as previously described with minor modifications (106). Briefly, 10- to 12-week old mice were fasted 2-4 h before experiments. For inhibitor studies, vehicle or GS-9667 was administered i.p. 30 min prior to start of the experiment. Mice were initially anesthetized with 2% isoflurane and maintained on 1.5% isoflurane. An incision was made to expose, isolate, and catheterize the left jugular vein. During the induction period (-30 to 0 min), mice were infused with D-[3-$^{3}$H] glucose at 0.17 μCi/min and either epinephrine (1 μg/kg/min) or saline. The clamp was started with a continuous infusion of insulin at 10 mU/kg/min and either epinephrine (1 μg/kg/min) or saline. Plasma glucose was maintained at 150 mg/dL by variable infusion of dextrose throughout the clamp.

## 2.8 LAD ARTERY LIGATION MODEL OF MYOCARDIAL INFARCTION

To model diet-induced obesity, wild-type (WT) mice were fed chow or high-fat diet (HFD) for 12 weeks. Blood was collected from the tail vein after 12 weeks as the basal timepoint. To induce myocardial infarction in lean or obese mice, the left anterior descending (LAD) artery ligation model was used (107). In brief, mice were anesthetized with 2% isoflurane, intubated, and ventilated with 40% oxygen using a rodent ventilator (Hugo Sachs). Mice were place in a supine position on a warming plate (Zevenaar) to maintain body temperature at 37.5 °C. For analgesia, mice received 0.1 mg/kg buprenorphine subcutaneously. Electrocardiography was recorded continuously during the procedure. Blood was collected from the tail vein before incision to account for anesthesia-induced changes. After lateral thoracotomy, the pericardium was dissected, and a 7-0 surgical prolene suture was passed underneath the LAD artery 1 mm from the

tip of the left auricle. The suture ends were passed through a piece of silicon tubing to form a snare occlude. Myocardial ischemia was produced by tightening the snare and was confirmed by both blanching of the myocardium and a change in the electrocardiography. After 35 min of ischemia, blood was collected from the tail vein for the ischemic stress timepoint. After a total of 45 min of ischemia, the snare was opened to initiate reperfusion. The suture was then removed, and the chest was closed. Mice were extubated after they regained spontaneous breathing. As postoperative analgesia, mice received 0.05-0.1 mg/kg buprenorphine every 8 h for up to 5 days. Blood was collected from the tail vein 1, 2, 8, and 16 days after surgery. On either day 8 or 16, mice were sacrificed by cervical dislocation, and tissues were harvested.

## 2.9 LIPID EXTRACTION

### 2.9.1 Extraction of Lipids for *in vitro* mTOR Complex Assays

A 6-cm plate of 3T3-L1 adipocytes or 100 µL of packed isolated adipocytes treated as indicated were washed twice with PBS (145 mM NaCl, 5.4 mM KCl, and 10 mM $Na_3PO_4$, pH 7.4) and homogenized in a buffer containing 1 mM EDTA, 1 mM ethylene glycol tetraacetic acid (EGTA), 1 mM dithiothreitol (DTT), 0.1% Tween 20, 10 mM $Na_3PO_4$, 50 mM β-glycerophosphate, pH 7.4 supplemented with 1 mM phenylmethylsulfonyl fluoride, 10 µg/mL leupeptin, 10 µg/mL aprotinin, 10 µg/mL pepstatin, and 0.5 µM microcystin LR. Homogenates were centrifuged at 16,000 x g for 10 min. A total of 400 µL of 1:1 hexane:ethyl acetate was added and mixed with the supernatants for 30 min followed by centrifugation at 8,000 x g for 2 min. The organic phase was moved to a fresh tube, and the organic solvent was evaporated. The dried residue was then resuspended and used in either the kinase or dissociation assay, as

specified. For the *in vitro* lipase treatment, resuspended lipids were treated with 2 U/mL lipase for 30 min at room temperature. Lipids were then reextracted.

### 2.9.2 Extraction of OxFA

Lipids were extracted from cellular media or mouse serum spiked with 25 nmol of internal standard (heptadecanoic acid, C17:0) using a chloroform/methanol extraction. To each glass tube of media or serum, 3 mL of extraction solvent (2:1 chloroform:methanol containing 50 μg/mL butylated hydroxytoluene to deter further lipid oxidation) was added. The tubes were then vortexed and placed on ice for 30 min before partitioning by centrifugation (2,000 x *g*, 5 min, 4 °C). After centrifugation, the lower organic layer was collected in a separate glass test tube. The remaining aqueous layer was subjected to a second extraction with 1.5 mL of extraction solvent. After vortexing, the samples were again partitioned by centrifugation and the lower organic layer collected and combined with that from the first extraction. The solvent from the collected extractions was evaporated under a stream of nitrogen before being suspended in 100 μL of methanol and analyzed by HPLC-MS/MS.

## 2.10 METABOLITE MEASUREMENTS

Blood glucose levels were measured at the tail vein by a handheld glucometer. NEFA levels in serum, media, and lipid extracts were measured using the HR series NEFA-HR detection kit (Wako Diagnostics) following manufacturer's protocol (32). Glycerol and glycerolipid levels in serum, media, and lipid extracts were measured using the free glycerol/glycerolipid determination kit (Sigma-Aldrich) following manufacturer's protocol. A commercial enzyme-linked immunosorbent assay (ELISA)

kit was used to detect resistin (RayBiotech) following manufacturer's protocol. All other circulating adipokines in serum were detected by Luminex Multiplex Assays at the University of Virginia flow core facility.

## 2.11 mTOR Complex Activity

### 2.11.1 Endogenous mTOR Complex Immunoprecipitation

Cell extracts from a 6-cm dish of 3T3-L1 were incubated at 4 °C with 2 μg of antibodies bound to either 15 μL of protein A-agarose beads for rabbit antibodies or 15 μL of protein G-agarose beads for mouse antibodies for 2 h with constant mixing. After incubation, the beads were washed with 1 mL of buffer containing 1 mM EDTA, 1 mM EGTA, 1 mM DTT, 0.1% Tween 20, 10 mM $Na_3PO_4$, 50 mM β-glycerophosphate, 0.5 mM NaCl, pH 7.4. Beads were then washed twice with 1 mL of buffer containing 1 mM EDTA, 1 mM EGTA, 1 mM DTT, 0.1% Tween 20, 10 mM $Na_3PO_4$, 50 mM β-glycerophosphate, pH 7.4. Protein was eluted from beads with Laemmli buffer.

### 2.11.2 Recombinant mTOR Complex Purification

A 15-cm plate of HEK293T cells were transiently transfected with 40 μg plasmid for HA-tagged mTOR and 10 μg plasmid for FLAG-tagged raptor (FLAG-tagged rictor for mTORC2) using 25 μL Lipofectamine 2000. A total of 18-24 plates were used for each purification. Each plate of cells was lysed in 0.3 mL lysis buffer (150 mM NaCl, 50 mM HEPES, 0.4% CHAPS, pH 7.4 with protease inhibitors). Cell lysates were centrifuged at 16,000 x g for 10 min. The supernatant was incubated with 10 μL anti-FLAG M2 beads for 2 h at 4 °C. Beads were isolated by centrifuging at 2,000 x g, and the supernatant was removed. The beads were packed onto a screening column (Fisher Scientific) and washed once with lysis buffer. The beads were then rinsed once with 3

mL wash buffer 1 (150 mM NaCl, 50mM HEPES, 0.1% CHAPS, pH 7.4) and twice with 1 mL wash buffer 2 (200 mM NaCl, 50 mM HEPES, 0.1% CHAPS, pH 7.4). mTOR complex was eluted by five 200 μL additions of elution buffer (500 mM NaCl, 50 mM HEPES, 0.1% CHAPS, pH 7.4) supplemented with 0.5 mg/mL FLAG peptide (Lifetein). The column was stopped with parafilm for 3 min during the third addition of elution buffer. The first three elution fractions were pooled and dialyzed three times against 150 mM NaCl, 50 mM HEPES, 50 mM β-glycerophosphate, pH 7.4. Purified mTOR complex was quantified by comparison of mTOR, raptor, and rictor bands to BSA standards on Coomassie Blue-stained sodium dodecyl sulfate-polyacrylamide gel electrophoresis.

### 2.11.3 mTOR Complex Kinase Assay *in vitro*

A total of 250 ng of purified mTORC1 and 1 μg of substrate (either 4E-BP1 or S6K) were suspended in 25 μL of kinase buffer (50 mM NaCl, 0.1 mM EGTA, 1 mM DTT, 2 mM $MnCl_2$, 10 mM HEPES, 50 mM β-glycerophosphate, 0.5 μM microcystin LR, pH 7.4). The kinase reactions were initiated by adding 5 μL of 3 mM ATP in kinase buffer supplemented with 1,000 mCi/mmol [$\gamma$-$^{32}$P]-ATP (PerkinElmer Life Sciences). The final ATP concentration was 500 μM. Reactions were incubated with shaking for 30 min at 30 °C. Assays were quenched by addition of Laemmli buffer. The amount of $^{32}$P incorporation was determined by sodium dodecyl sulfate-polyacrylamide gel electrophoresis followed by phosphoimaging. For lipid treatments, lipids were extracted, solubilized in 100 μL kinase buffer with 0.1% Tween-20, and 2 μL was added to each reaction.

### 2.11.4 mTOR Complex Dissociation Assay *in vitro*

Anti-HA beads were prepared by conjugating 2 μg anti-HA mouse antibody to 15 μL Protein-G agarose beads by constant mixing at 4 °C for 2 h. Purified, fluorescently-tagged HA-Venus-mTOR and FLAG-Cerulean-Raptor (FLAG-Cerulean-Rictor for mTORC2) were immobilized by immunoprecipitation with prepared anti-HA beads. The amount of mTOR complex in each assay was between 0.9-1.1 μg. When treated with extracted lipids, the dried lipid residue was solubilized in dissociation buffer (1 mM EDTA, 1 mM EGTA, 1 mM DTT, 10 mM sodium phosphate, 50 mM β-glycerophosphate, 0.1% Tween-20, pH 7.4) supplemented with protease inhibitors. The solubilized lipids were then mixed with the mTOR complexes on beads for 30 min at room temperature. The beads were then washed three times, suspended in 100 μL dissociation buffer, and transferred to a 96-well plate. Fluorescent emissions were detected on a TECAN infinite M200. Venus excitation and emission wavelengths are 495 and 528 nm, respectively, Cerulean excitation and emission wavelengths are 433 and 475 nm, respectively. For a positive control of mTOR complex dissociation, 1% Triton X-100 was included instead of 0.1% Tween-20. The presence of complex proteins was confirmed at the end of the assay by immunoblotting.

## 2.12 Pressure Overload-Induced Heart Failure Model

To cause pressure-overload induced heart failure in WT and iCMp38KO mice, we used angiotensin II (AngII) as a potent vasoconstrictor, leading to hypertension and increased cardiac workload. Osmotic mini-pumps (Alzet) were used to allow continuous AngII infusion. Pumps were filled 12-16 h before use with AngII (Sigma-Aldrich) or PBS according to manufacturer's recommendation and stored overnight at 37 °C in PBS.

Before implantation, mice were initially anesthetized with 3-4% isoflurane and, during the course of the procedure, were continuously delivered 1-3% isoflurane. An incision was made subcutaneously on the back for insertion of the osmotic mini-pump and sutured after implantation. After 4-6 h, pumps reached a constant infusion rate of 1.5 mg/kg/day AngII. For lipolysis inhibition studies, atglistatin was administered in the food at a dose of 0.4 mg/g food. To prepare atglistatin supplemented food, normal chow was crushed using a mortar and pestle, weighed, and mixed with the appropriate amount of atglistatin. The powdered mixture was then formed into a pellet using water and allowed to dry overnight. Atglistatin administration was started two days prior to osmotic mini-pump implantation and continued for two more days. Mice were fasted 4 h prior to blood collection and tissues being harvested.

## 2.13 Regioisomer-Independent Analysis of OxFA by HPLC-Electrospray (ESI)-MS/MS

### 2.13.1 ESI-MS/MS Conditions

Analysis was performed on an AB Sciex 4000 QTRAP hybrid triple quadrupole-linear ion trap mass spectrometer with a Turbo V source with positive-ion ionization. Instrument operation and data acquisition/analysis were performed using AB Sciex 1.6.3 Analyst software. General source parameters were set as follows: ion spray voltage (IS) to 5.5 kV, interface temperature (TEM) to 180 °C, curtain gas (CUR) to 30 psi, collision activated dissociation gas (CAD, nitrogen) to 4 psi, nebulizer gas (GS1) to 25 psi, and auxiliary gas (GS2) to 10 psi. Species-dependent MS/MS parameters, including declustering potential, CE, and collision exit potential, were optimized using direct infusion-MS/MS analysis of purchased standards.

Direct infusion-MS/MS analysis was performed on dilutions of 10 μM for individual standards or 100 μM for oxFA mixtures prepared in methanol supplemented with 200 μM sodium acetate. Standards for LA; AA; C17:0; ±13-hydroperoxy-9Z,11E-octadecadienoic acid (HPODE); ±13-hydroxy-9Z,11E-octadecadienoic acid (HODE); 9-oxo-10E,12Z-octadecadienoic acid (KODE); ±12-hydroperoxy-5Z,8Z,10E,14Z-eicosatetraenoic acid (HPETE); ±5-hydroxy-6E,8Z,11Z,14Z-eicosatetraenoic acid (HETE); and 5-oxo-6E,8Z,11Z,14Z-eicosatetraenoic acid (KETE) were purchased from Cayman Chemical (Ann Arbor, MI).Samples were continuously infused with a syringe pump at a rate of 20 μL/min. Optimized MS/MS conditions for improved detection were determined using the Compound Optimization tool in the Analyst software as well as confirmation of detection and fragmentation in manual tuning mode at a range of declustering potential and CE. All mass spectra were recorded over a mass-to-charge ratio (m/z) range of 50–500 in multi-channel analysis mode under optimized conditions. Full-scan mass spectra depict 238 cumulative scans of 0.5 s. Product ion scans depict 79 cumulative scans of 1.5 s.

For oxFA quantitation, HPLC-MS/MS analysis in multiple reaction monitoring mode was utilized. Using the DiffE QIM approach of species identification, two pseudo-molecular multiple reaction monitoring transitions, where both the parent ion and product ion mass were set to the molecular ion adduct, were monitored for each analyte: the quantitative transition had a low CE and the qualitative transition had a high CE yielding approximately 50% intensity (108). Species identification was performed by comparing the ratio of the quantitative and qualitative transitions under the specified conditions. The qualifier ion ratio (QIR) must be in the range of 75-125% of the pure reference standard

when the qualitative transition has an intensity of 20-50% of the quantitative transition. Further deviation indicates the likely presence of a confounding coeluting species (108–114). Quantification was achieved by comparison to five-point calibration curves ranging from 0.1 to 1000 pmol/injection. For each species, the lower limit of quantification (LOQ) was determined to be the concentration at which the lower intensity, qualitative transition has a signal-to-noise ratio of greater than 3:1. Because this method relies on DiffE QIM, the limit of detection and LOQ are the same, as the oxFA cannot be identified without the qualitative transition.

### 2.13.2 HPLC Conditions

A Shimadzu LC-20AD HPLC system was used in combination with a DGU-20A3 degasser, SIL-20ACHT autosampler, and a CTO-20A column oven. The autosampler was maintained at 4 °C and set to an injection volume of 10 μL. Analysis was performed with a Supelco Discovery C18 column (5 μm, 2.1 x 50 mm) in combination with a Supelguard Discovery C18 guard column (5 μm, 2.1 x 20 mm). Selective elution was achieved with a gradient of Solvent A (80:20 water:methanol) and Solvent B (methanol containing 200 μM sodium acetate) with an overall flow rate of 300 μL/min. The column was first equilibrated for 5 min with 100% Solvent A. After that, Solvent B was increased linearly to 100% over 4 min before being held constant for 4 min. Solvent A was then increased to 100% over 1 min and held constant for 3 min to rinse residual salt from the HPLC-MS/MS setup. Retention time variation was calculated for each oxFA species by comparing the retention times on five separate days. The HPLC was connected to a Sciex 4000 QTRAP operated using the settings indicated previously.

An alternate, compatible HPLC method for a shorter runtime utilizing the same column and HPLC setup is as follows. The column was first equilibrated for 2 min with 100% Solvent A. After that, Solvent B was increased linearly to 100% over 1 min before being held constant for 4 min. Solvent A was then increased to 100% over 1 min and held constant for 3 min to rinse residual salt. An alternate, compatible HPLC method for increased separation utilized the same HPLC setup but with a Thermo Fisher Acclaim 120 C18 column (5 μm, 4.6 x 100 mm). In this method, the column was first equilibrated for 2 min with 100% Solvent A. After that, Solvent B was increased linearly to 100% over 1 min before being held constant for 12 min. Solvent A was then increased to 100% over 1 min and held constant for 5 min to rinse residual salt.

### 2.13.3 Validation Procedure

For determination of method precision, five concentrations (0.1 to 1000 pmol/injection) of each oxFA standard were used. For intra-assay precision, the samples were measured three times each on the same day. For interassay precision, the samples were measured on five separate days. Precision values are expressed as the percent value of the standard deviation compared to the mean value. Accuracy was determined by measuring three different, known concentrations of oxFA standard five times. Accuracy values are expressed as the percent value of the calculated concentration compared to the known concentration.

## 2.14 Serum Collection for OxFA Measurement

For basal oxFA measurement, 6-month-old C57BL/6J mice (both male and female) were fasted for 2 h in the morning (fed state) while maintaining free access to water. In order to collect blood, mice were sacrificed by cervical dislocation under

isoflurane anesthesia and a cardiac puncture performed. For measurement of oxFA after lipolysis-stimulation, 12-week-old WT mice were fasted 4 h and i.p. injected with either with vehicle or 5 mg/kg CL316,243. After 15 min, blood was collected from the tail vein. For measurement of basal circulating levels of oxFA in obesity, WT mice were fed chow or HFD for 12 weeks. Mice were fasted 4 h and then blood was collected from the tail vein. Blood was kept on ice for 20 min to allow for coagulation. The clot was pelleted by centrifugation (1,500 x g, 10 min, 4 °C). The supernatant serum was removed into clean tubes for immediate storage at -80 °C.

## 2.15 Western Blot and Quantitative Analysis

### 2.15.1 Tissue Western Blots

Tissues were homogenized in lysis buffer containing 1 mM EDTA, 1 mM EGTA, 1 mM DTT, 0.1% Tween-20, 10 mM sodium phosphate, and 50 mM β-glycerophosphate, pH 7.4 supplemented with protease inhibitors. Samples were centrifuged at 16,000 x g for 10 min. Protein concentrations were measured using bicinchoninic acid (BCA) (Pierce). Samples were then boiled in Laemmli buffer, separated by sodium dodecyl sulfate-polyacrylamide gel electrophoresis, and transferred to polyvinylidene fluoride (PVDF) membrane. Immunoblotting was performed with antibodies to Akt, $pAkt^{S473}$, ATGL, β-actin, and β-tubulin (Cell Signaling Technology).

### 2.15.2 Cell Lysate Western Blots

Cells were rinsed with chilled PBS and homogenized using a syringe with a 20-gauge needle in buffer containing 1 mM EDTA, 1 mM EGTA, 1 mM DTT, 0.1% Tween 20, 10 mM $Na_3PO_4$, 50 mM β-glycerophosphate, pH 7.4 supplemented with 1 mM phenylmethylsulfonyl fluoride, 10 μg/mL leupeptin, 10 μg/mL aprotinin, 10 μg/mL

pepstatin, and 0.5 μM microcystin LR. Homogenates were centrifuged at 16,000 x g for 10 min. Supernatant lysates were then boiled in Laemmli buffer, separated by sodium dodecyl sulfate-polyacrylamide gel electrophoresis, and transferred to polyvinylidene fluoride (PVDF) membrane. Immunoblotting was performed with antibodies to p4E-BP1$^{T37/47}$, Akt, pAkt$^{S473}$, pAkt$^{T308}$, pAS160$^{S588}$, pHSL$^{S563}$, IR, pIR$^{Y1150/1151}$, mTOR, pPKA substrate, raptor, rictor, and pS6K$^{T389}$ (Cell Signaling Technology).

### 2.15.3 Cellular Media Western Blots

Media samples were collected in tubes and centrifuged at 2,500 x g for 10 min. Laemmli buffer was added to media supernatant, separated by sodium dodecyl sulfate-polyacrylamide gel electrophoresis, and transferred to polyvinylidene fluoride (PVDF) membrane. Immunoblotting was performed with an antibody to resistin (Cell Signaling Technology).

### 2.15.4 Quantitative Analysis

Alkaline phosphatase conjugated chemiluminescence was used to image blots (Fujifilm LAS-4000). Blots were quantified by densitometry using ImageJ software. Bands corresponding to protein were quantified by subtracting background exposure. Phosphorylated protein values were divided by total protein levels to account for differences in loading. Normalization for tissue blots was carried out in GraphPad Prism software by setting the largest relative value in each immunoblot to 100 and all other values adjusted accordingly. Normalization for cell lysate blots was carried out in GraphPad Prism software by setting vehicle-treated or WT cells in each immunoblot to 1 and all other values adjusted accordingly.

## ATTRIBUTION

Portions of this chapter were sampled from: Ahern KW, Serbulea V, Wingrove CL, Palas, ZT, Leitinger N, Harris TE. Regioisomer-independent quantification of fatty acid oxidation products by HPLC-ESI-MS/MS analysis of sodium adducts. *Scientific Reports*. 2019 July 22.; Mullins GR, Wang L, Raje V, Sherwood SG, Grande RC, Boroda S, Eaton JM, Blancquaert S, Roger PP, Leitinger N, Harris TE. Catecholamine-induced lipolysis causes mTOR complex dissociation and inhibits glucose uptake in adipocytes. *PNAS*. 2014 December 9.; Raje V, Ahern KW, Howell NL, Martinez BA, Oenarto V, Granade ME, Kim JW, Tundup S, Bottermann K, Gödecke A, Keller SR, Kadl A, Bland ML, Harris TE. Adipocyte lipolysis drives acute stress-induced insulin resistance and hyperglycemia. *Scientific Reports*. 2020 November 1.; and Serbulea V, Upchurch CM, Ahern KW, Bories G, Voigt P, DeWeese DE, Meher AK, Harris TE, Leitinger N. Macrophages sensing oxidized DAMPs reprogram their metabolism to support redox homeostasis and inflammation through a TLR2-Syk-ceramide dependent mechanism. *Mol Metab*. 2017 November 7.

# 3 CHAPTER 3: ADIPOCYTE LIPOLYSIS DRIVES ADRENERGIC STRESS-INDUCED INSULIN RESISTANCE AND mTOR COMPLEX DISSOCIATION

## 3.1 ABSTRACT

Acute hyperglycemia and systemic insulin resistance often develop after injury or surgery. This stress response leads to increased post-operative complications and mortality. However, the underlying mechanisms driving insulin resistance are unknown. It is, however, known that surgical animal models rapidly develop adipose insulin resistance. Impaired insulin action in adipose alone can result in whole body insulin resistance and hyperglycemia. Therefore, we investigated the contributions of adipocyte lipolysis to the metabolic response to acute stress. Both surgical injury with HS and epinephrine infusion profoundly stimulated adipocyte lipolysis and simultaneously induced insulin resistance and hyperglycemia. When lipolysis was inhibited, the stress-induced insulin resistance and hyperglycemia were largely abolished, demonstrating an essential requirement for adipocyte lipolysis. Interestingly, circulating NEFA levels did not increase with lipolysis or correlate with insulin resistance during acute stress. Instead, we show that impaired insulin sensitivity correlated with circulating levels of the adipokine resistin in a lipolysis-dependent manner. To further define the mechanism by which catecholamines impair insulin signaling in adipocytes, we modeled adrenergic-stress *in vitro*. We demonstrate that β-adrenergic-mediated lipolysis blunts glucose uptake by inhibiting mTOR complex activity. Furthermore, we show that products of lipolysis inhibit the mTOR complexes through complex dissociation. Defining the

mechanism by which catecholamine-stimulated lipolysis attenuates insulin signaling may provide novel therapeutic targets for improved post-operative glucose homeostasis.

## 3.2 INTRODUCTION

Severe trauma, such as severe illness and surgery, activates an acute stress response which results in systemic insulin resistance and hyperglycemia, even in patients without prior history of diabetes (1–4, 115). Of concern, hyperglycemia has been shown to be an independent risk factor for increased mortality and morbidity after major surgery (2–4, 116). As a result, the maintenance of euglycemia is a major therapeutic target in the ICU after injury or critical illness (5–7). However, intensive insulin therapy is only effective in some patients and requires careful monitoring and individualization, as it increases hypoglycemic incidents which often negate the positive effects of tight glucose control (1, 117, 118). Furthermore, this treatment does not correct the underlying insulin resistance, the mechanism of which remains unknown. Our research into the pathophysiology of acute insulin resistance in critical illness diabetes will set the stage for the development of a more targeted approach to maintaining glucose homeostasis in patients.

The acute stress response is characterized by inhibition of anabolic signaling and activation of catabolic signaling to provide substrates for tissue healing (47). Insulin is a key anabolic hormone, and its signaling is potently inhibited during acute stress (47). Insulin resistance is the inability of insulin to adequately stimulate glucose uptake or inhibit gluconeogenesis in the liver (1). The mechanism by which insulin resistance develops in chronic or acute conditions in various tissues is still largely unknown (1). Integral steps in the insulin signaling pathway are the mTOR complexes. The mTOR

complexes are serine/threonine kinases that function as key regulators of cell growth and metabolism. mTOR is found in two unique protein complexes: mTORC1, in which mTOR interacts with raptor and PRAS40; and mTORC2, in which it interacts with rictor and mSin (49). Association of mTOR with raptor or rictor is required for mTORC1 and mTORC2 kinase activity, respectively (50, 119, 120). Both mTOR complexes phosphorylate and activate downstream steps of the insulin signaling pathway, including the mTORC1 substrates S6K1 and 4E-BP1 and the mTORC2 substrate Akt (50). Of note, inhibition of these complexes has been strongly associated with the onset of insulin resistance. In support of this, our laboratory showed that adipose-specific loss of rictor not only inhibited insulin signaling in adipose tissue, but also led to whole-body insulin resistance and glucose intolerance (50). However, the mechanism by which adipose-specific loss of insulin signaling contributes to the development of peripheral insulin resistance is still unknown.

In addition to inhibiting insulin signaling, acute stress induces a sympathetic nervous system response and the rapid release of catecholamines, which are major catabolic hormones (1). Catecholamines, such as epinephrine, activate adrenergic receptors which lead to the breakdown of glycogen, production of glucose, and the induction of lipolysis (1, 47, 51, 52). Lipolysis is the breakdown of stored fats in the form of TAG from lipid droplets. The first and rate-limiting step of this process, the hydrolysis of a TAG to produce DAG, is catalyzed by ATGL (53). Mice lacking ATGL, such as our fat-specific knockout (FATA) mice, exhibit drastic reductions in their ability to begin the breakdown of TAGs and undergo lipolysis (54). The final products of the breakdown of TAGs are glycerol and NEFA. Glycerol serves as a gluconeogenic substrate for the liver,

and its increased abundance could contribute to hyperglycemia during critical illness diabetes (121–124). NEFA can undergo beta-oxidation to serve as a source of energy, be used as precursors for other lipids, or act as signaling molecules (51, 52, 125).

In this study, we investigated the role of adipocyte lipolysis in the development of acute stress-induced hyperglycemia and insulin resistance *in vivo* using a mouse model of surgical injury and HS. We quantified the effect of adipocyte lipolysis on insulin sensitivity using hyperinsulinemic-euglycemic clamps. Our findings show that adipocyte lipolysis is necessary for the development of acute stress-induced hyperglycemia and insulin resistance. In addition, adipose tissue releases the adipokine resistin, which has been strongly linked to the development of chronic insulin resistance, in a stress- and lipolysis-dependent manner. We further investigated *in vitro* the molecular mechanism by which lipolysis affects insulin signaling in adipocytes. We specifically investigated the effect of lipolysis on the critical mTOR complexes. We found that products of lipolysis themselves are capable of causing mTOR complex inhibition through dissociation of the complex, leading to the development of insulin resistance. Taken together, our data suggest adipocyte lipolysis may be a possible therapeutic target for reducing the maladaptive metabolic effects of the acute stress response.

## 3.3 RESULTS

### 3.3.1 Inhibition of Adipocyte Lipolysis Prevents Acute Adrenergic Stress-Induced Metabolic Derangements

Rodent models of surgical injury and hemorrhage develop severe adrenergic stress leading to acute metabolic derangements, including hyperglycemia and peripheral insulin resistance (115, 126–128). We robustly induced stress-dependent metabolic changes by

subjecting mice to surgical soft-tissue injury alone (sham) or with HS. To investigate the role of lipolysis in the development of these changes, we used atglistatin to specifically inhibit ATGL (129). In vehicle-treated mice, HS induced profound hyperglycemia compared to sham **(Figure 3-1A)**. This development was accompanied by the induction of lipolysis, as shown by an increase in the level of circulating glycerol **(Figure 3-1B)**. Mice treated with atglistatin exhibited inhibited lipolysis and were protected from the development of hyperglycemia **(Figure 3-1A, B)**. Notably, the increase in glycerol observed with HS in vehicle-treated mice was not accompanied by an increase in circulating NEFA levels **(Figure 3-1C)**. This disconnect between circulating glycerol and NEFA levels observed during HS has previously been ascribed to vasoconstriction in WAT. Glycerol is miscible in aqueous solution and can freely diffuse from adipose depots into systemic circulation through the interstitial fluid (130). However, NEFA are hydrophobic and require carrier proteins, such as albumin, for transport in aqueous solution. Vasoconstriction reduces the availability of these necessary carrier proteins within adipose depots, thus preventing NEFA transport (131–135). Hemorrhage also leads to elevated lactate levels and tissue acidification, thereby promoting increased fatty acid re-esterification within the adipose depot (136). In addition to the development of hyperglycemia and similar to previous reports, HS impaired insulin-induced $Akt^{S473}$ phosphorylation in peripheral tissues of vehicle-treated mice, including WAT, liver, and skeletal muscle (SKM) **(Figure 3-1D-F)** (126, 137, 138). Atglistatin-treated mice were protected from HS-induced disruptions in peripheral insulin signaling **(Figure 3-1D-F)**.

While atglistatin is a potent inhibitor of rodent ATGL, it has been found to be ineffective against the human isoform (139). Therefore, we chose to validate our results

with GS-9667, an A1-adenosine receptor partial agonist which blocks lipolysis by inhibiting cAMP production and has been shown to be effective in reducing circulating NEFA levels in human patients (140, 141). Similar to our findings with atglistatin, GS-9667 treatment protected mice from the development of HS-induced hyperglycemia and disruptions in peripheral insulin signaling **(Figure 3-1A-F)**.

To identify adipocytes as the necessary site of lipolysis, we genetically deleted *Pnpla2* specifically from adipocytes in mice ($FATA^{-/-}$) to create loss of ATGL within adipocytes. Successful adipose tissue-specific loss of ATGL was demonstrated by immunoblot **(Figure 3-2A)**. The functional consequences of this deletion were confirmed by subjecting mice to i.p. injection of epinephrine and measuring the release of lipolytic products. Both serum glycerol and NEFA were observed to increase in $WT^{fl/fl}$ mice, but this increase was prevented by genetic deletion of adipocyte ATGL in $FATA^{-/-}$ mice **(Figure 3-2B, C)**. To examine the role of adipocyte ATGL action in the context of acute stress, we subjected $FATA^{-/-}$ mice to HS. Similar to pharmacological inhibition, loss of ATGL in adipocytes alone lowered blood glucose levels **(Figure 3-2D)**. Hyperglycemia in $WT^{fl/fl}$ mice was again accompanied by elevations in circulating glycerol with no corresponding increase in systemic NEFA levels **(Figure 3-2E, F)**. As expected, HS disrupted peripheral insulin response in $WT^{fl/fl}$ mice **(Figure 3-2G-I)**. Interestingly, $FATA^{-/-}$ mice were largely protected from stress-induced insulin signaling disturbances not only in WAT, but also in liver and SKM **(Figure 3-2G-I)**. These studies suggest that stress-induced metabolic derangements such as hyperglycemia and defects in peripheral insulin signaling are dependent on adipocyte lipolysis but occur without apparent increases in circulating NEFA.

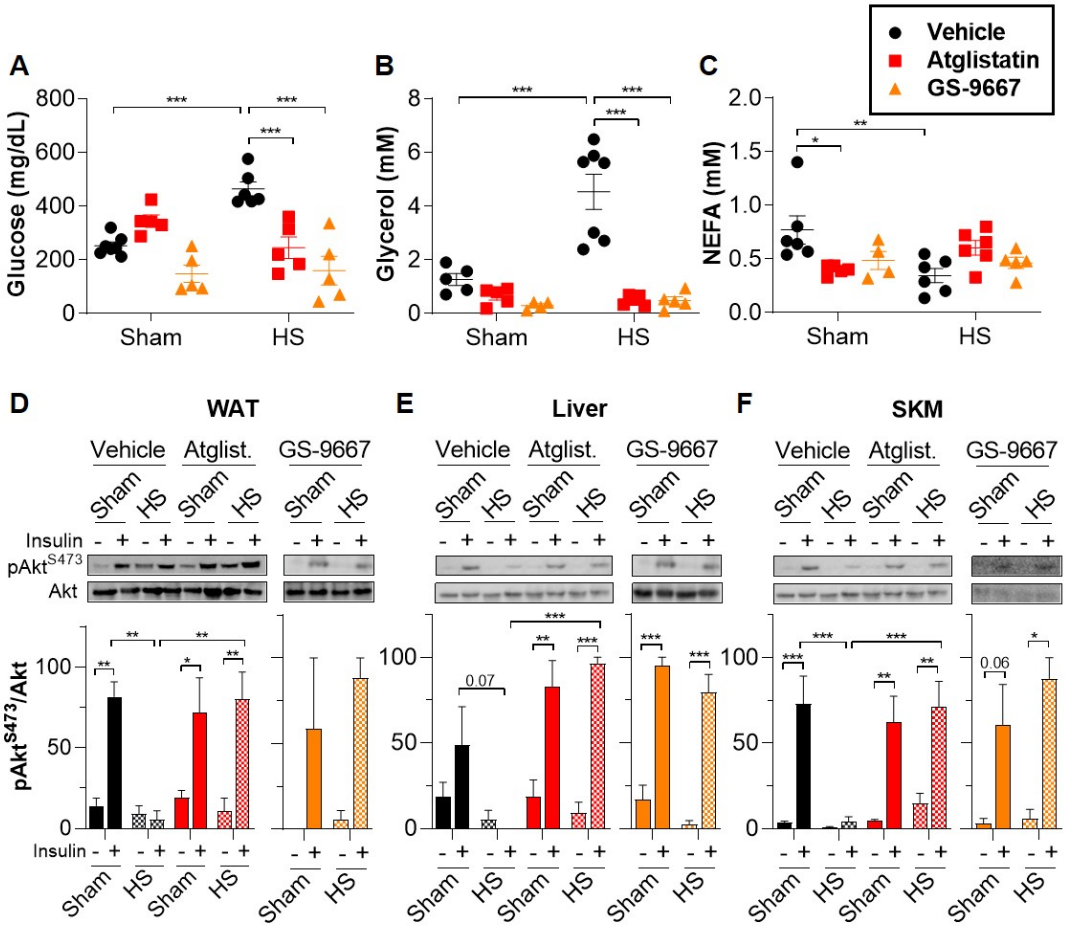


**Figure 3-1: Acute inhibition of lipolysis improves metabolic impairments in HS**

**Figure 3-1 Legend**

**A.** Blood glucose levels from WT mice fasted 4 h and pretreated either with vehicle, 1 mg/kg atglistatin, or 5 mg/kg GS-9667 before being subjected to sham or HS. After 30 min of sham or HS, the mice were injected with saline or 0.5 U insulin in the inferior vena cava, and tissues were harvested after 4 min.

**B.** Glycerol levels in serum from WT mice treated as in A.

**C.** NEFA levels in serum from WT mice treated as in A.

**D.** Representative immunoblots and quantitation for white adipose tissue (WAT, epididymal) from WT mice treated as in A.

**E.** Representative immunoblots and quantitation for liver from WT mice treated as in A.

**F.** Representative immunoblots and quantitation for skeletal muscle (SKM, gastrocnemius) from WT mice treated as in A.

$N$ = 2-7. Data are shown as mean ± standard error of mean (SEM). *$P$ < 0.05, **$P$ < 0.01, and ***$P$ < 0.001, as indicated. For A-C, statistical analyses were performed using two-way analysis of variance (ANOVA). For D-F, image quantitations were normalized by setting largest value in each immunoblot to 100. Statistical analyses on relative values for vehicle and atglistatin were performed using three-way ANOVA. Statistical analyses of GS-9667 relative values were performed using two-way ANOVA. All comparisons differing by one variable were made and adjusted for with ANOVA, and all significant comparisons are denoted as such.

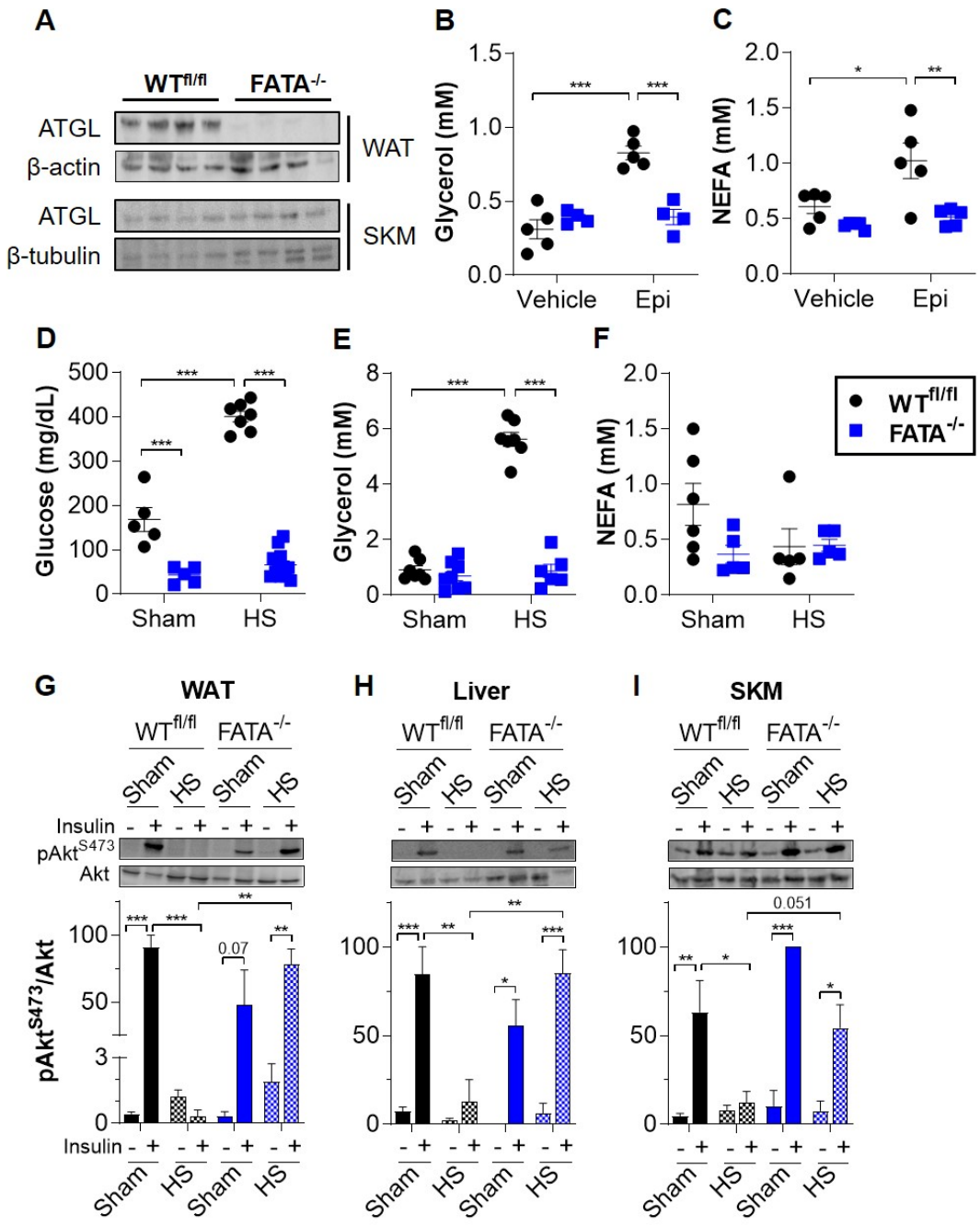


**Figure 3-2: Genetic deletion of adipocyte *Atgl* improves metabolic impairments in HS**

**Figure 3-2 Legend**

**A.** Representative immunoblots for white adipose tissue (WAT, epididymal) and skeletal muscle (SKM, gastrocnemius) of $WT^{fl/fl}$ and $FATA^{-/-}$ mice demonstrating adipocyte-specific ATGL knockout.

**B.** Glycerol level in serum from $WT^{fl/fl}$ and $FATA^{-/-}$ mice fasted 4 h, injected i.p. with 2 mg/kg epinephrine and had serum collected from the tail vein after 30 min.

**C.** NEFA levels in serum from $WT^{fl/fl}$ and $FATA^{-/-}$ mice treated as in B.

**D.** Blood glucose levels from $WT^{fl/fl}$ and $FATA^{-/-}$ mice fasted 4 h before being subjected to sham or HS. After 30 min of sham or HS, the mice were injected with saline or 0.5 U insulin in the inferior vena cava, and tissues were harvested after 4 min.

**E.** Glycerol levels in serum from $WT^{fl/fl}$ and $FATA^{-/-}$ mice treated as in D.

**F.** NEFA levels in serum from $WT^{fl/fl}$ and $FATA^{-/-}$ mice treated as in D.

**G.** Representative immunoblots and quantitation for WAT (epididymal) from $WT^{fl/fl}$ and $FATA^{-/-}$ mice treated as in D.

**H.** Representative immunoblots and quantitation for liver from $WT^{fl/fl}$ and $FATA^{-/-}$ mice treated as in D.

**I.** Representative immunoblots and quantitation for SKM (gastrocnemius) from $WT^{fl/fl}$ and $FATA^{-/-}$ mice treated as in D.

$N$ = 3-12. Data are shown as mean ± SEM. *$P < 0.05$, **$P < 0.01$, and ***$P < 0.001$, as indicated. For A-F, statistical analyses were performed using two-way ANOVA. For G-I, image quantitations were normalized by setting largest value in each immunoblot to 100. Statistical analyses on relative values were performed using three-way ANOVA. All comparisons differing by one variable were made and adjusted for with ANOVA, and all significant comparisons are denoted as such. Experiments in B and C were performed by Katelyn Ahern.

### 3.3.2 The Development of Catecholamine-Induced Insulin Resistance is Dependent on Adipocyte Lipolysis

While the degree of $pAkt^{S473}$ in our experiments suggests the development of peripheral insulin resistance, in agreement with previous results, we were interested in a more quantitative assessment of insulin sensitivity in peripheral tissues (126, 137, 138). To definitively investigate the role of stress-induced lipolysis on the development of insulin resistance *in vivo* under controlled conditions, we infused epinephrine in anesthetized vehicle- or GS-9667-treated mice during hyperinsulinemic-euglycemic clamp (106). Blood glucose levels were maintained at roughly 150 mg/dL for all groups during the steady-state period **(Figure 3-3A)**. As expected, epinephrine infusion induced lipolysis in vehicle-treated mice, as seen by an increase in circulating glycerol **(Figure 3-3B)**. Glycerol levels also increased in GS-9667-treated mice, but to a lesser extent, indicating an inhibited lipolytic response. Corroborating previously published results and our $pAkt^{S473}$ observations, vehicle-treated mice exhibited an epinephrine-dependent decline in glucose infusion rate (GIR), indicating the development of insulin resistance **(Figure 3-3C)** (121, 142). GS-9667-treated mice were protected from an epinephrine-dependent decline in GIR and the development of insulin resistance.

To confirm the critical role of adipocyte lipolysis in the development of peripheral insulin resistance, we performed hyperinsulinemic-euglycemic clamps on anesthetized $WT^{fl/fl}$ or $FATA^{-/-}$ mice. Again, blood glucose levels were maintained at roughly 150 mg/dL for all groups during the steady-state period **(Figure 3-3D)**. Epinephrine infusion induced lipolysis in $WT^{fl/fl}$ but not $FATA^{-/-}$ mice **(Figure 3-3E)**. Additionally, $WT^{fl/fl}$ mice exhibited an epinephrine-dependent decline in GIR, indicating the development of insulin resistance **(Figure 3-3F)**. Conversely, $FATA^{-/-}$ mice were not only protected from

epinephrine-dependent induction of peripheral insulin resistance, but actually became more insulin sensitive. These results further validate our finding that stress-induced peripheral insulin resistance is dependent on adipocyte lipolysis.

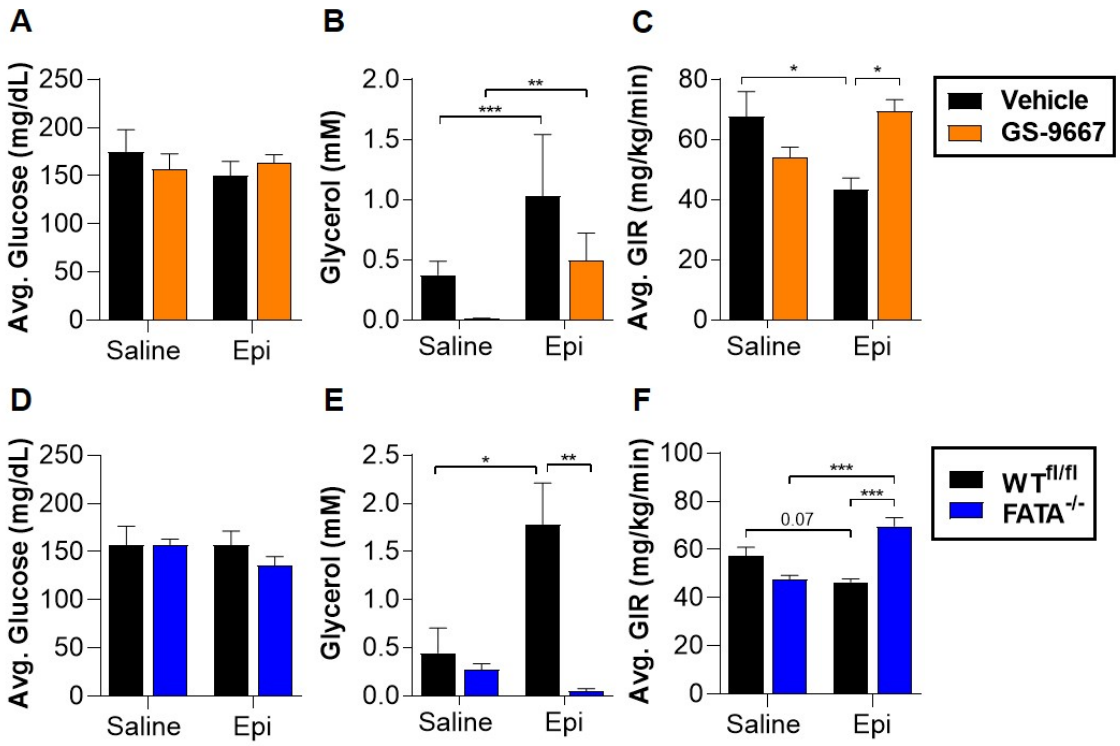


**Figure 3-3: Inhibition of lipolysis abolishes epinephrine-induced impairments in glucose uptake during hyperinsulinemic-euglycemic clamps**

**Figure 3-3 Legend**

- **A.** Average blood glucose during steady state of WT mice fasted 4 h and pretreated 30 min prior with vehicle or 5 mg/kg GS-9667. Mice were infused with either saline or epinephrine (Epi, 1 μg/kg/min) and subjected to a 30 min basal period (-30 to 0 min) followed by a hyperinsulinemic-euglycemic clamp (0-120 min). Steady state was the last 30 min of the clamp (90-120 min).
- **B.** Glycerol levels in serum from WT mice treated as in A.
- **C.** Average glucose infusion rates (GIR) during steady state from WT mice treated as A.
- **D.** Average blood glucose during steady state of $WT^{fl/fl}$ and $FATA^{-/-}$ mice fasted 4 h before being infused with either saline or Epi (1 μg/kg/min) and subjected to a 30 min basal period (-30 to 0 min) followed by a hyperinsulinemic-euglycemic clamp (0-120 min). Steady state was the last 30 min of the clamp (90-120 min).
- **E.** Glycerol levels in serum from $WT^{fl/fl}$ and $FATA^{-/-}$ mice treated as in D.
- **F.** Average GIR during steady state from $WT^{fl/fl}$ and $FATA^{-/-}$ mice treated as D.

  $N$ = 4-7. Data are shown as mean ± SEM. *$P < 0.05$, **$P < 0.01$, and ***$P < 0.001$, as indicated. Statistical analyses were performed using two-way ANOVA. All comparisons differing by one variable were made and adjusted for with ANOVA, and all significant comparisons are denoted as such.

### 3.3.3 Glycerol Produced by Adipocyte Lipolysis is Necessary for Acute Adrenergic Stress-Induced Hyperglycemia

Stress hormone action, particularly epinephrine, rapidly induces adipocyte lipolysis causing an increase in glycerol levels in systemic circulation. Glycerol can be utilized by the liver as a substrate for gluconeogenesis (143). As glycerol was observed to be elevated during HS in mice that developed hyperglycemia and peripheral insulin resistance, we next investigated the specific contribution of glycerol in the development of stress-induced metabolic disturbances. After lipolysis, glycerol enters circulation through aquaporin 7 (AQP7), the primary membrane channel responsible for glycerol release in adipocytes. Mice deficient for AQP7 (*Aqp7*$^{-/-}$) cannot release glycerol into circulation in response to adrenergic stimulation (101, 144). As expected, when we subjected *Aqp7*$^{-/-}$ mice to HS, we did not observe the increase in circulating glycerol seen in the WT mice **(Figure 3-4A)**. Furthermore, *Aqp7*$^{-/-}$ mice were protected from characteristic increase in blood glucose, demonstrating that glycerol is necessary for stress-induced hyperglycemia **(Figure 3-4B)**.

To determine if glycerol is sufficient to produce hyperglycemia during acute stress, we administered glycerol to vehicle- and atglistatin-treated mice to achieve similar systemic levels between groups **(Figure 3-4C)**. After glycerol injection, hyperglycemia was observed in both sham and HS conditions **(Figure 3-4D)**. Furthermore, atglistatin-treated mice were no longer protected from the development of hyperglycemia and exhibited increased blood glucose under both sham and HS conditions after glycerol administration **(Figure 3-4D)**. Of note, injection of glycerol did not affect the observed disruptions to Akt$^{S473}$ phosphorylation. Despite the presence of hyperglycemia in all groups, vehicle-treated mice only exhibited disturbances in insulin signaling after HS,

and atglistatin-treated mice were still protected from the development of insulin resistance **(Figure 3-4E)**. These studies show that glycerol is an important contributor to acute stress-induced hyperglycemia but does not account for the development of peripheral insulin resistance.

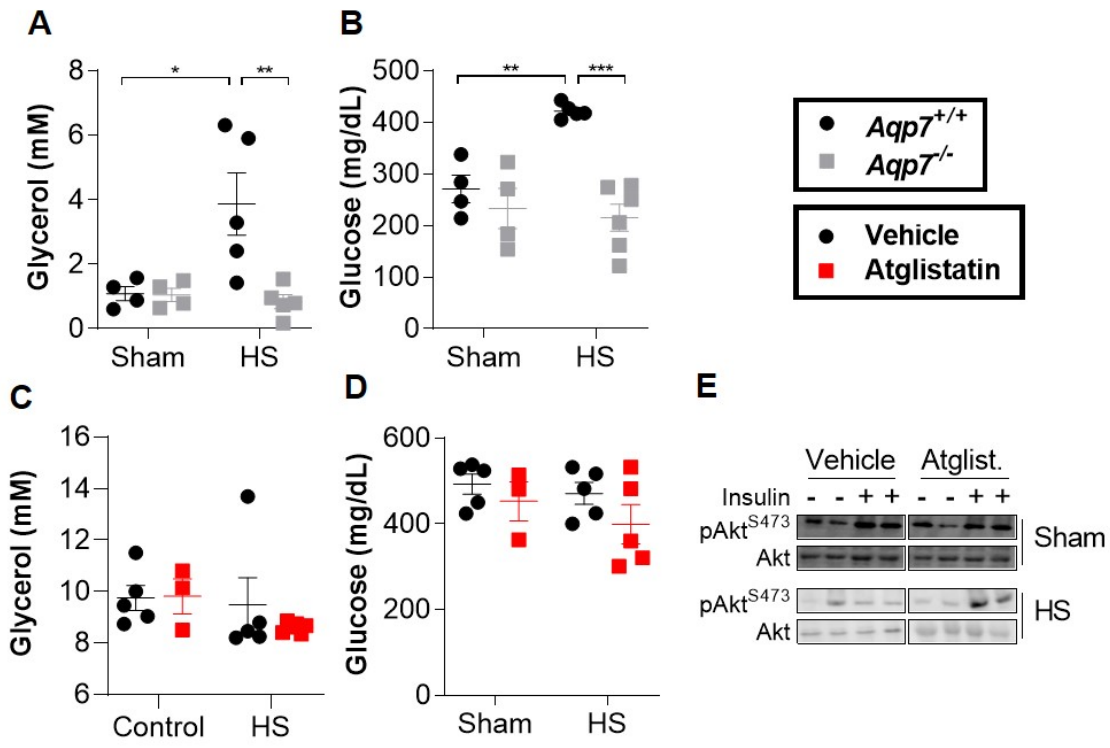


**Figure 3-4: Glycerol release contributes to hyperglycemia but not insulin resistance**

**Figure 3-4 Legend**

**A.** Glycerol levels in serum from WT and *Aqp7*$^{-/-}$ mice fasted 4 h then subjected to sham or HS for 30 min.

**B.** Blood glucose levels from WT and *Aqp7*$^{-/-}$ treated as in A.

**C.** Glycerol levels in serum from WT mice pretreated with vehicle or 1 mg/kg atglistatin and an i.p. bolus of glycerol (3 g/kg) then subjected to sham or HS. After 30 min of sham or HS, the mice were injected with saline or 0.5 U insulin in the inferior vena cava, and tissues were harvested after 4 min.

**D.** Blood glucose levels from WT mice treated as in C.

**E.** Representative immunoblots for white adipose tissue (epididymal) of WT mice treated as in C.

$N$ = 2-6. Data are shown as mean ± SEM. *$P$ < 0.05, **$P$ < 0.01, and ***$P$ < 0.001, as indicated. Statistical analyses were performed using two-way ANOVA. All comparisons differing by one variable were made and adjusted for with ANOVA, and all significant comparisons are denoted as such.

### 3.3.4 The Adipokine Resistin Correlates with Stress-Induced Insulin Resistance in a Lipolysis-Dependent Manner

In addition to storing and mobilizing TAG, adipose tissue has been increasingly appreciated for its role in endocrine signaling, such as through the release of adipokines (79). The ability of adipokines such as adiponectin and leptin to improve insulin sensitivity has been well-documented (145, 146). In both pharmacologic or genetic inhibition of lipolysis, adiponectin levels were found to be unaffected by HS or presence of lipolysis **(Figure 3-5A, E)**. Circulating levels of PAI-1 and leptin were found to be elevated or trend towards increased with HS, but independent of lipolysis inhibition **(Figure 3-5B, C, F, G)**. Resistin is a pro-inflammatory adipokine that has previously been shown to positively correlate with hyperglycemia and insulin resistance in obesity, and both peripheral and hypothalamic administrations of resistin impair insulin signaling (147, 148). Interestingly, resistin showed a robust induction with HS, which was attenuated with lipolysis inhibition **(Figure 3-5D, H)**. In addition, epinephrine infusion during hyperinsulinemic-euglycemic clamps increased circulating resistin levels with inhibition of lipolysis abrogating this response **(Figure 3-5I, J)**. Furthermore, circulating resistin levels were positively correlated with net lipolysis as shown by glycerol levels **(Figure 3-5K)**. Numerous clinical studies observed correlations between circulating resistin levels and the development of stress-induced metabolic dysfunction and morbidity, including in instances of hemorrhage (91–97). While not providing definitive mechanistic evidence, our data does corroborate a strong relationship between resistin and stress-induced insulin resistance and supports a lipolysis-mediated resistin release during acute stress.

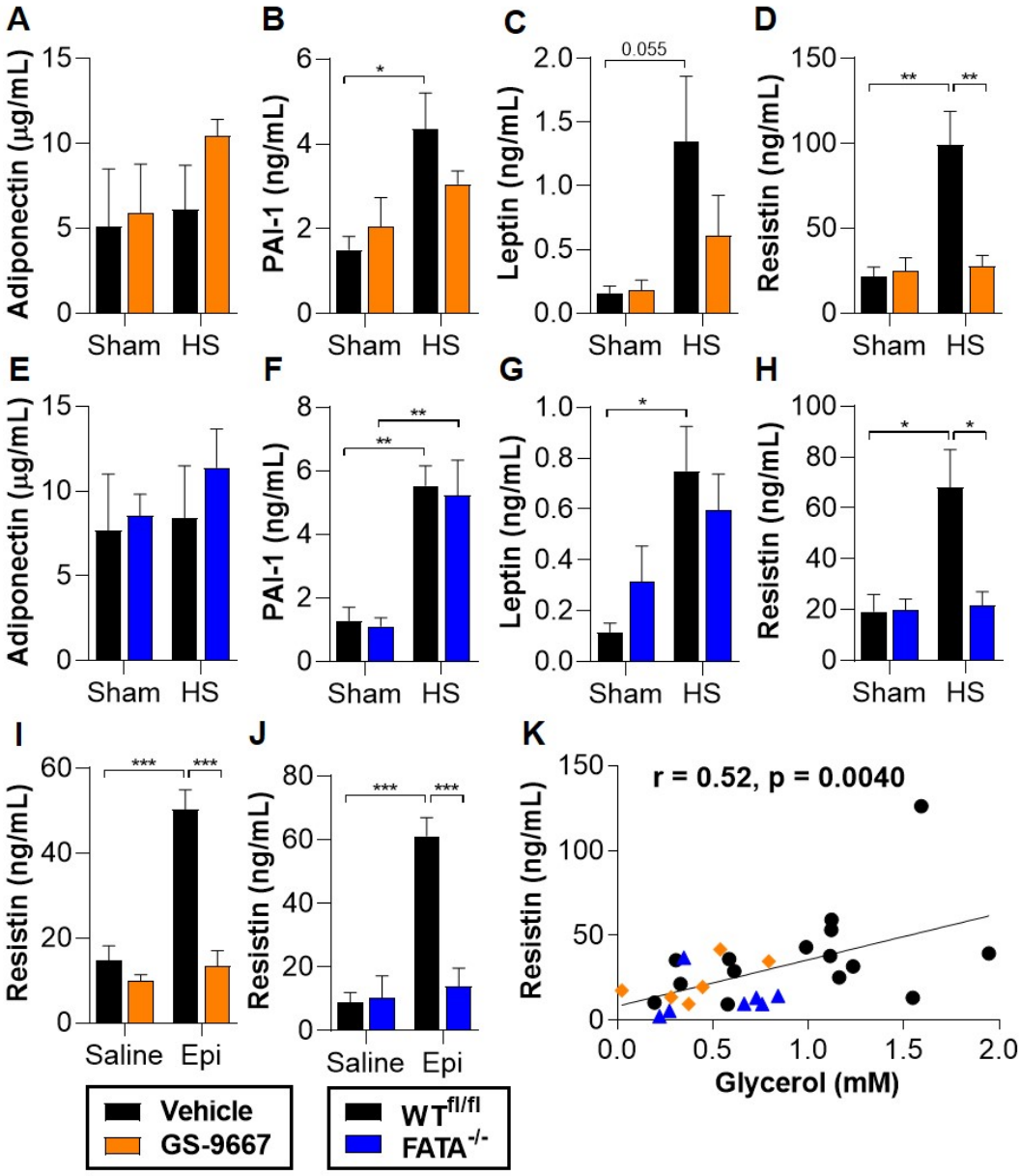


**Figure 3-5: Resistin levels correlate with lipolysis during adrenergic-stress**

**Figure 3-5 Legend**

**A.** Adiponectin levels determined by Luminex in serum from WT mice fasted 4 h and pretreated either with vehicle or 5 mg/kg GS-9667 before being subjected to sham or HS for 30 min.

**B.** PAI-1 levels determined by Luminex in serum from vehicle- or GS-9667-treated mice treated as in A.

**C.** Leptin levels determined by Luminex in serum from vehicle- or GS-9667-treated mice treated as in A.

**D.** Resistin levels determined by ELISA in serum from vehicle- or GS-9667-treated mice treated as in A.

**E.** Adiponectin levels determined by Luminex in serum from $WT^{fl/fl}$ and $FATA^{-/-}$ mice fasted 4 h before being subjected to sham or HS for 30 min.

**F.** PAI-1 levels determined by Luminex in serum from $WT^{fl/fl}$ and $FATA^{-/-}$ mice treated as in E.

**G.** Leptin levels determined by Luminex in serum from $WT^{fl/fl}$ and $FATA^{-/-}$ mice treated as in E.

**H.** Resistin levels determined by ELISA in serum from $WT^{fl/fl}$ and $FATA^{-/-}$ mice treated as in E.

**I.** Resistin levels determined by ELISA in serum during steady state of WT mice fasted 4 h and pretreated 30 min prior with vehicle or 5 mg/kg GS-9667. Mice were infused with either saline or epinephrine (Epi, 1 μg/kg/min) and subjected to a 30 min basal period (-30 to 0 min) followed by a hyperinsulinemic-euglycemic clamp (0-120 min). Steady state was the last 30 min of the clamp (90-120 min).

**J.** Resistin levels determined by ELISA in serum during steady state of $WT^{fl/fl}$ and $FATA^{-/-}$ mice fasted 4 h before being infused with either saline or Epi (1 μg/kg/min) and subjected to a 30 min basal period (-30 to 0 min) followed by a hyperinsulinemic-euglycemic clamp (0-120 min). Steady state was the last 30 min of the clamp (90-120 min).

**K.** Pearson correlation between circulating resistin and glycerol from mice subjected to sham or HS with and without genetic or pharmacological inhibition of lipolysis.

$N$ = 3-6. Data are shown as mean ± SEM. *$P < 0.05$, **$P < 0.01$, and ***$P < 0.001$, as indicated. Statistical analyses were performed using two-way ANOVA. All comparisons differing by one variable were made and adjusted for with ANOVA, and all significant comparisons are denoted as such.

### 3.3.5 The β-Adrenergic Pathway Impairs Insulin Signaling in Adipocytes by Inhibiting the mTOR Complexes

To investigate the molecular mechanism by which catecholamine-induced lipolysis disrupts insulin signaling within adipose tissue, we isolated primary adipocytes from WT and *Atgl*$^{-/-}$ mice for further *in vitro* studies. To ensure that adrenergic stress-induced metabolic disturbances that are observed *in vivo* could be replicated in our *in vitro* culture, we treated primary adipocytes with the catecholamine ISO, a β-adrenergic receptor agonist, and assessed glucose uptake. Both WT and *Atgl*$^{-/-}$ adipocytes increased glucose uptake in response to insulin **(Figure 3-6A)**. However, adipocytes from WT mice exhibited a blunted response to insulin stimulation when treated with ISO, which replicates the development of hyperglycemia and reduced GIR that we observed *in vivo*. *Atgl*$^{-/-}$ adipocytes were protected from the isoproterenol-mediated loss in insulin-stimulated glucose uptake, just as lipolysis inhibition protects mice from the development of hyperglycemia and reduced GIR *in vivo*. When we examined the effect of ISO treatment on the ability of insulin to cause Akt$^{S473}$ phosphorylation, we observed decreased pAkt$^{S473}$ with isoproterenol treatment in WT adipocytes **(Figure 3-6B, C)**. *Atgl*$^{-/-}$ adipocytes maintained insulin-stimulated pAkt$^{S473}$ levels even with ISO treatment, replicating our *in vivo* finding that lipolysis inhibition protects against catecholamine-induced loss in Akt$^{S473}$ phosphorylation **(Figure 3-6B, C)**. Taken together, these data validate our ability to replicate our *in vivo* findings in adipocytes *in vitro*, allowing us to probe the molecular mechanism behind lipolysis-mediated insulin resistance.

We had consistently observed decreased insulin-stimulated pAkt$^{S473}$ with HS *in vivo* or ISO *in vitro*, but had yet to investigate what other steps of the insulin signaling cascade might be disrupted **(Figure 3-7A)**. Therefore, we treated cultured 3T3-L1

adipocytes with FSK, a potent activator of downstream β-adrenergic signaling through adenylyl cyclase, and immunoblotted for various phosphorylation events in the insulin signaling cascade. While signaling upstream of the mTOR complexes was unaffected, such as insulin receptor and PDK1-mediated $Akt^{T308}$ phosphorylation, downstream signaling was observed to be inhibited **(Figure 3-7B)**. We found that FSK action significantly decreased levels of both $pAkt^{S473}$ and $pS6K^{T389}$, phosphorylation events that are performed by mTORC1 and mTORC2, respectively **(Figure 3-7B, C)**. To determine whether this observed inhibition of the mTOR complexes is dependent on lipolysis, we incubated cultured 3T3-L1 adipocytes with atglistatin or the general lipase inhibitor E600 and again treated with FSK and probed the levels of $pS6K^{T389}$ and $pAkt^{S473}$. As expected, we observed a decrease in insulin-stimulated $pS6K^{T389}$ and $pAkt^{S473}$ with FSK treatment, however, pretreatment with either atglistatin or E600 rescued mTOR complex-mediated phosphorylation **(Figure 3-7D, E)**. Taken together, these data demonstrate that β-adrenergic signaling inhibits the mTOR complexes in adipocytes in a lipolysis-dependent manner, which likely contributes to acute stress-induced insulin resistance.

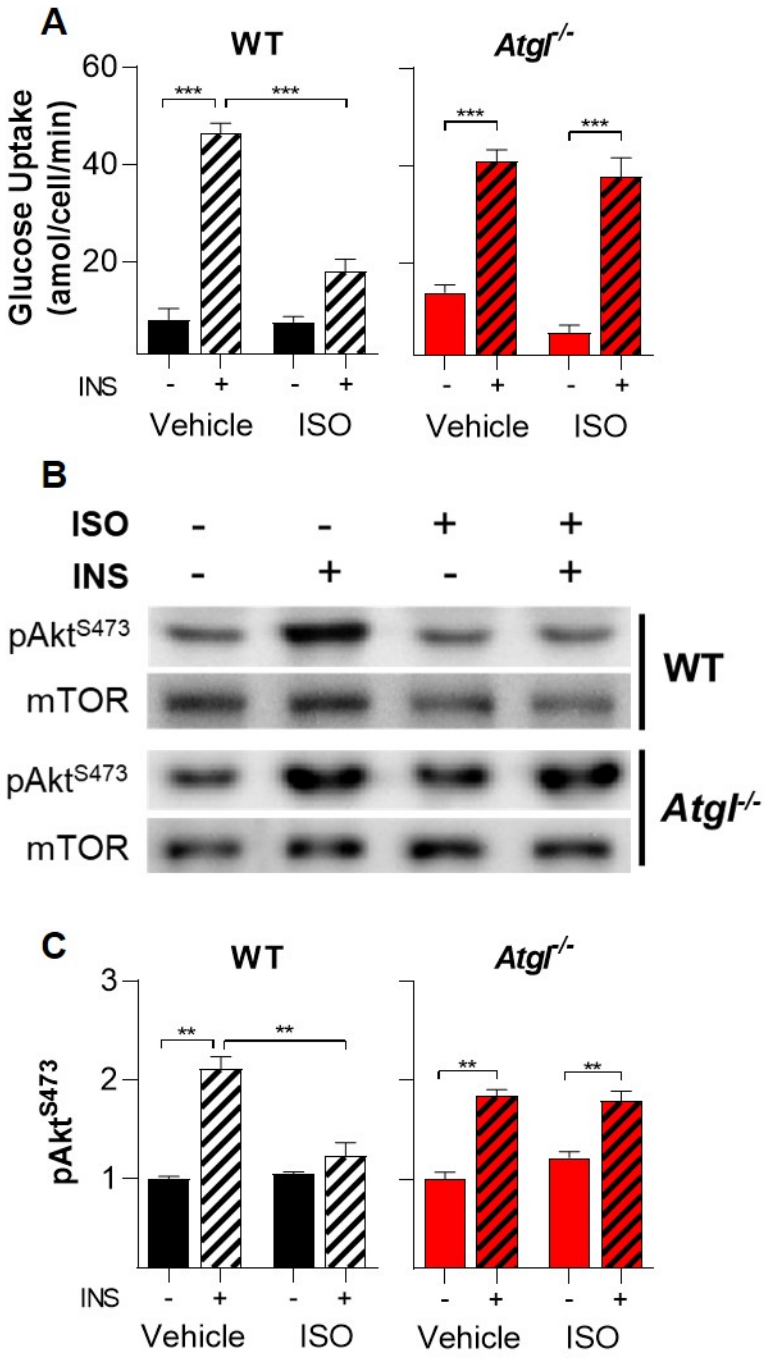


**Figure 3-6: Catecholamine-induced insulin resistance *in vitro* requires lipolysis**

**Figure 3-6 Legend**

**A.** Glucose uptake in WT and *Atgl*$^{-/-}$ primary mouse adipocytes. Isolated adipocytes were treated with or without 10 nM insulin (INS) in the presence or absence of 100 nM isoproterenol (ISO) for 30 min followed by 10 μM [U-$^{14}$C]-D-glucose for 20 min.

**B.** Representative immunoblots for WT and *Atgl*$^{-/-}$ primary mouse adipocytes treated with or without 10 nM INS in the presence or absence of 100 nM ISO for 30 min.

**C.** Quantitation of immunoblots for WT and *Atgl*$^{-/-}$ primary mouse adipocytes treated as in B.

$N = 3$. Data are shown as mean ± SEM. $^{**}P < 0.01$ and $^{***}P < 0.001$, as indicated. Statistical analyses were performed using two-way ANOVA. All comparisons differing by one variable were made and adjusted for with ANOVA, and all significant comparisons are denoted as such.

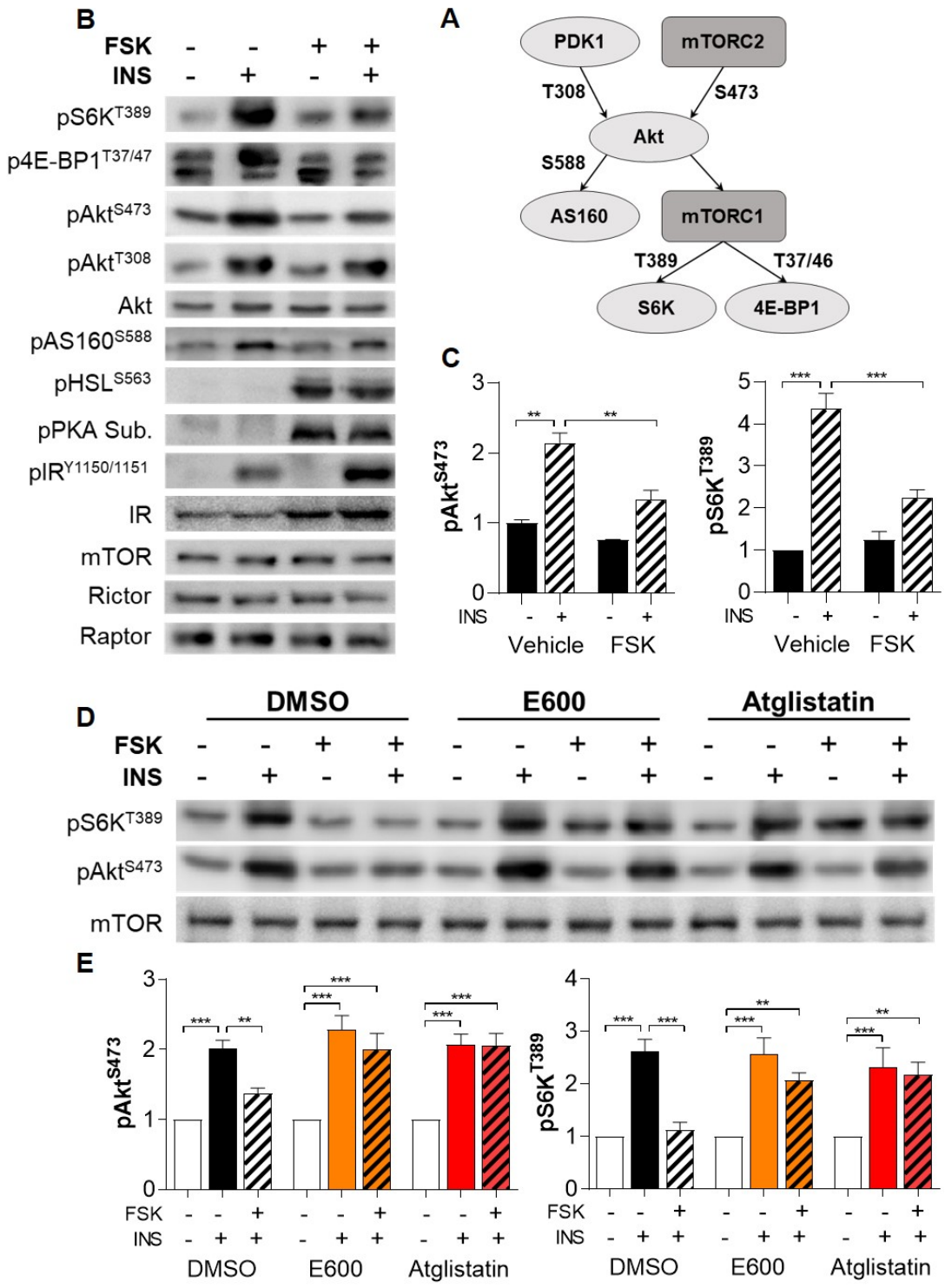


**Figure 3-7: β-adrenergic pathway-stimulated lipolysis disrupts insulin signaling by inhibiting the mTOR complexes**

**Figure 3-7 Legend**

**A.** Illustration of the roles of mTOR complexes in the insulin signaling pathway.

**B.** Representative immunoblots of insulin signaling for 3T3-L1 adipocytes incubated 30 min with or without 10 μM forskolin (FSK) before treatment with or without 10 nM insulin (INS) for 15 min.

**C.** Quantitation of immunoblots for mTOR complex mediated phosphorylation events in 3T3-L1 adipocytes treated as in B.

**D.** Representative immunoblots of 3T3-L1 adipocytes incubated with or without 150 μM E600 or 10 μM atglistatin before treatment with or without 10 μM FSK for 10 min then treatment with or without 10 nM INS for 15 min.

**E.** Quantitation of immunoblots for 3T3-L1 adipocytes treated as in D.

$N = 3$. Data are shown as mean ± SEM. $^{**}P < 0.01$ and $^{***}P < 0.001$, as indicated. Statistical analyses were performed using two-way ANOVA. All comparisons differing by one variable were made and adjusted for with ANOVA, and all significant comparisons are denoted as such.

### 3.3.6 Lipolytic Products Inhibit *in vitro* mTOR Complex Activity

Lipolysis of TAG produces multiple potential signaling molecules, including DAG, MAG, FA, and glycerol. To determine if one of these lipolytic products is responsible for the observed lipolysis-dependent inhibition, we assessed their ability to inhibit purified recombinant mTOR complex *in vitro*. We extracted lipids from WT and *Atgl*$^{-/-}$ primary adipocytes treated with or without ISO to stimulate lipolysis and included these lipids in mTOR kinase assays. We found that only lipids extracted from WT adipocytes undergoing catecholamine-induced lipolysis were capable of inhibiting *in vitro* mTOR complex activity **(Figure 3-8A)**. Lipids extracted from WT adipocytes that were not treated with ISO or lipids from *Atgl*$^{-/-}$ adipocytes did not affect mTOR complex activity **(Figure 3-8A)**. Notably, though lipids extracted from unstimulated WT cells did not affect mTOR complex activity, treatment of the extracted lipids with a lipase *in vitro* generated products capable of inhibiting the complexes **(Figure 3-8B)**. Furthermore, it was found that lipids isolated from lipolytic adipocytes inhibited mTOR complex activity in a dose-dependent manner **(Figure 3-8C)**. To investigate if a specific lipolytic product was responsible for inhibiting the mTOR complex, we included purified lipid standards of glycerolipids or fatty acids in our mTOR complex kinase assay. Interestingly, none of the lipids tested showed any significant effect on mTOR complex activity **(Figure 3-8D)**. Taken together, these data suggest that while lipolytic products are capable of inhibiting mTOR complex activity, it may be a particular specialized lipid released from lipolysis, such as an oxFA, that is acting as the inhibitor and not lipolytic products in general.

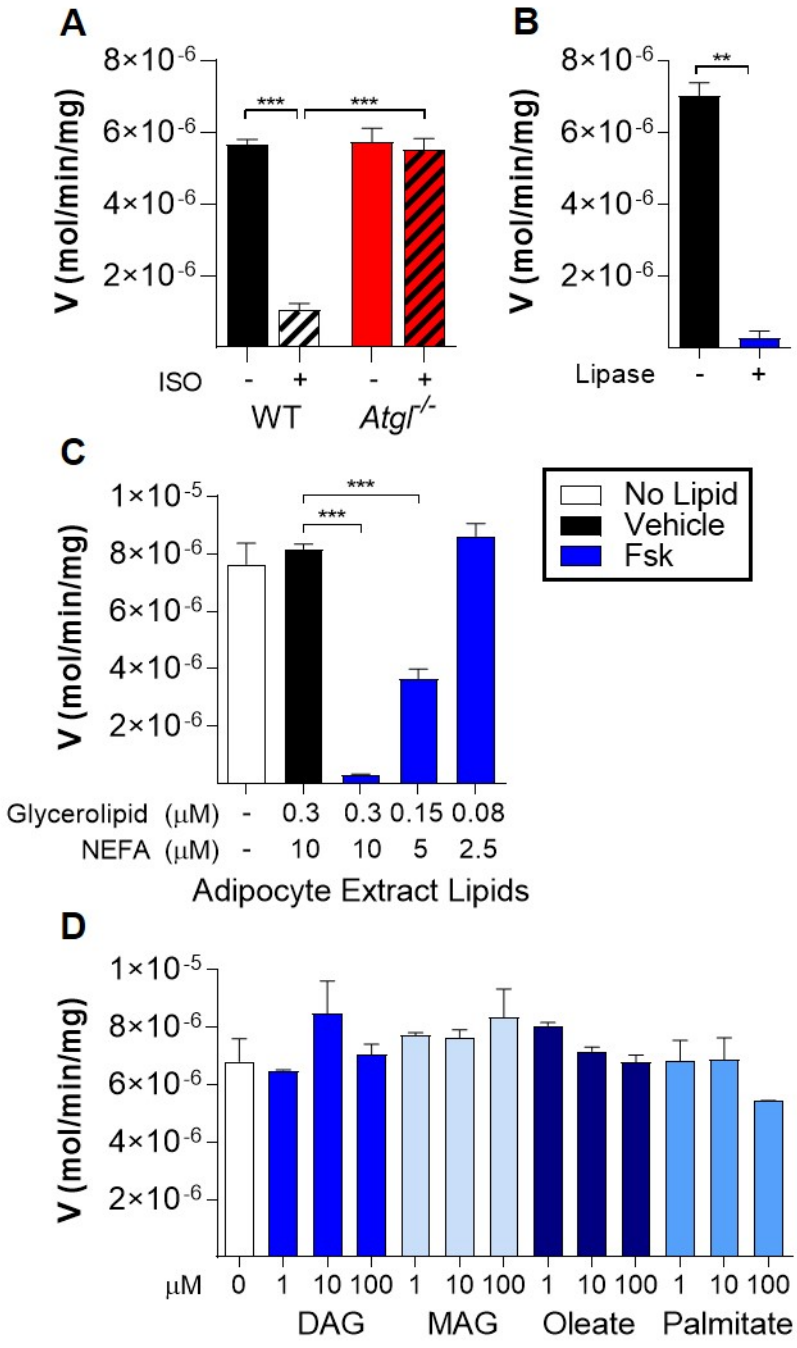


**Figure 3-8: Lipolytic products inhibit mTOR complex activity *in vitro***

**Figure 3-8 Legend**

**A.** mTOR complex activity determined by radioactive *in vitro* kinase assay. Lipids were extracted from either WT or *Atgl*$^{-/-}$ primary mouse adipocytes after treatment with or without 10 μM isoproterenol (ISO) for 30 min. Kinase assay was carried out using purified recombinant mTORC1 with 4E-BP1 as substrate. Extracted lipids were added to the assay 10 min before the addition of [γ-$^{32}$P]-ATP.

**B.** mTOR complex activity determined by radioactive *in vitro* kinase assay. Lipids were extracted from 3T3-L1 adipocytes then treated with or without lipase *in vitro*. Kinase assay was carried out as in A.

**C.** mTOR complex activity determined by radioactive *in vitro* kinase assay. Lipids were extracted from cultured 3T3-L1 adipocytes treated with or without 10 μM forskolin (FSK) for 30 min. Kinase assay was carried out as in A. No lipid, vehicle, or extracted lipids were added in the specified amounts.

**D.** mTOR complex activity determined by radioactive *in vitro* kinase assay. Kinase assay was carried out as in A. Pure DAG (1-palmitoyl-2-oleoyl-sn-glycerol), monoacylglycerol (2-oleoyl-glycerol), oleate, or palmitate were added in the specified amounts.

$N = 3$. Data are shown as mean ± SEM. $^{**}P < 0.01$ and $^{***}P < 0.001$, as indicated. Statistical analyses were performed using two-way ANOVA. All comparisons differing by one variable were made and adjusted for with ANOVA, and all significant comparisons are denoted as such.

### 3.3.7 Lipolytic Products Inhibit mTOR Complex Activity Through Complex Dissociation

While attempting to purify endogenous mTOR complex from adipocytes, we observed that the complexes were dissociated in cells treated with FSK **(Figure 3-9A)**. To determine if this was the mechanism of lipolysis-dependent mTOR complex inhibition, we developed an *in vitro* mTOR complex dissociation assay using fluorescently-tagged recombinant proteins: Venus-tagged mTOR with either Cerulean-tagged raptor or rictor, for mTORC1 or mTORC2 respectively **(Figure 3-9B)**. These fluorescent tags can be detected spectrophotometrically allowing for efficient determination and quantitation of complex dissociation *in vitro*. Using this assay, we showed that only lysates from adipocytes actively undergoing lipolysis caused dissociation of both mTORC1 and mTORC2, as seen by the loss in Cerulean-tagged raptor and rictor signal, respectively **(Figure 3-9C)**. Subsequently, when the lysate was subjected to a two-phase extraction, only the organic phase from lipolytically active adipocytes was capable of dissociating the mTOR complex **(Figure 3-9D)**. Additionally, when the organic phase of unstimulated adipocytes was treated with a lipase *in vitro*, the resulting extract gained the ability to dissociate the mTOR complex, further validating our hypothesis that a lipid produced during lipolysis is responsible for the complex dissociation and resulting inhibition **(Figure 3-9E)**. Complementary to our previous results, pretreatment of adipocytes with the lipolysis inhibitors atglistatin or E600 prevented FSK-induced complex dissociation **(Figure 3-9F)**. Taken together, these data show that lipolytic products facilitate mTOR complex inhibition through complex dissociation and serves as one mechanism of catecholamine-induced insulin resistance.

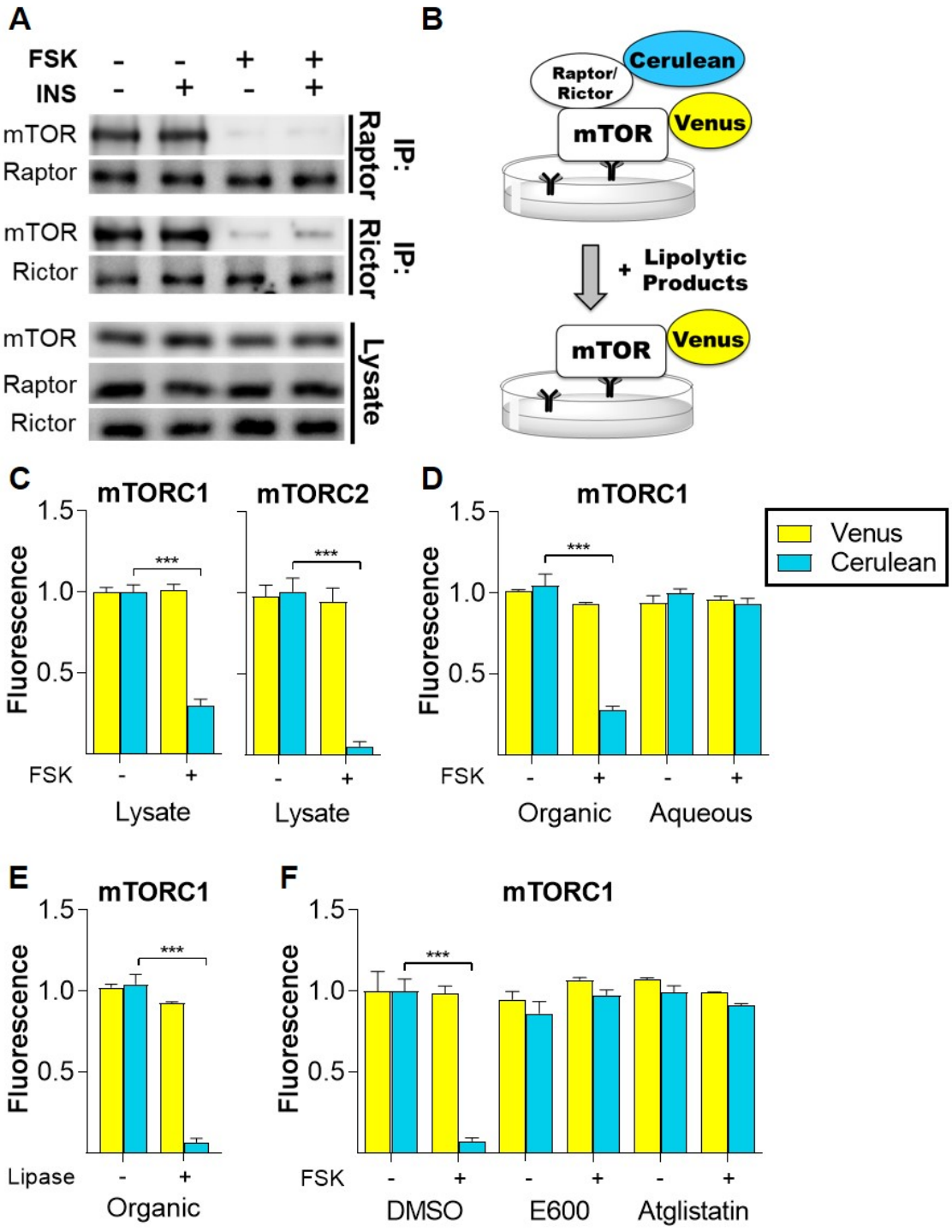


**Figure 3-9: Lipolytic products dissociate the mTOR complexes**

**Figure 3-9 Legend**

**A.** Representative immunoblots of mTORC1 and mTORC2 coimmunoprecipitations against raptor and rictor, respectively, from 3T3-L1 adipocytes incubated with or without 10 μM forskolin (FSK) for 30 min before treatment with or without 10 nM insulin (INS) for 15 min.

**B.** Illustration of the mTOR complex dissociation using fluorescently-tagged recombinant proteins.

**C.** mTOR complex integrity determined by *in vitro* mTOR complex dissociation assay. 3T3-L1 adipocytes were treated with or without 10 μM FSK. Purified fluorescently-tagged mTORC1 or mTORC2 was incubated with the adipocyte lysate for 30 min before washing and detection of fluorescence.

**D.** mTOR complex integrity determined by *in vitro* mTOR complex dissociation assay. 3T3-L1 adipocytes were treated with or without 10 μM FSK before being subjected to two-phase extraction. Purified fluorescently-tagged mTORC1 was incubated with either extracted organic or aqueous phases for 30 min before washing and detection of fluorescence.

**E.** mTOR complex integrity determined by *in vitro* mTOR complex dissociation assay. Lipids were extracted from 3T3-L1 adipocytes then treated with or without lipase *in vitro*. Purified fluorescently-tagged mTORC1 was incubated with extracted lipids for 30 min before washing and detection of fluorescence.

**F.** mTOR complex integrity determined by *in vitro* mTOR complex dissociation assay. Lipids were extracted from 3T3-L1 adipocytes incubated with vehicle, 150 μM E600, or 10 μM atglistatin before treatment with or without 10 μM FSK. Purified fluorescently-tagged mTORC1 was incubated with either extracted lipids for 30 min before washing and detection of fluorescence.

$N = 3$. Data are shown as mean ± SEM. $***P < 0.001$, as indicated. Statistical analyses were performed using two-way ANOVA. All comparisons differing by one variable were made and adjusted for with ANOVA, and all significant comparisons are denoted as such.

## 3.4 DISCUSSION AND CONCLUSIONS

This study shows that adrenergic action and subsequent adipocyte lipolysis is necessary for the development of stress-induced disturbances in glucose homeostasis and peripheral insulin resistance. Interestingly, catecholamines and lipolysis were shown to affect the secretion profile of adipokines from adipose tissue. Of particular interest was resistin which was released in a stress- and lipolysis-dependent manner and has previously been linked to the development of chronic insulin resistance in obesity (84, 86, 148). Furthermore, we show that the mechanism of insulin resistance in adipocytes may be through dissociation of the mTOR complexes. We found that lipolytic products that partition to the organic phase, likely lipids, are able to inhibit and dissociate the mTOR complexes *in vitro*. It is likely the lipids themselves are able to act as signaling molecules and do not require further enzymatic action because products produced through *in vitro* lipase treatment were also able to dissociate the mTOR complexes. Our observations suggest a critical role for adipose tissue in the metabolic response to acute stress.

Even though insulin resistance depends on insulin action in various tissues, multiple studies have supported adipose tissue as a central player in controlling peripheral insulin signaling. For example, adipose-specific loss of GLUT4 causes mice to develop hyperglycemia and peripheral insulin resistance, whereas adipose-specific overexpression of GLUT4 enhanced insulin sensitivity (72, 73). Previous work from our laboratory demonstrated that decreased rictor expression in adipose tissue led to hyperglycemia and systemic insulin resistance (50). This indicates that impaired insulin action in adipose tissue alone is sufficient to drive hyperglycemia and whole-body insulin resistance. Our

*in vitro* studies show that adipocyte lipolysis regulates acute mTOR complex inhibition which may lead to impaired insulin signaling in adipocytes and thus may impact the development of peripheral insulin resistance during adrenergic stress. Our data also demonstrate a novel mechanism of mTOR complex inhibition and dissociation by lipolytic products. This mechanism further highlights the importance of lipolytic products to regulate cell signaling events as well as potentially impact signaling in peripheral tissues.

Glycerol, one of the products of the lipolysis, serves an important substrate for gluconeogenesis (143). Under basal conditions, glycerol is a minor contributor to gluconeogenesis, however during acute stress, the need for glycerol for hepatic gluconeogenesis increases drastically (149). This is because trauma and injury induce a strong counterregulatory response, including significantly upregulating catecholamines such as epinephrine (127, 150). Epinephrine indirectly promotes hepatic gluconeogenesis (121, 122). Previous studies have demonstrated that the ability of insulin to suppress hepatic gluconeogenesis is actually an indirect effect based on inhibition of adipocyte lipolysis (122). Our studies show that blocking the release of glycerol into circulation in *Aqp7*$^{-/-}$ mice prevented the development of HS-induced hyperglycemia. In addition, infusion of glycerol resulted in stress-induced hyperglycemia, even when lipolysis was inhibited. These findings indicate the glycerol produced by adipocyte lipolysis is an important contributor to elevated blood glucose during acute stress.

Adipose tissue has long been recognized for its role in energy storage and as a regulator of energy homeostasis, but in recent years, the importance of adipose tissue as an endocrine organ has been increasingly appreciated (151). For example, adipose-

derived factors such as cytokines, adipokines, and lipid intermediates have been demonstrated to impair insulin-stimulated glucose disposal (151). One such adipokine is resistin which has been shown to be increased in obesity in mice and obesity and type 2 diabetes in humans (84, 148). Recent studies have also found elevated circulating levels of resistin in critically ill patients, with a strong positive correlation observed between circulating resistin and mortality (91–97). Our data demonstrates for the first time that acute resistin release requires lipolysis which correlated with the development of insulin resistance and impaired glucose homeostasis. Thus, our studies suggest that resistin may contribute to acute peripheral insulin resistance during trauma and surgery.

One limitation of our *in vivo* studies is the short time frame investigated. While catecholamines play an important role during the initial response to acute stress, other hormones play significant roles in the days to weeks following injury, including glucagon, cortisol, and inflammatory cytokines. It is important to note that while these hormones are induced at different times and have tissue-specific effects, all of these hormones may act similarly as they all oppose insulin action and induce adipocyte lipolysis (116). By focusing on one important hormonal component in the early acute stress response, we have demonstrated adipocyte lipolysis as a key regulator of catecholamine-induced metabolic impairments.

In summary, using both pharmacological and genetic methods, we show that adipocyte lipolysis is required for the development of HS- and adrenergic-induced hyperglycemia and insulin resistance. Furthermore, we have identified a novel mechanism of anabolic and catabolic signaling crosstalk by which lipolytic products inhibit insulin signaling through dissociation of the mTOR complexes. Our data suggest

that improved glucose control and insulin sensitivity observed with lipolysis inhibition may be due to decreased resistin release from adipose tissue and improved mTOR complex activity within adipocytes. These findings have important implications for understanding the early metabolic changes in the development of acute stress-induced hyperglycemia and may open up new therapeutic avenues to improve glucose control and insulin sensitivity commonly encountered in surgical and critically ill patients.

## ATTRIBUTION

Portions of this chapter (text and figures) were sampled from: Raje V, Ahern KW, Howell NL, Martinez BA, Oenarto V, Granade ME, Kim JW, Tundup S, Bottermann K, Gödecke A, Keller SR, Kadl A, Bland ML, Harris TE. Adipocyte lipolysis drives acute stress-induced insulin resistance and hyperglycemia. *Sci. Rep*. 2020 November 1. and Mullins GR, Wang L, Raje V, Sherwood SG, Grande RC, Boroda S, Eaton JM, Blancquaert S, Roger PP, Leitinger N, Harris TE. Catecholamine-induced lipolysis causes mTOR complex dissociation and inhibits glucose uptake in adipocytes. *PNAS*. 2014 December 9.

## ACKNOWLEDGEMENTS

We thank Dr. Eugene Barrett for helpful comments and discussion of manuscript, Gilead Sciences for providing GS-9667, and the Vanderbilt Mouse Metabolic Phenotyping Center for training in the Glucose Clamping the Conscious Mouse course. This work was funded by grants from the US National Institutes of Health R01DK101946 (T.E.H.), R01DK099601 (M.L.B.), R01DK096076 (N.L.), training grant support from T32HL007284 (K.W.A.), T32GM007055 (B.A.M.), and T32GM008715 (M.E.G.), the University of Virginia's Launchpad award (A.K. and T.E.H.), the American Heart Association Predoctoral Fellowships 14PRE20480252 (G.R.M.), 17PRE33660609 (K.W.A.), the German Research Foundation (DFG) through IRTG1902 (V.O.), American Diabetes Association Junior Faculty Award 7-11-JF-21, grants from the Belgian Fonds de la Recherche Scientifique (P.P.R.), and Télévie fellowships (S.B.)

## DECLARATION OF INTERESTS

Dr. Vidisha Raje, Dr. Alexandra Kadl, and Dr. Thurl Harris are inventors on a patent application relevant to this study filed by the University of Virginia through the UVA Licensing & Ventures Group (15/760,990). No other authors declare competing interests.

## AUTHOR CONTRIBUTIONS

These studies were driven primarily by Dr. Garrett Mullins and Dr. Vidisha Raje. The studies were designed by Dr. Thurl Harris, Dr. Garrett Mullins, Dr. Vidisha Raje, and Dr. Lifu Wang. Experimental work was performed by Katelyn Ahern (*Atgl*$^{-/-}$ tissue Western blots [data not shown] and FATA$^{-/-}$ knockout confirmation), Dr. Salome Alpert, Dr. Sara Blancquaert, Dr. Katharina Bottermann, Dr. James Eaton, Mitchell Granade, Rebecca Grande, Dr. Thurl Harris, Dr. Nancy Howell, Jae Woo Kim, Brittany Martinez, Dr. Garrett Mullins, Dr. Vici Oenarto, Dr. Vidisha Raje, Samantha Sherwood, Dr. Smanla Tundup, and Dr. Lifu Wang. Data analysis was performed by Katelyn Ahern (all data visualization and confirmation of statistical analysis for Raje et al. manuscript), Dr. Salome Alpert, Dr. Sara Blancquaert, Dr. Michelle Bland, Dr. Katharina Bottermann, Dr. James Eaton, Mitchell Granade, Rebecca Grande, Dr. Axel Gödecke, Dr. Thurl Harris, Dr. Nancy Howell, Dr. Alexandra Kadl, Dr. Susanna Keller, Jae Woo Kim, Dr. Norbert Leitinger, Brittany Martinez, Dr. Garrett Mullins, Dr. Vici Oenarto, Dr. Vidisha Raje, Dr. Pierre Roger, Samantha Sherwood, Dr. Smanla Tundup, and Dr. Lifu Wang. The manuscripts were written by Katelyn Ahern (editing and response to revisions for Raje et al. manuscript), Dr. Thurl Harris, Dr. Garrett Mullins, and Dr. Vidisha Raje. Funding was

provided by Katelyn Ahern, Dr. Sara Blancquaert, Dr. Michelle Bland, Mitchell Granade, Dr. Thurl Harris, Dr. Alexandra Kadl, Dr. Norbert Leitinger, Brittany Martinez, Dr. Garrett Mullins, Dr. Vici Oenarto, and Dr. Pierre Roger.

# 4 CHAPTER 4: REGIOISOMER-INDEPENDENT QUANTIFICATION OF FATTY ACID OXIDATION PRODUCTS BY HPLC-ESI-MS/MS ANALYSIS OF SODIUM ADDUCTS

## 4.1 ABSTRACT

Despite growing acknowledgement of the role of oxFA as cellular signaling molecules and in the pathogenesis of disease, developing methods to measure these species in biological samples has proven challenging. Here we describe a novel method utilizing HPLC-ESI-MS/MS to identify and quantify multiple full-length oxFA species in a regioisomer-independent manner without the need for time-consuming sample preparation or derivatization. Building on recent progress in the characterization of NEFA and their oxidation products by MS/MS, we employed positive-ion ionization by measuring sodium adducts in conjunction with DiffE QIM to unequivocally verify the presence of the hydroperoxide, hydroxide, and ketone oxidation products of LA and AA. Our HPLC method achieved separation of these oxidized species from their unoxidized counterparts while maintaining regioisomer-independent elution, allowing quantification over a 5 $\log_{10}$ range with a lower LOQ of 0.1 picomoles. With a simple sample preparation and a runtime as low as 11 minutes, our method allows the rapid and facile detection and measurement of full-length oxFA in biological samples. We believe this approach will allow for new insight and further investigation into the role of oxFA in metabolic disease.

## 4.2 INTRODUCTION

Impaired redox homeostasis has been implicated in a wide array of pathologies, including obesity, stress-induced insulin resistance, atherosclerosis, rheumatoid arthritis, and hypertension (152–155). One hallmark of oxidative stress in these pathologies is increased lipid oxidation (5, 156). While oxidized lipids can be produced enzymatically in a tightly regulated fashion by lipoxygenases and cyclooxygenases to form signaling molecules, such as leukotrienes and prostaglandins, non-enzymatic lipid oxidation during oxidative stress may surpass cellular control and lead to destructive biological processes, such as membrane damage, protein modification, DNA oxidation, deposition of atherogenic plaque, and tissue inflammation (45, 63–65, 67, 68). Due to the wide-ranging implications, there has been much interest in examining the diverse species of the oxidized lipidome and their differential biological functions.

Of note, recent work by our group has demonstrated relative changes in the components of this oxidized lipidome, specifically increases in full-length oxidized phospholipids (oxPL), to be associated with the onset of high-fat diet–induced obesity leading to dramatic differences in adipose tissue macrophage polarization and tissue inflammation (45). These effects on macrophages were found to be entirely dependent on the oxFA. Remarkably, treatment with non-esterified oxAA alone was able to comparably induce antioxidant, metabolic, and proinflammatory gene expression (44). As a result, a means of specifically identifying and quantifying these full-length oxFA in biological samples is of great importance.

Due to rapid expansion of the lipidomics field, analytical methods have been compiled by various groups such as LIPID MAPS. HPLC-MS is gaining in popularity as

the preferred way to identify and quantify various lipid classes; the major exception is FA, which have been traditionally measured by gas chromatography-MS following derivatization (157, 158). While gas chromatography methods measuring NEFA have high sensitivity and resolution, they have inherent problems and require extensive sample preparation, making them unsuitable for measuring oxFA. Gas chromatography requires high temperatures to produce volatile analytes for detection that would be destructive to oxFA, which are thermolabile (67). To improve volatilization and prevent breakdown, oxFA would require multiple derivatization steps (159). Not only are these steps time-consuming, but they inherently prevent the distinction of various oxFA species, such as hydroperoxides and hydroxides. Without derivatization, NEFA are measured by mass spectrometry (MS) using negative ion formation due to the loss of the acidic hydrogen of the carboxylic acid which is enhanced under basic conditions. However, HPLC methods used in conjunction with MS for NEFA measurement usually rely on reverse phase chromatography which requires the presence of a weak acid to keep the carboxylic acid in its protonated state and allow retention on the column for separation. As such, formation of the carboxylate anion in the electrospray droplets is usually suppressed (160–162). With reactive oxFA naturally present at much lower levels than their unoxidized counterparts, this loss of sensitivity has further hindered their measurement. As such, much work and many technological improvements have been dedicated to developing means of measuring NEFA and their oxidation products by HPLC-MS.

Recent progress towards utilizing HPLC-MS to measure NEFA oxidation has primarily focused on identifying specific regioisomers either through an untargeted approach, which only has relative quantitation capability, or through a targeted approach,

of which some methods allow absolute quantitation (67, 159, 163–167). Meanwhile, methods focused on measuring these species irrespective of regioisomer rely predominantly on HPLC with chemiluminescence detection, which, while easily quantitated, is inherently limited in its specificity. These methods measure oxFA solely based on the oxidized moiety and are unable to distinguish between individual NEFA backbones (68, 168, 169). A method that could quantitate specific oxFA in a regioisomer-independent manner would be highly biologically relevant, as it is likely that the sum total oxidation products, rather than the formation of one particular isomer, is more important in pathologies implicating chronic oxidative stress (45, 170). Thus, our goal was to utilize HPLC coupled with ESI-MS/MS to develop a targeted, species-specific method using positive-ion ionization that could identify and quantitate multiple full-length oxFA species in a regioisomer-independent manner without relying on time-consuming sample preparation, such as derivatization.

## 4.3 RESULTS

### 4.3.1 Species-Dependent Condition Determination using Synthetic Standards

In addition to allowing measurement with the more compatible positive-ion ionization, previous studies have noted that sodium and other metal adducts result in increased charge-remote fragmentation of lipid species which generates structurally informative product ions (63, 100, 165, 171, 104, 108–114). This observation has been further extended to oxidized lipid species and has been particularly successful for studying lipid hydroperoxides (63, 165, 171). Of note, Ito et al. demonstrated the use of alkali metal adducts, particularly sodium, as a fragmentation enhancer of NEFA hydroperoxides (165, 171). Despite this success, it has yet to be investigated whether

these improvements in fragmentation can be extended to other full-length oxFA, such as hydroxides and ketones. To address this, we fragmented and analyzed sodium adducts of full-length oxidation products of the polyunsaturated NEFA, LA, and AA **(Figure 4-1)**.

The formation and detection of sodium adducts was confirmed by directly infusing individual standards in the presence of sodium ions into the ESI-MS/MS system. Because the inclusion of nonvolatile salts can impair solvent vaporization and lead to instrument buildup, the level of sodium acetate was adjusted to minimize ion suppression and stress on the ESI-MS/MS system while still promoting adequate adduct formation. To further improve solvent vaporization, an elevated interface temperature was chosen that had been previously been demonstrated to be compatible with measuring sodium adducts of hydroperoxide oxFA, the least stable of the full-length oxFA species of interest (165, 171). Based on the masses observed in the full-scan spectra, the sodium adduct was formed by coordination of a sodium ion with the carbonyl oxygen in the carboxylic acid of the NEFA. A less abundant double adduct formed by the displacement of the acidic hydrogen by a second sodium ion was also observed. MS/MS conditions were optimized for enhanced detection of the single adduct of each species **(Table 4-1)**. As such, the predominant peak in the full MS scan for the oxFA of interest was the single adduct, with the double adduct detectable but at a lower intensity **(Figure 4-2)**. Some unidentified, lower intensity peaks were also observed in the full MS scan, particularly of the hydroxide and hydroperoxide species. These peaks are likely due to low abundance contaminants and adducts from the methanol, which has been shown to contain trace levels of ammonium, sodium, and potassium that vary between lots and brands (52, 172). As their presence has been shown to have no adverse effects on calibration and a linear

concentration response, no impairment of method capabilities is expected. The formation of the single sodium adduct was also detected for the unoxidized NEFA **(Figure 4-3)**.

Fragmentation of the oxFA sodium adducts was examined by product ion scans of the directly-infused standards. As expected based on previous literature, sodium adducts of both hydroperoxides produced stable, characteristic fragment ions **(Figure 4-2)** (165). 13-HPODE exhibited a fragment of 247 Da, with the loss of 88 Da likely due to cleavage of the bond between C-13 and C-14 and elimination of a hydroxide. 12-HPETE exhibited a fragment of 231 Da with a similar fragmentation pattern (cleavage between C-12 and C-13 and loss of a hydroxide). Despite the enhanced fragmentation of hydroperoxide sodium adducts, the same improvements were not observed for the hydroxides. As seen with many previously published methods, the product ion spectra of HODE and HETE were dominated by the unfragmented molecular ion (in this case, the single sodium adduct) and an uncharacteristic fragment resulting from the loss of water (the most stable product ion formed) (63, 67, 173, 174, 100, 108, 112, 114, 159, 163, 165, 168). Due to this stability, the uncharacteristic loss of water was also observed in the full MS scans of the hydroperoxide and hydroxide species **(Figure 4-2).** For the ketone product ion spectra, again, no stable fragments were produced for either KODE or KETE. Similar to their hydroxide products, LA and AA sodium adducts did not display stable fragmentation, as seen by product ion spectra dominated by the molecular ion **(Figure 4-3)**. Taken together, these data suggest that the enhancement of fragmentation seen by sodium adduct formation for hydroperoxides cannot be generalized to all full-length oxFA species.

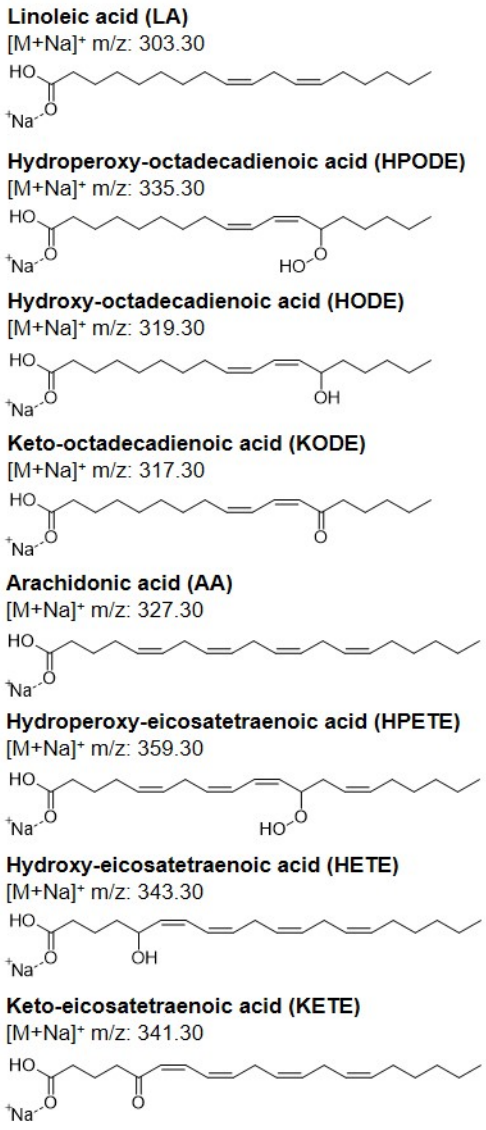


**Figure 4-1: Chemical structures for the sodium adducts of LA and AA and their full-length oxidation products**

**Figure 4-1 Legend**

Chemical structures of the specific regioisomer standards purchased and used for initial condition optimization are shown. Structures are depicted with a coordinated sodium ion as the single adduct is the molecular ion of interest. Note that structures are depicted with all double bonds in their *cis* form but can also naturally exist with a *trans* conformation.

| Fatty Acid Species | Molecular Ion | Molecular Ion *m/z* | DP (eV) | Quantitative Transition | Quantitative Transition CE (eV) | Qualitative Transition | Qualitative Transition CE (eV) | CXP (eV) | QIR | QIR Range (75-125%) |
|---|---|---|---|---|---|---|---|---|---|---|
| LA | $[M+Na]^+$ | 303.3 | 46 | 303.3 → 303.3 | 10 | 303.3 → 303.3 | 16 | 14 | 2.09 | 1.56-2.61 |
| AA | $[M+Na]^+$ | 327.3 | 36 | 327.3 → 327.3 | 13 | 327.3 → 327.3 | 17 | 6 | 1.97 | 1.47-2.46 |
| HPODE | $[M+Na]^+$ | 335.3 | 70 | 335.3 → 335.3 | 10 | 335.3 → 335.3 | 19 | 14 | 1.96 | 1.47-2.45 |
| HODE | $[M+Na]^+$ | 319.3 | 76 | 319.3 → 319.3 | 13 | 319.3 → 319.3 | 18 | 8 | 1.96 | 1.47-2.45 |
| KODE | $[M+Na]^+$ | 317.3 | 81 | 317.3 → 317.3 | 13 | 317.3 → 317.3 | 22 | 10 | 1.91 | 1.43-2.39 |
| HPETE | $[M+Na]^+$ | 359.3 | 46 | 359.3 → 359.3 | 7 | 359.3 → 359.3 | 14 | 14 | 1.72 | 1.29-2.15 |
| HETE | $[M+Na]^+$ | 343.3 | 56 | 343.3 → 343.3 | 13 | 343.3 → 343.3 | 16 | 10 | 2.18 | 1.63-2.73 |
| KETE | $[M+Na]^+$ | 341.3 | 71 | 341.3 → 341.3 | 13 | 341.3 → 341.3 | 20 | 12 | 1.94 | 1.45-2.43 |
| C17:0 | $[M+Na]^+$ | 293.5 | 51 | 293.5 → 293.5 | 7 | 293.5 → 293.5 | 13 | 10 | 1.68 | 1.26-2.10 |

**Table 4-1: Optimized MS/MS conditions for oxFA detection and quantification**

**Table 4-1 Legend**

MS/MS conditions were optimized for detection of the single sodium adduct of each analyte; specifically, declustering potential (DP), quantitative transition collision energy (CE), qualitative transition CE, and collision exit potential (CXP). Values are listed in electronvolts (eV). The listed qualifier ion ratio (QIR) is based on the noted pseudo-molecular transitions measured using the listed optimized MS/MS conditions in combination with the HPLC method outlined in the text. Based on the intensity of the qualitative transition chosen and accepted standards for QIR variation (75-125%), the tolerable range in QIR for each species was calculated.

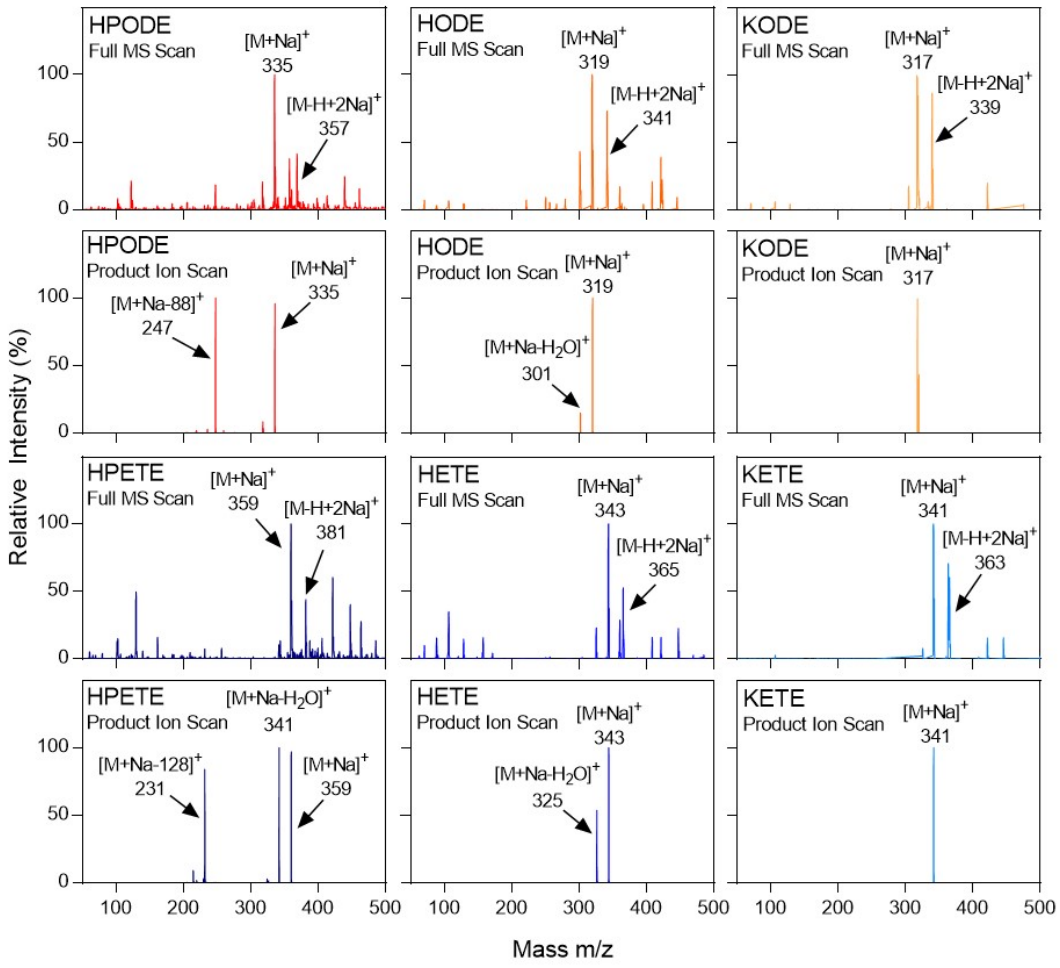


**Figure 4-2: Direct infusion-MS/MS detection and fragmentation of oxFA sodium adducts with positive-ion ionization**

**Figure 4-2 Legend**

Full MS scan from direct infusion of individual oxFA standards (10 μM) in the presence of sodium ions (200 μM sodium acetate). Full MS scan in multi-channel analysis mode depicts 238 cumulative scans of 0.5 s. The molecular ion of interest (the single sodium adduct) is denoted $[M+Na]^+$. The double sodium adduct is denoted $[M-H+2Na]^+$. Product ion scan of oxFA single sodium adducts from direct infusion of individual oxFA standards (10 μM) in the presence of sodium ions (200 μM sodium acetate). Product ion scan in multi-channel analysis mode depicts 79 cumulative scans of 1.5 s. Characteristic fragments are denoted as $[M+Na-X]^+$, with X being the mass lost. The uncharacteristic water-loss fragment is denoted as $[M+Na-H_2O]^+$. For both full MS and product ion scans, peak height is displayed relative to the intensity of the largest peak in the spectra.

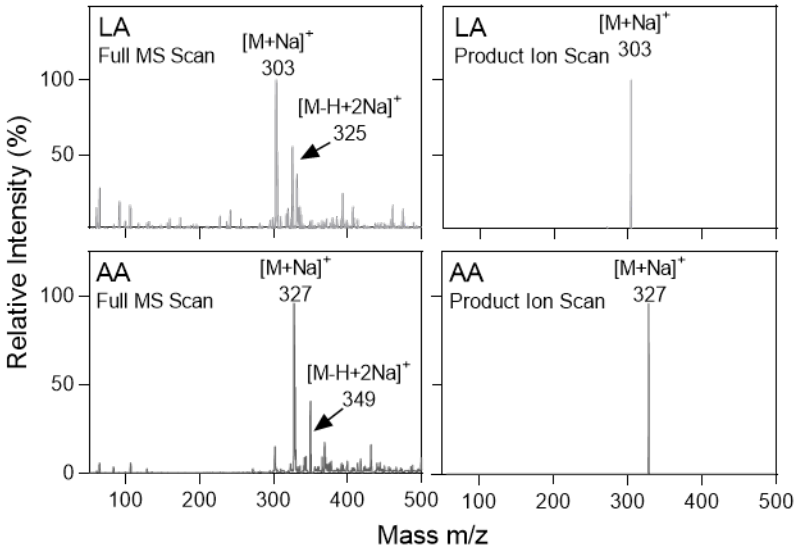


**Figure 4-3: Direct infusion-MS/MS detection and fragmentation of unoxidized LA and AA sodium adducts with positive-ion ionization**

**Figure 4-3 Legend**

Full MS scan from direct infusion of individual LA and AA standards (10 μM) in the presence of sodium ions (200 μM sodium acetate). Full MS scan in multi-channel analysis mode depicts 238 cumulative scans of 0.5 s. The molecular ion of interest (the single sodium adduct) is denoted $[M+Na]^+$. The double sodium adduct is denoted $[M-H+2Na]^+$. Product ion scan of LA and AA single sodium adducts from direct infusion of individual standards (10 μM) in the presence of sodium ions (200 μM sodium acetate). Product ion scan in multi-channel analysis mode depicts 79 cumulative scans of 1.5 s. Peak height is displayed relative to the intensity of the largest peak in the spectra.

.

### 4.3.2 Differential Energy Qualifier Ion Monitoring of Full-Length OxFA

Due to the lack of regioisomer-independent characteristic fragments necessary for traditional identification by MS/MS, DiffE QIM was employed. Traditional QIM allows high selectivity by monitoring two or more transitions for each analyte. The most intense transition is used for quantification, while lower intensity transitions are used for identity confirmation. This confirmation is accomplished by calculating the relative intensities between the quantitative and qualitative transitions, known as the QIR (175). The QIR is a constant property of a species under a given set of MS/MS conditions with adequate chromatographic separation, regardless of the matrix (176–178). Due to the lack of regioisomer-independent, stable fragmentation of oxFA, traditional QIM is not possible. However, Hellmuth et al. recently established the technique of DiffE QIM for use with FA, which relies on the unique relationship of CE to molecular ion signal intensity (108, 179). The quantitative and qualitative transitions are set to the same pseudo-molecular mass transition with the parent ion and product ion mass set to the molecular ion adduct but with increased CE for the qualitative transition **(Table 4-1)**. The ratio of these transitions was demonstrated to specifically identify NEFA in biological samples (179). As such, we looked to extend this technique for the first time to oxFA species. The unique relationship between the intensity of the pseudo-molecular transition and CE was determined for the unoxidized NEFA and their full-length oxFA products **(Figure 4-4)**. The CE that yielded the highest transition intensity was designated for the quantitative transition, while the CE that yielded an intensity of roughly 50% was chosen for the qualitative transition. Based on these differential energy transitions, the QIR was determined for each oxFA **(Table 4-1)**. Based on industry and government standards, with a qualitative transition intensity of 50% of the quantitative transition, the acceptable

QIR range for identification is 75-125% of the QIR of the reference standard (175, 176, 178–182).

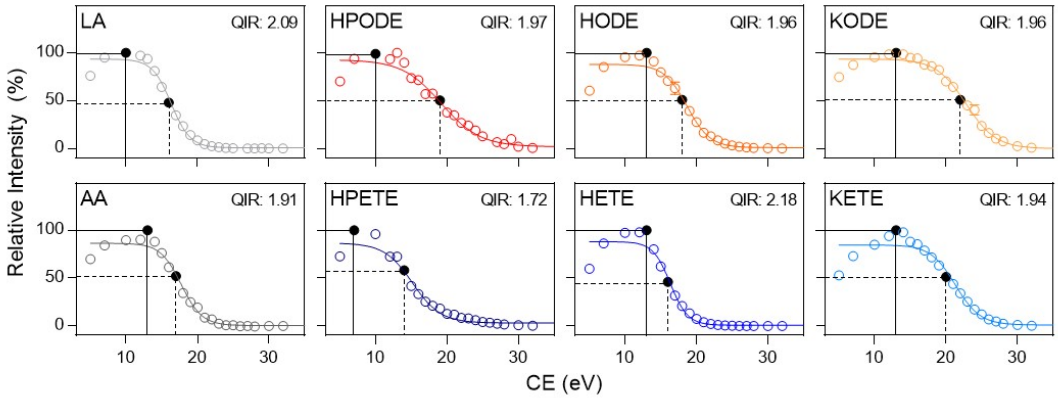


**Figure 4-4: DiffE transition intensity curves for oxFA and NEFA species**

**Figure 4-4 Legend**

The curves were fit with a sigmoidal non-linear regression. The intensities are displayed relative to the highest intensity transition. The collision energy (CE) yielding the highest intensity transition was designated as the quantitative transition (solid line). The CE yielding an intensity of roughly 50% of maximal was designated at the qualitative transition (dashed line). The qualifier ion ratio (QIR) was calculated based on the intensities of these two transitions. Differential energy curves were performed in triplicate with data expressed as mean ± SEM.

### 4.3.3 Chromatographic Separation and Quantification of Synthetic Standards

Recent studies examining oxFA have been focused on regioisomer identification and have thus relied heavily on chromatographic separation of these species by chiral columns (165, 171). In contrast, our goal was to quantitate full-length oxFA independent of regioisomer, since it is probable that the sum total of oxidation products, rather than the formation of a specific regioisomer, is more relevant in the pathophysiology of chronic oxidative stress diseases (45, 170). As such, the chromatographic method employed should separate the oxFA from other potentially conflicting lipid entities while still allowing collective elution of all the regioisomers of a given oxFA species in a single peak. To this end, reverse phase chromatography was selected, since the primary distinguishing characteristic of oxFA compared to other lipids is their increased polarity imparted by the oxidized moiety and amplified by their relatively small size. As previously mentioned, if not properly accommodated, the inclusion of nonvolatile salts, such as sodium acetate, can reduce performance of the ESI-MS/MS system by leading to residual salt within the system. This build-up could further confound our results by increasing the formation of the double sodium adduct of the oxFA. To limit these potential issues, sodium acetate was confined to the primary elution solvent (Solvent B), and a 10 column-volume wash with salt-free Solvent A was programmed between samples. The inclusion of a thorough wash prevented the accumulation of salt within the HPLC and ESI and allowed for the stable formation of the single sodium adduct. This can be demonstrated by the precision and accuracy values calculated during validation of the method **(Table 4-2)**. The washes had the added benefit of reducing carryover between samples, a common problem in lipid analysis (164). To maximize solvent vaporization

and thus analyte detection, a low flow rate, which gave the highest signal intensity for the standards, was selected.

Under these chromatographic conditions, high-quality peaks with extremely stable retention times were obtained with a distinct separation of the oxFA standards from their unoxidized counterpart **(Table 4-2, Figure 4-5)**. The oxidized species were found to elute earlier, reflective of their increased polarity. Furthermore, peaks for the quantitative and qualitative transitions were observed to have corresponding retention times and fell in the expected range of QIR for each species **(Figure 4-5)**. Though there was less than a minute separation between the oxidized and unoxidized species, this was deemed sufficient separation in order to maintain a short overall runtime. In fact, the method was able to be even further reduced without significant effects on the method capability, yielding a rapid 11 runtime **(Figure 4-6A)**. If increased separation is the priority, the published HPLC method can easily be adapted for use with a longer column **(Figure 4-6B)**.

Linearity over a 5 $\log_{10}$ range was achieved for each analyte of interest, with a coefficient of determination ($R^2$ value) of at least 0.988 **(Figure 4-7)**. As shown in the full MS scans of oxFA, the double adduct is present in all samples in addition to the single adduct of interest. To ensure that the presence of the double adduct does not hinder reliability, the precision and accuracy of the method were analyzed. The intraassay and interassay precision of the analytes were in the range of 0.8-6.5% and 4.3-10.8%, respectively **(Table 4-2)**. Based on comparison to a calibration curve of the pure reference standard, the accuracy of samples with a known concentration were all within the accepted range of 80-120% **(Table 4-2)**. As a result, we concluded that presence of

the double adduct was sufficiently accounted for in our method design. The LOQ for each species was determined to be the concentration at which the qualitative transition has a signal-to-noise ratio of greater than 3:1 **(Table 4-2)**. Because this method relies on DiffE QIR, the limit of detection and LOQ are identical, as a species cannot be definitively identified in the absence of the qualitative transition. The LOQ for the oxFA species were determined to be 0.1 pmol. The LOQ for the unoxidized NEFA species were lower at 0.01 pmol, likely due to their increased stability compared to oxFA. These LOQ values are similar to reported LOQ values for unoxidized NEFA quantification by HPLC-MS/MS using the QIR approach to species confirmation (179). The LOQ values for our oxFA and previously published unoxidized NEFA methods are slightly above those reported for HPLC-MS/MS methods quantifying derivatized NEFA (183, 184).

| Fatty Acid Species | Intra-assay Precision (%) | Interassay Precision (%) | Accuracy (%) | LOQ (pmol) | Retention Time (min) | Relative Retention Time |
|---|---|---|---|---|---|---|
| LA | 0.8 | 5.2 | 96-109 | 0.01 | 10.89 ± 0.019 | 0.95 |
| AA | 1.7 | 6.9 | 88-104 | 0.01 | 10.85 ± 0.022 | 0.95 |
| HPODE | 3.7 | 6.0 | 82-101 | 0.1 | 10.50 ± 0.011 | 0.90 |
| HODE | 1.2 | 8.0 | 94-104 | 0.1 | 10.31 ± 0.031 | 0.90 |
| KODE | 6.5 | 10.0 | 98-110 | 0.1 | 10.27 ± 0.028 | 0.90 |
| HPETE | 2.5 | 8.2 | 81-100 | 0.1 | 10.37 ± 0.023 | 0.91 |
| HETE | 2.0 | 4.3 | 91-111 | 0.1 | 10.47 ± 0.027 | 0.92 |
| KETE | 6.2 | 10.8 | 98-113 | 0.1 | 10.42 ± 0.025 | 0.91 |
| C17:0 | 1.7 | 8.0 | 95-102 | 10 | 11.11 ± 0.055 | 1.00 |

**Table 4-2: Method validation parameters**

**Table 4-2 Legend**

The intra-assay precision was determined by measuring five concentrations three times each on the same day. The interassay precision was determined by measuring five concentrations on five days. Precision values are expressed as the percent value of the standard deviation compared to the mean value. Accuracy was determined by measuring three different, known concentrations five times. Accuracy values are expressed as the percent value of the calculated concentration compared to the known concentration. The lower limit of quantification (LOQ) was determined to be the concentration at which the qualitative transition had a signal-to-noise ratio of greater than 3:1. The variation in retention time was determined by comparing retention times on five days and is expressed as the average retention time and standard deviation. The relative retention time compared to the internal standard C17:0 was calculated for each species. This value is constant for all three described HPLC methods.

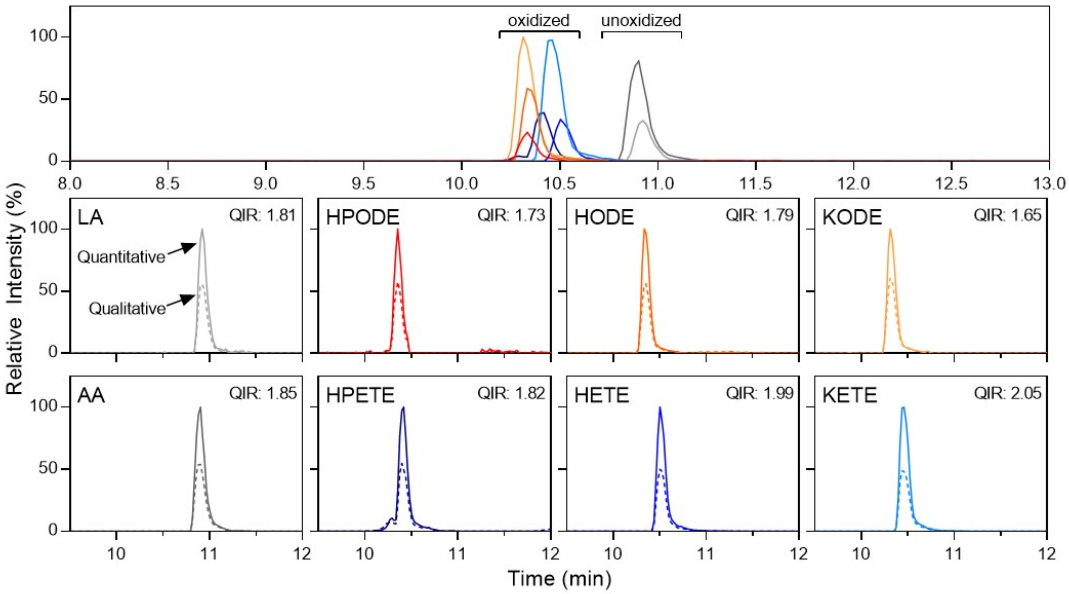


**Figure 4-5: HPLC-MS/MS approach to quantification of oxFA sodium adducts with positive-ion ionization**

**Figure 4-5 Legend**

Chromatogram of 10 μM standard mix of oxFA species. Zoomed chromatograms of the individual analytes with both the quantitative (solid line) and qualitative transitions (dashed line) visualized with the calculated qualifier ion ratio (QIR). Peak height is displayed relative to the highest intensity peak in each chromatogram.

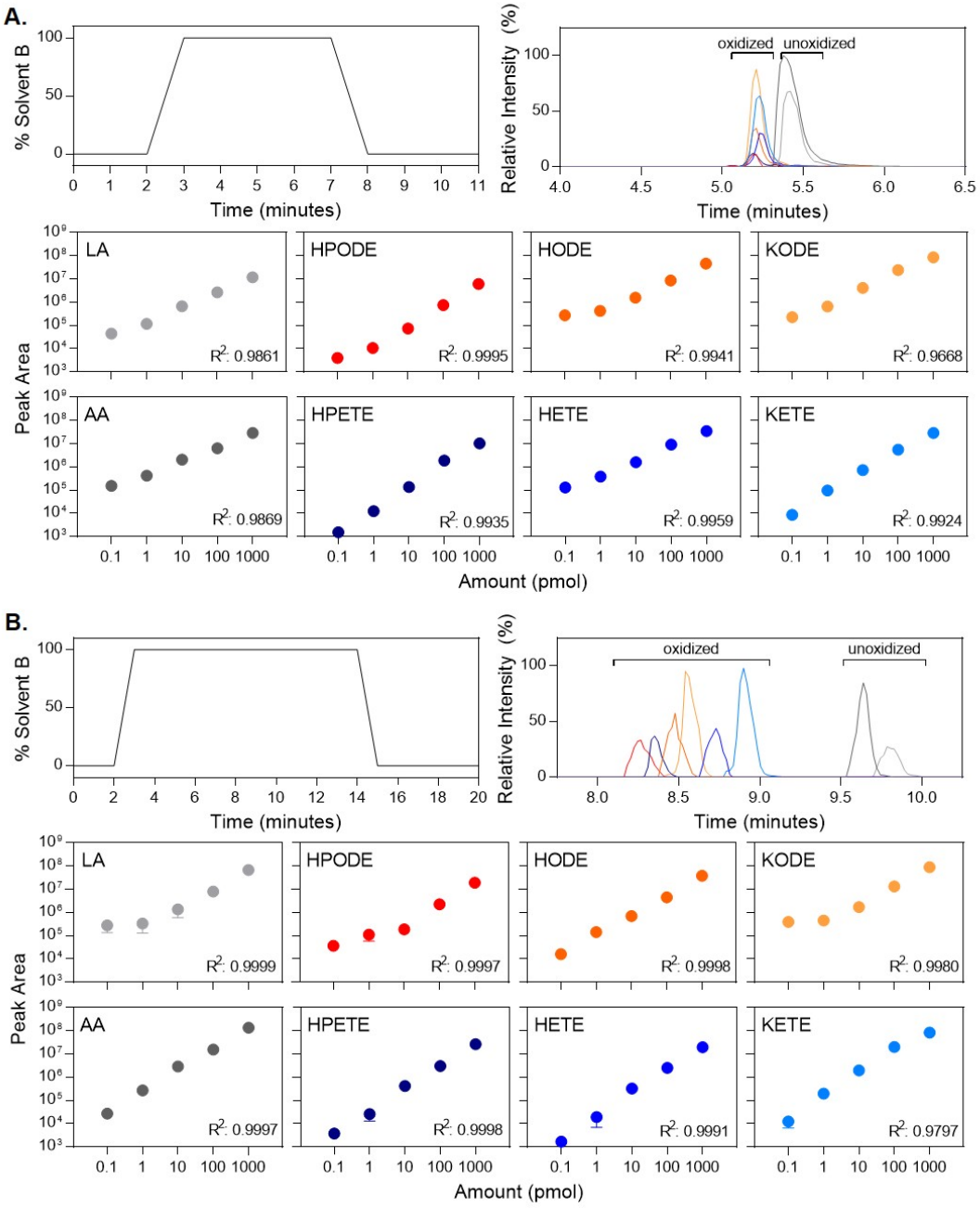


**Figure 4-6: Alternate, compatible HPLC methods**

**Figure 4-6 Legend**

**A.** Chromatogram of 10 μM standard mix of oxFA species and calibration curves of individual oxFA standards generated using a shorter runtime HPLC method. The solvent gradient approach for a shorter runtime is depicted as the percent of Solvent B over time. Chromatogram peak height is displayed relative to the highest intensity peak. Linearity was achieved over a 5 log10 range for each analyte with a high coefficient of determination ($R^2$ value). Calibration curves were performed in triplicate with data expressed as mean ± SEM.

**B.** Chromatogram of 10 μM standard mix of oxFA species and calibration curves of individual oxFA standards generated using a HPLC method with a longer column. Calibration curves were performed in triplicate with data expressed as mean ± SEM. The solvent gradient approach for a shorter runtime is depicted as the percent of solvent B over time. Chromatogram peak height is displayed relative to the highest intensity peak. Linearity was achieved over a 5 log10 range for each analyte with a high coefficient of determination ($R^2$ value). Calibration curves were performed in triplicate with data expressed as mean ± SEM.

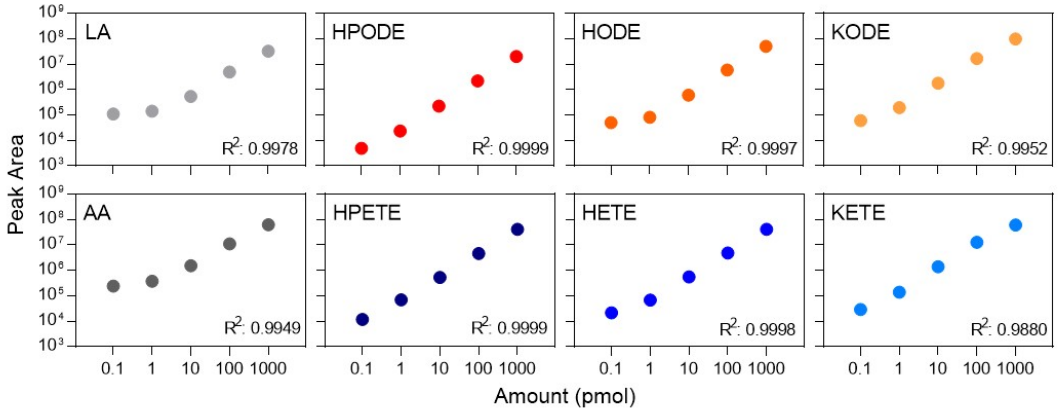


**Figure 4-7: HPLC-MS/MS calibration curves for oxFA and unoxidized NEFA species**

**Figure 4-7 Legend**

Linearity was achieved over a 5 $\log_{10}$ range for each analyte with a high coefficient of determination ($R^2$ value) using the standard HPLC method. Quantification of oxFA in samples was based on comparison to the corresponding curve. Calibration curves were performed in triplicate with data expressed as mean ± SEM.

### 4.3.4 Regioisomer-Independent Analysis of Complex Oxidized Mixtures by HPLC-MS/MS

Because characterization and optimization were performed with pure standards of a single regioisomer, a mixture of oxFA was required to ensure the optimized conditions could definitively identify the full-length species of interest within a mixture, independent of regioisomer. To create a diverse mixture of species and regioisomers, auto-oxidation of LA and AA was performed. Progression of oxidation was monitored over time by directly infusing the mixture in the presence of sodium ions into the ESI-MS/MS, and the time point with the highest intensity of full-length species is represented **(Figure 4-8A)**. This occurred much more rapidly for AA than LA (12 h compared to 48 h), likely due to the increased number of susceptible allylic carbons. At each of these time points, a significant peak corresponding to the unoxidized NEFA was still observed. Based on comparison with the full-scan and product ion mass spectra of the pure standards, the presence of sodium adducts of the hydroperoxide, hydroxide, and ketone oxidation products for both LA and AA could be identified, indicating that the determined species-specific conditions could be used to detect the full-length oxidized species of interest, regardless of regioisomer, within a complex lipid mixture.

To ensure that all regioisomers eluted collectively under the determined chromatographic conditions, the auto-oxidized mixture containing a variety of oxidized species and regioisomers was again employed. Similar to the chromatogram observed for the standards, separation of the full-length oxFA from their unoxidized counterparts was obtained, with a singular peak for each analyte observed, indicating unified elution of all regioisomers **(Figure 4-8B)**. Furthermore, species identity within the complex mixture was able to be confirmed, since the QIR for each analyte fell within the acceptable range.

To confirm our ability to quantitate total levels of full-length oxFA, various time points throughout auto-oxidation of LA and AA were collected, and the production of each full-length oxFA and reduction of its unoxidized counterpart were quantified over time. In agreement with the observation by direct infusion analysis, AA oxidized on a more rapid timescale than LA **(Figure 4-9)**. Of the time points analyzed, peak levels of full-length oxFA were achieved after 48 h for LA and 12 h for AA. The percentage of full-length oxFA present reached a higher maximum for LA compared to AA. This is likely due to the different rates of oxidation progression for LA and AA. Just as AA forms full-length oxFA more quickly due to the increased number of susceptible allylic carbons, these species undergo further oxidation at a more rapid pace. As such, equilibrium of full-length oxFA formation and further oxidation is likely established at a lower level for AA than LA. Based on these data, our HPLC-ESI-MS/MS method implementing DiffE QIM was validated for measuring and quantifying full-length oxFA species independent of regioisomer within a complex mixture.

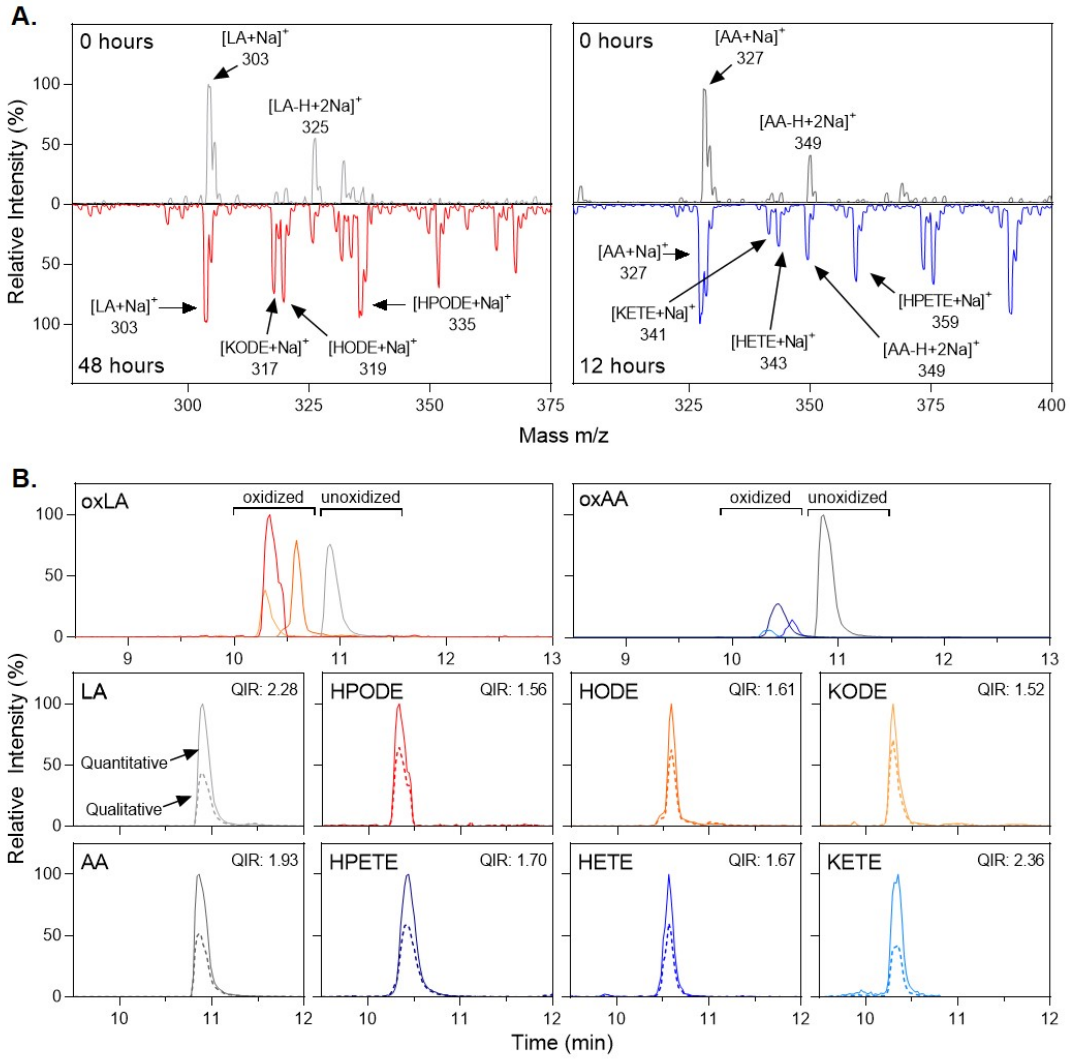


**Figure 4-8: Method validation with a complex mixture of species and isoforms**

**Figure 4-8 Legend**

**A.** Full MS scan of oxFA mixtures produced by auto-oxidation of LA and AA for specified time period. Both unoxidized and auto-oxidized spectra were measured under the optimized conditions for the unoxidized species. Peak height is displayed relative to the highest intensity peak in the spectra.

**B.** Chromatograms of 100 μM LA and AA auto-oxidized for specified amount of time. Zoomed chromatograms of the individual analytes with both the quantitative (solid line) and qualitative transitions (dashed line) visualized with the calculated qualifier ion ratio (QIR). Peak height is displayed relative to the highest intensity peak in each chromatogram.

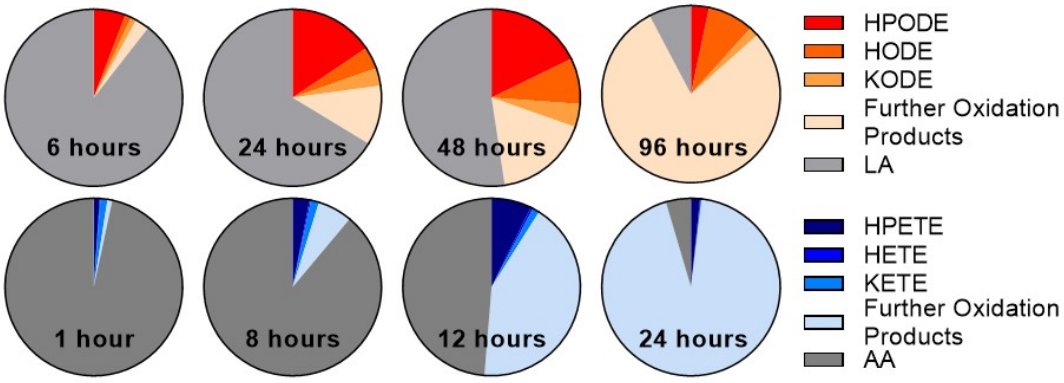


**Figure 4-9: Quantification validation with a complex mixture of species and isoforms**

**Figure 4-9 Legend**

The auto-oxidation of LA over 96 h and AA over 24 h, as represented by pie charts visualizing the relative amount of each species. Further oxidation products was defined as the portion of the known starting amount of unoxidized NEFA that could not be accounted for by the quantification of our species of interest. Auto-oxidation time course was performed in triplicate.

### 4.3.5 Quantification of Full-Length OxFA Species in Biological Samples

In order to confirm our ability to measure these lipid species in a regioisomer-independent manner within a complex biological sample, we next examined the basal levels of oxFAs circulating in mouse serum. Before HPLC-ESI-MS/MS analysis, the serum was subjected to a simple chloroform/methanol lipid extraction. While acidified extraction methods are frequently employed for more polar lipids, this was found to not be compatible with full-length oxFA species due to their acid lability (163). To correct for extraction efficiency, C17:0 was implemented as an internal standard. C17:0 has similar polarity and partitioning qualities as LA and AA but is not naturally occurring within mammalian cells, making it a viable internal standard for our purposes (185). The MS and HPLC conditions for the C17:0 sodium adduct were determined following the same procedure as for the oxFA species **(Figure 4-10)**.

Based on comparison of peak retention time and QIR to the oxFA standards, all NEFA and oxFA species were identified **(Figure 4-11A)**. The levels of circulating LA and AA were found to be 291 μM and 26 μM, respectively, matching previously measured concentrations in the literature **(Figure 4-11B)** (186–189). The concentrations of LA-derived HPODE, HODE, and KODE were found to be 45 nM, 2.2 μM, and 0.4 μM, respectively. HODE had the highest concentration, likely because it is the most stable of the three species. The concentrations of AA-derived HPETE, HETE, and KETE were found to be 161 nM, 600 nM, and 306 nM, respectively. Again, the hydroxyl product, HETE, was measured at the highest levels due to its increased stability. The sum of just these full-length oxidation products were found to compose approximately 1% of circulating LA, whereas they makeup approximately 4% of circulating AA. These results

correspond with our auto-oxidized time course where we demonstrated that AA oxidizes nearly four times as quickly as LA **(Figure 4-8, Figure 4-9)**. Based on these results, our method is capable of measuring full-length oxFA species in an isoform-independent manner in serum and can likely be extended to other biological samples.

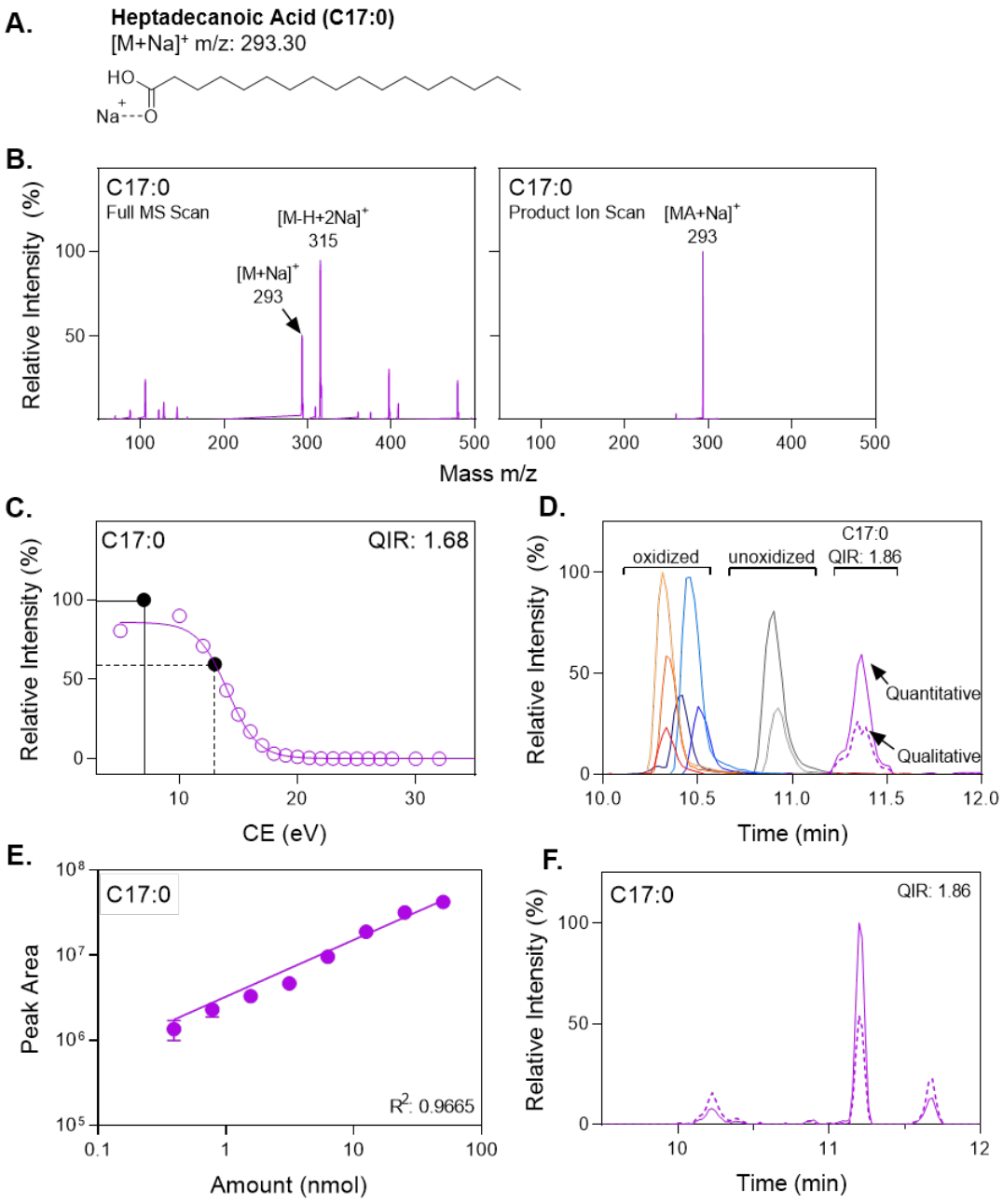


**Figure 4-10: Internal standard conditions and validation**

**Figure 4-10 Legend**

**A.** Chemical structure for the single sodium adduct of C17:0.

**B.** Direct infusion-MS/MS full MS scan of C17:0 standard (10 μM) in the presence of sodium ions (200 μM sodium acetate). Full MS scan in multi-channel analysis mode depicts 238 cumulative scans of 0.5 s. The molecular ion of interest (the single sodium adduct) is denoted $[M+Na]^+$. The double sodium adduct is denoted $[M-H+2Na]^+$. Product ion scan of C17:0 single sodium adduct from direct infusion of 10 μM standard in the presence of sodium ions (200 μM sodium acetate). Product ion scan in multi-channel analysis mode depicts 79 cumulative scans of 1.5 s. For both full MS and product ion scans, peak height is displayed relative to the intensity of the largest peak in the spectra.

**C.** The differential energy transition intensity curve fit with a sigmoidal non-linear regression. The intensities are displayed relative to the highest intensity transition. The collision energy (CE) yielding the highest intensity transition was designated as the quantitative transition (solid line). The CE yielding an intensity of roughly 50% of maximal was designated at the qualitative transition (dashed line). The differential energy curves were performed in triplicate with data expressed as mean ± SEM.

**D.** HPLC-MS/MS chromatogram of 10 μM standard mix of oxFA species. C17:0 quantitative (solid line) and qualitative transitions (dashed line) visualized with the calculated qualifier ion ratio (QIR). Peak height is displayed relative to the highest intensity peak in chromatogram.

**E.** HPLC-MS/MS calibration curve for C17:0. Linearity was achieved over a 5 $\log_{10}$ range with a high coefficient of determination ($R^2$ value). Quantification in samples was based on comparison to the curve. Calibration curve was performed in triplicate with data expressed as mean ± SEM.

**F.** Representative chromatogram of C17:0 in basal mouse serum samples. C17:0 quantitative (solid line) and qualitative transitions (dashed line) visualized with the calculated QIR. Peak height is displayed relative to the highest intensity peak in chromatogram.

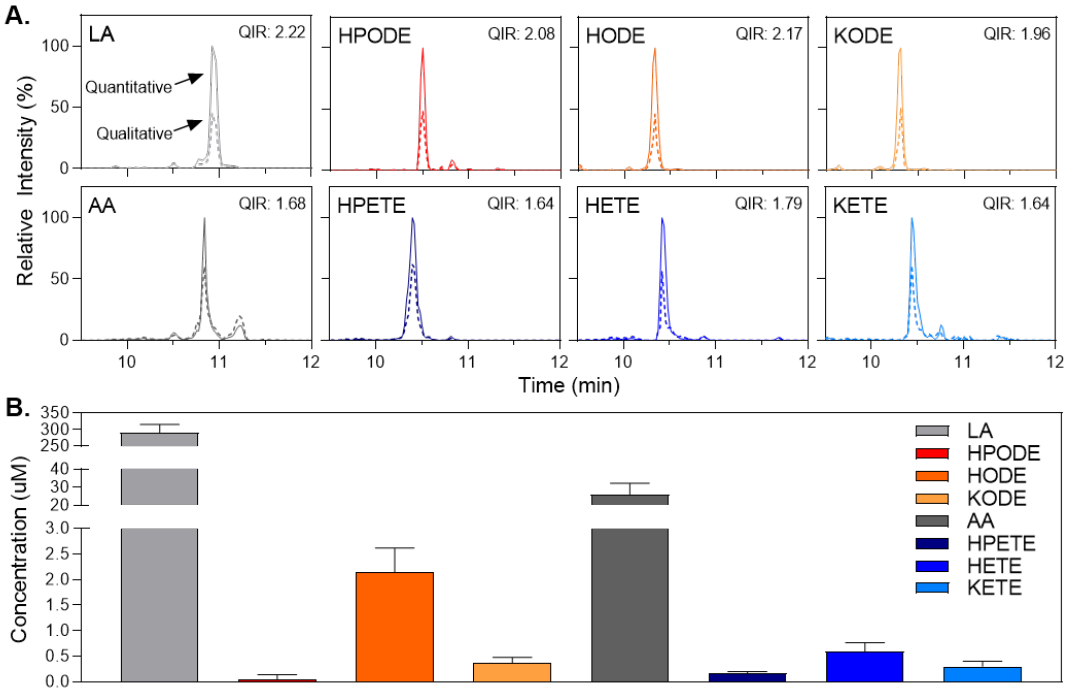


**Figure 4-11: Quantification of oxFA species in biological sample**

**Figure 4-11 Legend**

**A.** Representative chromatogram of oxFA in basal mouse serum samples. Quantitative (solid line) and qualitative transitions (dashed line) visualized with the calculated qualifier ion ratio (QIR). Peak height is displayed relative to the highest intensity peak in each chromatogram.

**B.** Concentration of oxFA in mouse serum. Blood was collected by cardiac puncture from anesthetized mice. Serum was isolated, subjected to a lipid extraction, and measured by HPLC-MS/MS. Data shown is from 12 mice and expressed as mean ± SEM.

## 4.4 DISCUSSION AND CONCLUSIONS

Despite the importance of oxFA as signaling molecules and their roles in the pathophysiology of metabolic disease, the development of HPLC-ESI-MS/MS methods to quantify these species has been slow. Recent methods developed to measure NEFA oxidation have focused heavily on identifying specific regioisomers either through an untargeted approach with only relative quantitation capability or through a targeted approach, of which some methods allow absolute quantitation (67, 159, 163–167, 171). However, it is likely that the sum total oxidation products, rather than the formation of one particular regioisomer, is more important in pathologies implicating chronic oxidative stress (45, 167). Unfortunately, methods focused on measuring these species irrespective of regioisomer rely predominantly on HPLC with chemiluminescence detection, which, while easily quantitated, is inherently limited in its specificity. These methods usually measure oxFA solely based on the oxidized moiety and are unable to distinguish between individual NEFA backbones (68, 168, 169). Therefore, a method that could quantitate specific oxFA in a regioisomer-independent manner would be highly biologically relevant. Our method represents significant progress toward this goal.

While it is true that untargeted methods allow for a far greater number of species to be monitored, these methods usually rely on relative quantitation, are amenable only to measurement of specific regioisomers, and are generally less facile to implement than targeted methods. Our targeted method outlined in this report is able to identify and absolutely quantify multiple full-length oxFA species independent of regioisomer with a relatively short runtime. We have shown our method is highly sensitive, without requiring time-consuming and destructive derivitization steps, due to the utilization of

sodium adducts to take advantage of positive-ion ionization and DiffE QIM to quantify based on regioisomer-independent, high intensity, pseudo-molecular transitions. The implementation of DiffE QIM also circumvents the difficulty of fragmentation since it does not rely on characteristic fragmentation. To our knowledge, this is the first study implementing DiffE QIM to measure oxFA, and based on our success measuring full-length oxFA, could likely be applied to other oxFA for regioisomer-independent quantification. Furthermore, our results in mouse serum indicate that our approach could be extended for oxFA quantification in other biological samples.

Additionally, as lipid oxidation frequently occurs on esterified fatty acids, this method could be readily applied to measuring the oxidized acyl chains of TAG and phospholipids with the addition of a lipase treatment to the sample preparation. This is of importance as we have previously shown that oxAA-containing phosphatidylcholine drives pro-inflammatory and antioxidant gene expression in macrophages, and these effects can be recapitulated with products of non-esterified AA oxidation (44). Numerous studies have identified distinct biological functions not only for a variety of individual oxidized lipids, but also for sets of oxidized lipids with similar functional moieties. Even so, prior to this study, there has not been a regioisomer-independent, targeted HPLC-ESI-MS/MS method with which to measure oxFA. Our method provides a simple and reliable means for measuring oxFA and elucidating their growing role in human disease. The ability to faithfully quantify individual oxFA, regardless of regioisomer, is a currently unmet need in the oxidized lipids field, and should be further pursued in order to measure oxFA in a robust and comprehensive manner in biological samples.

## ATTRIBUTION

Portions of this chapter (text and figures) were written as published in Ahern KW, Serbulea V, Wingrove CL, Palas, ZT, Leitinger N, Harris TE. Regioisomer-independent quantification of fatty acid oxidation products by HPLC-ESI-MS/MS analysis of sodium adducts. *Sci. Rep*. 2019 July 22.

## ACKNOWLEDGEMENTS

I want to thank Anne Schofield for donating her time as an editor of this manuscript. I would also like to thank the other members of the Harris and Leitinger labs for their continued support. This research was funded by NIH Cardiovascular Research Training Grant T32 HL0007284-41 (K.W.A.), American Heart Association Predoctoral Fellowship 17PRE33660609 (K.W.A.), NIH NRSA Predoctoral Fellowship 5F31DK108553-02 (V.S.), NIH R01 1R01DK096076 (N.L.), and NIH R01 1R01DK101946 (T.E.H.).

## AUTHOR CONTRIBUTIONS

The studies were designed by Katelyn Ahern, Dr. Thurl Harris, Dr. Vlad Serbulea, and Catherine Wingrove. Experimental work was performed Katelyn Ahern, Zachary Palas, and Catherine Wingrove. Data analysis was performed Katelyn Ahern, Zachary Palas, Dr. Vlad Serbulea, and Catherine Wingrove. The manuscript was written by Katelyn Ahern, Dr. Thurl Harris, and Dr. Vlad Serbulea. Funding was provided by Katelyn Ahern, Dr. Thurl Harris, Dr. Norbert Leitinger, and Dr. Vlad Serbulea.

# 5 CHAPTER 5: OXFA SERVE A CRITICAL ROLE IN PATHOLOGIES CHARACTERIZED BY INSULIN RESISTANCE

## 5.1 ABSTRACT

Oxidative stress has been implicated in the development of both acute and chronic insulin resistance, such as during acute stress and obesity, respectively. In addition, our previous work demonstrated a critical role for adipocyte lipolysis in the development of acute stress-induced impairments in insulin signaling through dissociation of the mTOR complexes. However, traditional lipolytic products were found to have no effect on mTOR complex activity. This led us to hypothesize that oxFA may be responsible for acute insulin resistance. Levels of oxFA were found to be increased in response to adipocyte lipolysis both *in vitro* and *in vivo*. Furthermore, the production of ROS was found to be critical for the mTOR complex inhibition, with antioxidants rescuing complex integrity and increased oxidative stress decreasing mTOR complex activity. Preliminary data suggest that the lipid responsible for mTOR complex inhibition is a product of oxLA. Because oxidative stress and oxPL have also been linked to obesity, we investigated the role of oxFA in the development of maladaptive phenotypes during obesity. Levels of oxFA were found to be increased with HFD. In addition, oxAA was capable of inducing changes to macrophage gene expression to the same extent as oxPL, including increases in inflammatory gene expression which is a hallmark of ATM in obesity. Taken together, our results provide evidence for an active role for oxFA in acute and chronic metabolic disturbances. Further studies are required to elucidate the mechanisms by with oxFA exert their effects in both acute stress and obesity.

## 5.2 INTRODUCTION

Impaired redox homeostasis and the production of ROS has been implicated in the development of chronic insulin resistance, such as type 2 diabetes, obesity, and cardiovascular disease (152–155, 190–194). One hallmark of oxidative stress is increased lipid oxidation (5, 156). While oxidized lipids can be produced enzymatically in a highly regulated fashion to form signaling molecules, in disease states, production of oxidized lipids by ROS during oxidative stress may surpass cellular control mechanisms, leading to destructive biological processes (45, 63–65, 67, 68). Due to the pathological implications, there has been much interest in studying the diverse species of the oxidized lipidome and their unique biological functions.

To this end, work from our collaborators demonstrated that obesity led to relative changes in the components of the oxidized lipidome (45). Specifically, HFD-induced increases in adiposity led to a disproportional increase in full-length oxPL compared to truncated oxPL species. This increase in full-length oxPL was observed within circulation as well as within the stromal vascular fraction of the adipose tissue itself. Furthermore, full-length oxPL were found to promote a pro-inflammatory gene expression within macrophages, another characteristic phenotype of obesity pathology (42, 195). However, it was not yet known whether other classifications of lipids within the oxidized lipidome, such as oxFA, also exhibited a shift towards full-length species during obesity. It was also unclear whether the intact oxPL or the oxFA was responsible for the phenotypic changes observed in macrophages.

In addition to pathologies of chronic insulin resistance, studies have implicated a critical role for ROS in the development of acute insulin resistance, such as during acute

stress caused by trauma, surgery, and critical illness (5). A study using the same HS mouse model as our acute stress studies demonstrated a correlation between levels of ROS and hepatic insulin sensitivity after HS (5). Furthermore, reduction of ROS levels by superoxide dismutase overexpression or antioxidant treatment rescued HS-induced hepatic insulin resistance. This data demonstrating the importance of ROS combined with our studies demonstrating the necessity of adipocyte lipolysis suggests a potentially critical role for oxidized lipids in the development of acute stress-induced peripheral insulin resistance.

We hypothesized that oxFA play a crucial role in pathologies characterized by insulin resistance, including acute cases such as during acute stress and chronic cases such as during obesity. To this end, we investigated whether oxFA are produced during adipocyte lipolysis and their acute effect on the insulin signaling cascade, specifically their ability to inhibit and dissociate the mTOR complexes. We also tested whether full-length oxFA are increased with HFD-feeding and whether oxFA are capable of inducing similar changes in macrophage phenotype, as is observed for oxPL.

## 5.3 RESULTS

### 5.3.1 Adrenergic-Induced Lipolysis Increases OxFA in Circulation

We demonstrated that adipocyte lipolysis is necessary for the development of acute stress-related insulin resistance. Previous research demonstrated a critical role for ROS production in the development of stress-induced hepatic insulin resistance (5). As such, we hypothesized that oxFA may be produced during adrenergic-stimulated adipocyte lipolysis and released into circulation to promote peripheral resistance. To test this, we employed our novel HPLC-MS/MS method based on DiffE QIM and sodium

adducts to identify and quantify the production of oxFA during lipolysis. For this purpose, we again utilized the 3T3-L1 mouse cell line as an *in vitro* model of adipocytes. Differentiated 3T3-L1 adipocytes were treated with ISO to stimulate β-adrenergic receptors leading to the potent induction of lipolysis (52). The cellular media was collected 0, 15, and 45 min after treatment, and lipolysis was confirmed by the release of the products NEFA and glycerol **(Figure 5-1A)**. When measured by HPLC-MS/MS, all the oxFA species of interest, except HPETE, were found to be present in the cellular media after induction of lipolysis based on peak retention time and QIR **(Figure 5-1B)**. The lack of HPETE in our cultured cell sample is likely due to its high reactivity and cellular peroxidase-driven breakdown to HETE (196). We observed significant increases in the level of oxFA by 15 min after induction of lipolysis, and these levels were maintained or continued to increase as quantified at 45 min **(Figure 5-1C)**. These results indicate that oxFA are quickly produced and released during adipocyte lipolysis.

To confirm the production and release of these oxFA species into circulation *in vivo*, we injected WT mice i.p. with CL316,243, a specific $\beta_3$-adrenergic receptor agonist ($\beta_3$-adrenergic receptors are primarily expressed on adipose tissue in rodents), to stimulate adipocyte lipolysis (197). Serum was collected 15 min after CL316,243 injection, and lipolysis was confirmed by measurement of the products NEFA and glycerol **(Figure 5-2A)**. After 15 min of CL316,243 stimulation, NEFA levels were significantly increased in circulation indicating induction of lipolysis, but glycerol levels were unchanged. This is not unexpected given the short time period being tested. Glycerol is only released after cleavage of all three fatty acid tails and thus increases in circulating glycerol lag NEFA levels. When the serum was measured by HPLC-MS/MS,

all of the oxFA species of interest were found to be present in the serum **(Figure 5-2B)**. Furthermore, the levels of the oxLA species HPODE and KODE were significantly increased in 15 min with HODE trending towards increased. A similar profile was observed for the oxAA species with HPETE and KETE significantly increased in circulation compared to vehicle-treated mice. Taken together, these studies suggest that oxFA are rapidly produced and released into circulation during adrenergic-stimulated adipocyte lipolysis, such as during acute stress.

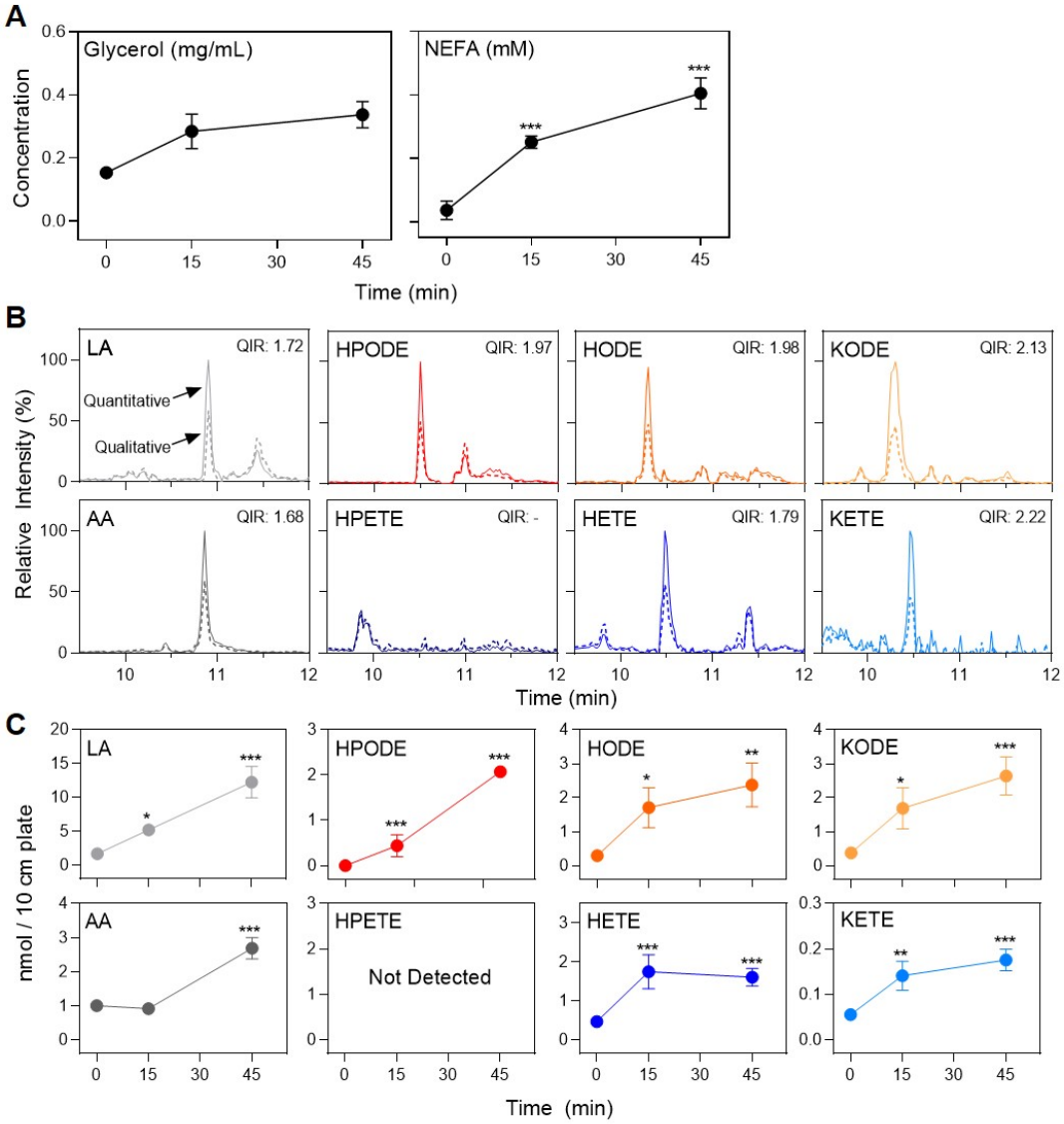


**Figure 5-1: Adrenergic-stimulated lipolysis in adipocytes produces oxFA**

**Figure 5-1 Legend**

**A.** Glycerol and NEFA levels in the media of 3T3-L1 adipocytes serum-starved in high glucose DMEM + 0.5% FA-free BSA for 1 h before being treated with 10 μM ISO. Media was collected after 0, 15, and 45 min of treatment. Glycerol and NEFA were measured in the media using their respective kits.

**B.** Representative chromatogram of oxFA measured by HPLC-MS/MS in media of 3T3-L1 adipocytes treated as in A. Quantitative (solid line) and qualitative transitions (dashed line) visualized with the calculated QIR. Peak height is displayed relative to the highest intensity peak in each chromatogram.

**C.** Levels of oxFA determined by HPLC-MS/MS released into media from 3T3-L1 adipocytes treated as in A.

$N = 4$. Data are shown as mean ± SEM. $*P < 0.05$, $**P < 0.01$ and $***P < 0.001$, as indicated. Statistical analyses were performed using one-way ANOVA. All comparisons differing by one variable were made and adjusted for with ANOVA, and all significant comparisons are denoted as such.

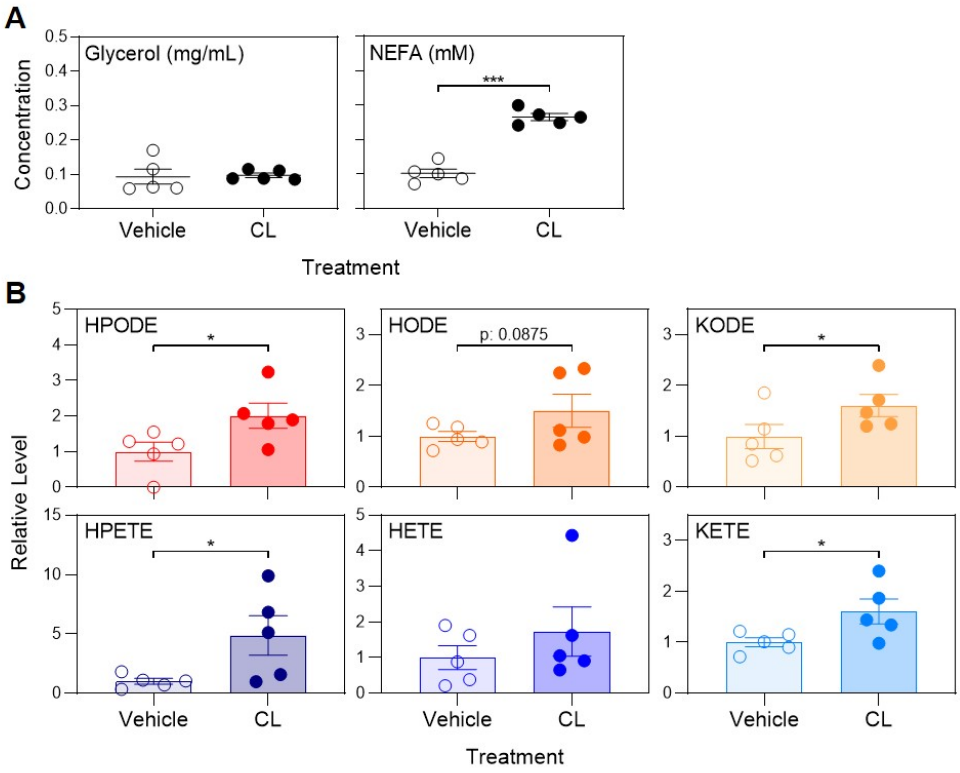


**Figure 5-2: Adipocyte lipolysis increases levels of oxFA in circulation *in vivo***

**Figure 5-2 Legend**

**A.** Glycerol and NEFA levels in the serum of WT mice fasted 4 h and i.p. injected with either with vehicle or 5 mg/kg CL316,243. After 15 min, blood was collected. Glycerol and NEFA were measured in the media using their respective kits.

**B.** Relative levels of oxFA determined by HPLC-MS/MS in serum of WT mice treated as in A.

$N = 5$. Data are shown as mean ± SEM. $*P < 0.05$ and $***P < 0.001$, as indicated. Statistical analyses were performed using an unpaired t-test. All significant comparisons are denoted as such.

### 5.3.2 Oxidized Lipolytic Products Inhibit mTOR Complex Activity

Our previous work demonstrated that adrenergic-stimulated lipolysis inhibits insulin signaling in adipocytes through mTOR complex inhibition and dissociation. However, while lipolytic products can disrupt the mTOR complexes, typical products such as DAG, MAG, and NEFA had no effect. This led us to hypothesize that a specialized product of lipolysis may be responsible, such as an oxFA. To test whether oxidized lipid production is necessary, we pretreated adipocytes with either vehicle or an antioxidant: TBAP, a superoxide dismutase mimic, or EUK, a ROS scavenger. We then treated with combinations of insulin and FSK and immunoblotted for mTOR complex-catalyzed phosphorylation events in the insulin signaling cascade **(Figure 5-3A)**. The lipolysis pathway was stimulated by FSK treatment as seen by increases in $pHSL^{S563}$. Furthermore, treatment with FSK inhibited mTORC1-catalyzed $pS6k^{T389}$ and mTORC2-catalyzed $pAkt^{S473}$. However, insulin signaling was rescued after pretreatment with either TBAP or EUK, complementary to previous findings that *in vivo* antioxidant treatment during acute stress prevented peripheral insulin resistance (5). We next tested whether pretreatment with antioxidants prevented the production of lipolytic products capable of dissociating the mTOR complexes **(Figure 5-3B)**. We again pretreated differentiated adipocytes with vehicle or an antioxidant, TmPyP, a superoxide dismutase mimic, or EUK, before treatment with FSK. Lipids were extracted and included in our *in vitro* mTOR complex dissociation assay with Venus-tagged mTOR and Cerulean-tagged raptor. As in our previous experiments, FSK-stimulated cells produced lipids that resulted in mTOR complex dissociation. However, pretreatment with either TmPyP or EUK prevented the production of lipids with dissociating activity, even with FSK treatment. Since treatment with antioxidants rescues mTOR complex association and adipocyte

insulin signaling, we next investigated whether stimulating ROS production further exacerbated mTOR complex inhibition. Differentiated 3T3-L1 adipocytes were pretreated with TBH, an oxidizing agent, before stimulation with FSK. Lipids were extracted and included in an *in vitro* mTOR complex kinase assay **(Figure 5-3C)**. As in our previous experiments, treatment with FSK resulted in lipids that were capable of inhibiting mTOR complex activity. In addition, pretreatment with TBH resulted in further inhibition. However, TBH alone was not sufficient to produce inhibitory lipids and lipolysis stimulation was still required to inhibit mTOR complex activity. Taken together, these data suggest that ROS play a critical role in the production of lipolytic products capable of inhibiting the mTOR complexes.

Using our HPLC-MS/MS method, we demonstrated that oxFA are produced by adipocyte lipolysis *in vitro* and *in vivo*. We next wanted to test whether isolated oxFA are capable of inhibiting mTOR complex. We included either vehicle, LA, or auto-oxidized LA in an *in vitro* mTOR complex kinase assay **(Figure 5-3D)**. We observed that high doses of oxLA were capable of inhibiting mTOR activity compared to vehicle or LA. While 100 μM may seem like a supraphysiological level of oxLA, it is worth noting that the concentration is based on the starting amount of LA subjected to auto-oxidation. Our data and previous literature have shown basal circulating levels of LA to be around 250 μM. Furthermore, the oxLA used in the kinase assay is a mixture of LA oxidation products. It is likely that the oxFA species with inhibitory activity is present at a much lower concentration. Taken together, these studies demonstrate that oxidation is critical for the production of mTOR complex-inhibiting lipolytic products. In addition, we provide preliminary data suggesting that the species responsible is an oxFA.

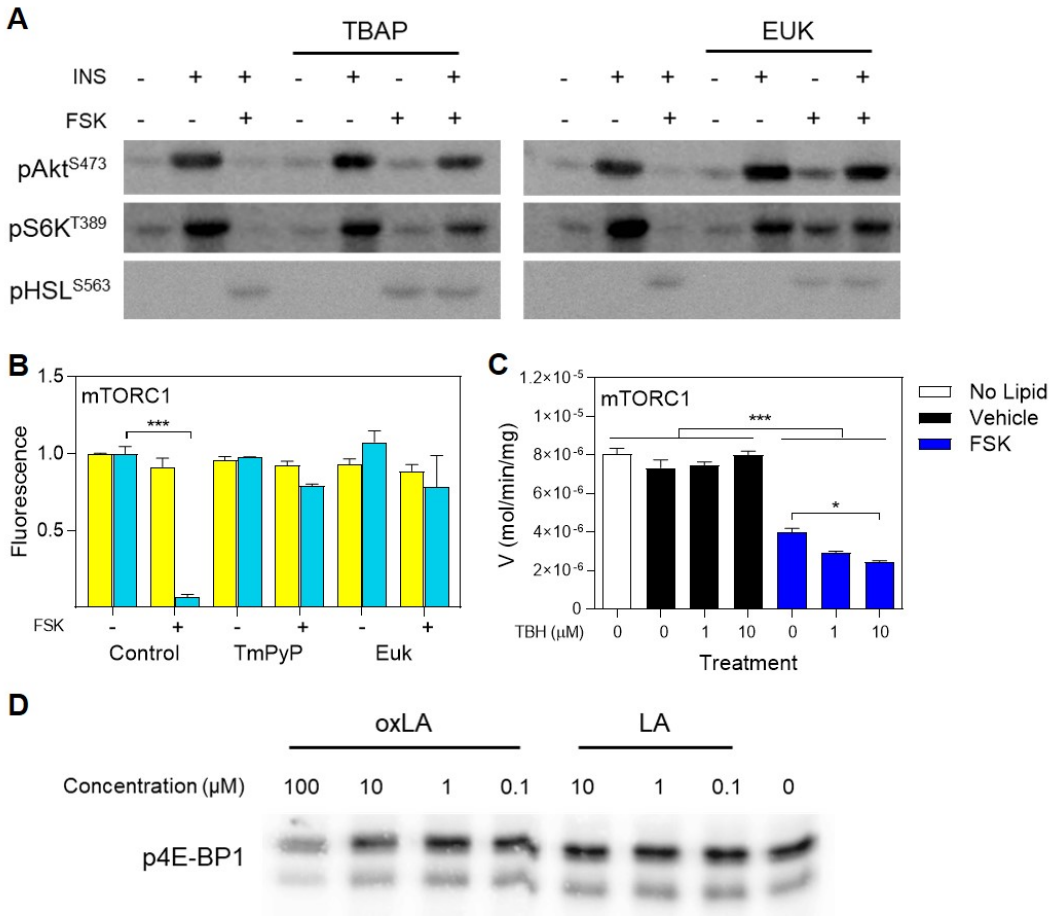


**Figure 5-3: OxFA inhibit mTOR complex activity through complex dissociation**

**Figure 5-3 Legend**

**A.** Representative immunoblots of 3T3-L1 adipocytes incubated with or without 100 μM TBAP or 100 μM EUK before treatment with or without 10 μM forskolin (FSK) for 10 min then treatment with or without 10 nM insulin (INS) for 15 min.

**B.** mTOR complex integrity determined by *in vitro* mTOR complex dissociation assay. Lipids were extracted from 3T3-L1 adipocytes incubated with vehicle, 100 μM TmPyP, or 100 μM EUK before treatment with or without 10 μM FSK. Purified fluorescently-tagged mTORC1 was incubated with either extracted lipids for 30 min before washing and detection of fluorescence.

**C.** mTOR complex activity determined by radioactive *in vitro* kinase assay. Lipids were extracted from cultured 3T3-L1 adipocytes that were incubated with TBH overnight at the noted concentration before treatment with or without 10 μM FSK for 30 min. Kinase assay was carried out using purified recombinant mTORC1 with 4E-BP1 as substrate. Extracted lipids were added to the assay 10 min before the addition of [$\gamma$-$^{32}$P]-ATP.

**D.** Representative phosphoimage of substrate from radioactive *in vitro* kinase assay. Kinase assay was carried out as in C.

$N = 3$. Data are shown as mean ± SEM. $*P < 0.05$ and $***P < 0.001$, as indicated. Statistical analyses were performed using two-way ANOVA. All comparisons differing by one variable were made and adjusted for with ANOVA, and all significant comparisons are denoted as such.

### 5.3.3 Obesity Elevates Levels of OxFA Species Capable of Disturbing Adipose Tissue Macrophage Function

Obesity is associated with adipose tissue dysfunction, including elevated oxidative stress, changes in adipocyte metabolism, and increased inflammation from ATM (42, 43, 154, 195). Previous collaborative studies using HPLC-MS/MS to measure oxPL levels in the stromal vascular fraction showed that HFD-induced increases in adiposity lead to a disproportionate increase in full-length species compared to truncated species (45). When the effect on macrophages was tested *in vitro*, these full-length oxPL induced macrophage phenotypes characteristic of obesity, including increased proinflammatory gene expression (45). However, it was not yet known whether this increase in full-length species was specific to oxPL or other oxidized lipids as well, particularly oxFA. Furthermore, it had yet to be studied whether the oxidized moiety of the oxPL alone was capable of inducing the same macrophage phenotypic changes. To assess the prevalence of full-length oxFA in obesity, we used our HPLC-MS/MS method to measure oxFA levels in serum of HFD-fed mice **(Figure 5-4A)**. We observed significantly increased levels of KODE and HETE with a trend towards increased levels of HPETE, indicating the full-length oxFA species increase with HFD-induced adiposity. Because oxAA species were particularly elevated, we tested the effect oxAA treatment on macrophages *in vitro* **(Figure 5-4B)**. We found that oxAA increased antioxidant, inflammatory, and metabolic gene expression to largely the same extent as oxPL treatment. Taken together, these results indicate that full-length species of oxidized lipids increase during obesity, including oxPL and oxFA, and that the oxFA moiety is responsible for the effects of oxPL exposure on macrophage phenotype.

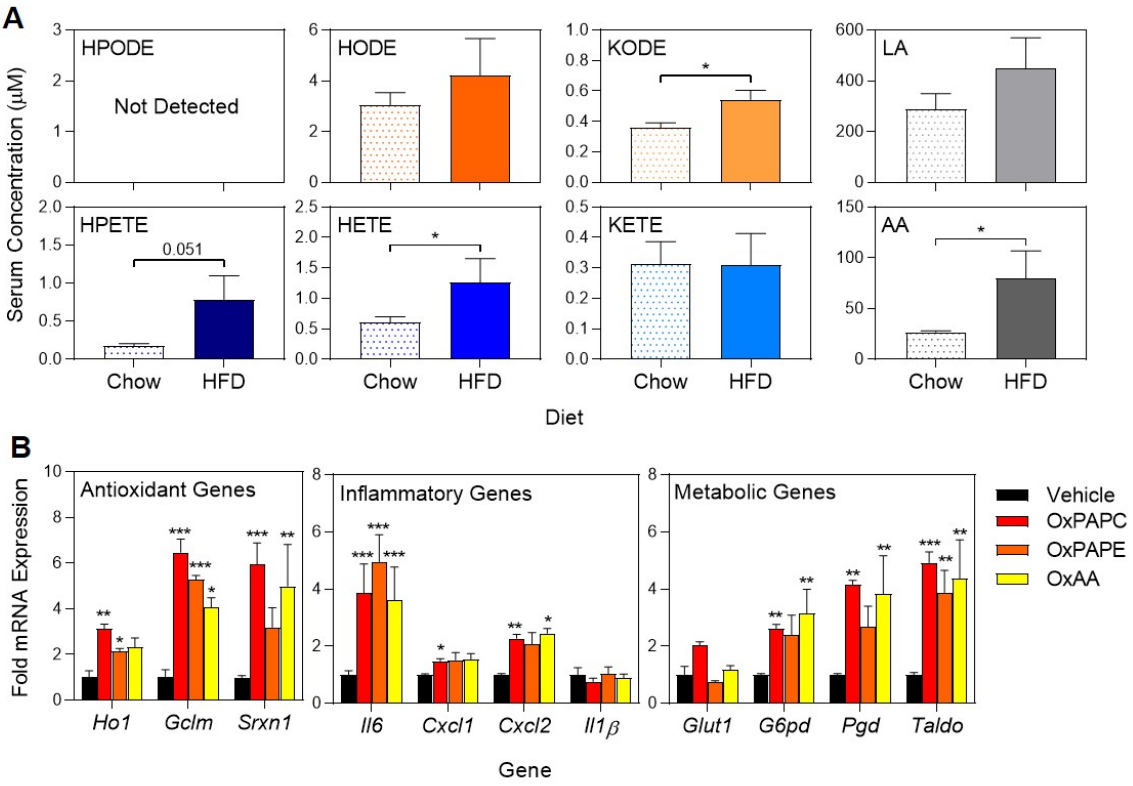


**Figure 5-4: OxFA increase with HFD and affect macrophage gene expression**

**Figure 5-4 Legend**

**A.** OxFA levels determined by HPLC-MS/MS in the serum of WT mice fed chow or HFD for 12 weeks. Mice were fasted 4 h before blood was collected.

**B.** Relative mRNA expression measured by qPCR of antioxidant, inflammatory, and metabolic genes in bone marrow-derived macrophages treated with vehicle, 6.4 μM oxPAPC, 6.4 μM oxPAPE, or 6.4 μM oxAA for 4 h.

$N$ = 3-4. Data are shown as mean ± SEM. *$P < 0.05$, **$P < 0.01$ and ***$P < 0.001$, as indicated. Statistical analyses of MS data were performed using unpaired t-test. Statistical analyses of qPCR data were performed using two-way ANOVA. All comparisons differing by one variable were made and adjusted for with ANOVA. All significant comparisons are denoted as such.

## 5.4 DISCUSSION AND CONCLUSIONS

In response to surgery and HS, previous studies have shown that oxidative stress increases, correlates with insulin sensitivity, and is required for the development of stress-induced insulin resistance. Our data further demonstrate that adipocyte lipolysis is necessary for the development of peripheral insulin resistance. As such, we hypothesized that oxidized lipids would be increased in response to adrenergic-stimulated lipolysis during acute stress. Indeed, levels of oxFA were found to be increased in response to adipocyte lipolysis both *in vitro* and *in vivo*. Adipocytes have vast stores of TAG in the form of lipid droplets, and we and others have found that, even under basal conditions, there is a considerable quantity of oxidized esterified acyl chains on TAG (198). It is possible during lipolysis that these oxidized acyl chains are hydrolyzed and released into the cell as oxFA. However, we cannot rule out the possibility that these oxFA are produced by oxidation after hydrolysis. While it is likely that both oxFA production mechanisms contribute to the increase observed after lipolysis, more studies are needed to determine the level of contribution from each pathway. Of note, we measured increased oxFA in extracellular media and in circulation. Our data does not delineate whether these oxFA are produced in the cell, such as from hydrolysis of oxidized TAG, and exported, or if the NEFA are exported from the cell and become oxidized in circulation. Again, further studies are needed to determine the potential method of export and degree of contribution from each oxFA production mechanism.

In addition, our previous work demonstrated a critical role for adipocyte lipolysis in the development of impairments in insulin signaling through dissociation of the mTOR complexes. However, traditional lipolytic products were found to have no effect on

mTOR complex activity. This led us to hypothesize that oxFA may be responsible for acute insulin resistance. The production of ROS was found to be critical for mTOR complex inhibition with antioxidants rescuing complex integrity and increased oxidative stress decreasing mTOR complex activity. Preliminary data suggest that the lipid responsible for mTOR complex inhibition is a product of oxLA. Further studies are needed to confirm that an oxLA species is responsible and which species have mTOR complex inhibition activity. Currently, our data does not provide a mechanism for how oxFA species dissociate the mTOR complexes. Previous studies have shown that phosphatidic acid binds directly to the rapamycin-FKBP12 binding domain of mTOR and positively regulates activity (71, 199). It is hypothesized that phosphatidic acid activates mTOR complexes through strengthening the association of the complex, and that the mTOR complexes dissociate in the absence of phosphatidic acid. Therefore, it is possible that the oxFA competes with phosphatidic acid for binding to mTOR, thus resulting in complex dissociation. Further studies are needed to test this potential mechanism.

Because oxidative stress and oxPL have also been linked to obesity, we also investigated the role of oxFA in the development of maladaptive phenotypes during obesity. Previous work by our collaborators demonstrated that, while obesity led to an overall increase in the fraction of phospholipid species that were oxidized, there was a disproportional increase in full-length oxPL compared to truncated oxPL species (45). Our data show that levels of full-length oxFA increased with HFD feeding, corroborating data that oxidized lipids increase overall with obesity. However, we did not measure truncated oxFA species. These species would need to be measured in order to determine whether full-length oxFA species disproportionately increase, similar to what is observed

in oxPL. In addition, we observed that oxAA was capable of inducing changes to macrophage gene expression to the same extent as oxPL, including increases in inflammatory gene expression which is a hallmark of ATM in obesity. More studies are needed to determine if oxAA are capable of inducing other phenotypic changes mediated by oxPL, such as changes in mitochondrial respiration and glycolytic capacity.

In summary, we demonstrated that levels of oxFA are increased in circulation *in vitro* and *in vivo* in response to acute adrenergic-stimulated lipolysis. Our data suggest that oxFA produced by adipocyte lipolysis may be responsible for mTOR complex inhibition. When we investigated in the chronic condition of obesity, levels of oxFA were found to be increased with HFD feeding. In addition, oxAA was capable of inducing changes to macrophage phenotype, such as is observed *in vivo* in obese animals. Taken together, our results provide evidence for an active role for oxFA in acute and chronic metabolic disturbances. Further studies are required to elucidate the mechanisms by which oxFA exert their effects in both acute stress and obesity.

## ATTRIBUTION

Portions of this chapter (text and figures) were written as published in Ahern KW, Serbulea V, Wingrove CL, Palas, ZT, Leitinger N, Harris TE. Regioisomer-independent quantification of fatty acid oxidation products by HPLC-ESI-MS/MS analysis of sodium adducts. *Sci. Rep*. 2019 July 22. Portions of this chapter (text and figures) were sampled from Serbulea V, Upchurch CM, Ahern KW, Bories G, Voigt P, DeWeese DE, Meher AK, Harris TE, Leitinger N. Macrophages sensing oxidized DAMPs reprogram their metabolism to support redox homeostasis and inflammation through a TLR2-Syk-ceramide dependent mechanism. *Mol Metab*. 2017 November 7.

## ACKNOWLEDGEMENTS

This research was funded by NIH Cardiovascular Research Training Grant T32 HL0007284-41 (K.W.A.), American Heart Association Pre-doctoral Fellowship 17PRE33660609 (K.W.A.), NIH Pharmacological Sciences Training Grant T32 GM007055-40 (V.S.), NIH NRSA Predoctoral Fellowship 5F31DK108553-02 (V.S.), American Heart Association Predoctoral Fellowship 15PRE255600036 (V.S.), SFRBM Mini-Fellowship (V.S.), UVA Double-Hood Research Award (V.S. and D.E.D.), NIH Pharmacological Sciences Training Grant T32 GM007055-43 (C.M.U.), National Scientist Development Grant 14SDG20380044 (A.K.M.), NIH R01 1R01DK096076 (N.L.), P01 HL120840 (N.L.), and NIH R01 1R01DK101946 (T.E.H.).

## AUTHOR CONTRIBUTIONS

The studies were designed by Katelyn Ahern, Dr. Thurl Harris, Dr. Norbert Leitinger, Dr. Garrett Mullins, Dr. Vlad Serbulea, and Catherine Wingrove. Experimental work was performed by Nicole Aaron, Katelyn Ahern, Dr. Gael Bories, Hannah Chung, Dory DeWeese, Dr. Akshaya Meher, Dr. Garrett Mullins, Zachary Palas, Dr. Vlad Serbulea, Clint Upchurch, Paxton Voigt, and Catherine Wingrove. Data analysis was performed by Katelyn Ahern, Dr. Gael Bories, Hannah Chung, Dory DeWeese, Dr. Garrett Mullins, Zachary Palas, Dr. Vlad Serbulea, Clint Upchurch, Paxton Voigt, and Catherine Wingrove. The manuscripts were written by Katelyn Ahern, Dr. Thurl Harris, Dr. Norbert Leitinger, and Dr. Vlad Serbulea. Funding was provided by Katelyn Ahern, Dory DeWeese, Dr. Thurl Harris, Dr. Norbert Leitinger, Dr. Akshaya Meher, Dr. Vlad Serbulea, and Clint Upchurch.

# 6 CHAPTER 6: THE ADIPOKINE RESISTIN IS ACUTELY RELEASED DURING CATECHOLAMINE-INDUCED LIPOLYSIS

## 6.1 ABSTRACT

Resistin, an adipose-derived hormone, has been linked to the development of chronic insulin resistance in both humans and rodents. However, little effort has been put towards investigating whether resistin is released acutely and its potential involvement in transient insulin resistance. We previously demonstrated *in vivo* that resistin is released in a surgery- and lipolysis-dependent manner. When we further investigated this mechanism *in vitro*, we observed a significant, lipolysis-dependent release of resistin from adipocytes into the media. Furthermore, overnight pretreatment with the antioxidant EUK prevented lipolysis-dependent resistin secretion, suggesting a role for oxidized lipid signaling in the acute release of resistin.

In humans, the development of acute stress-induced metabolic disturbances has been well-documented in cardiovascular disease-associated events. In a pressure overload-induced heart failure model, we demonstrated that inhibiting lipolysis reduced circulating levels of resistin. In the context of myocardial infarction, we found that circulating resistin levels spiked during ischemia and again during recovery. Interestingly, while obese mice had higher basal levels of resistin, they did not exhibit a spike during ischemia and had more stable resistin levels over the course of recovery. Based on these studies, we propose that resistin is acutely released in response to products of stress-stimulated lipolysis. By elucidating this mechanism, our work could

provide insight into the role of resistin in the development of acute and chronic insulin resistance.

## 6.2 INTRODUCTION

Severe trauma activates an acute stress response which results in systemic insulin resistance and hyperglycemia, even in patients without prior history of diabetes (1–4, 115). While a variety of trauma and critical illness can stimulate the acute stress response, cardiovascular events and surgery have been well-documented to cause metabolic impairments in humans (2–4). Previous studies have shown that hyperglycemia during cardiopulmonary bypass surgery is an independent risk factor for death and complications, even in nondiabetic patients (3). In addition, a 50% decrease in insulin sensitivity after cardiac surgery increased the risk of major complications by more than 5-fold and the risk of severe infection by more than 10-fold (2, 4). This is particularly worrisome because patients can lose up to 90% of insulin sensitivity during major surgery (2). Though controlling surgery-induced metabolic impairments is of clear clinical importance, the mechanism underlying the development of stress-induced insulin resistance is largely unknown. Our work has shown that adipocyte lipolysis is necessary for the development of hyperglycemia and insulin resistance during HS and surgery. This observation is supported by previous studies which demonstrated a role for adipose tissue and lipolysis during cardiovascular stress, such as heart failure (200, 201). Interestingly, our data also suggested a novel role for resistin which we found to be released in a stress- and lipolysis-dependent manner.

Resistin is an adipocytokine that is released by adipocytes in rodents (84–88). Resistin acquired its name due to its initial association with the development of insulin

resistance (84, 87). Initial characterization of resistin showed that circulating levels were increased in mouse models of obesity. Manipulating levels of resistin altered blood glucose and insulin function (84). For example, administration of recombinant resistin impaired glucose tolerance and led to insulin resistance while treatment with an anti-resistin antibody improved blood glucose and insulin sensitivity. Interestingly, while circulating levels of resistin have been shown to also increase in obesity in humans, resistin was found to be secreted by macrophages in humans as opposed to adipocytes (86–88). In humans, resistin is associated with inflammation rather than adiposity (87). However, a characteristic of obesity is increased basal inflammation and infiltration of macrophages into adipose tissue. Furthermore, inflammatory cytokines have previously been linked to the development of insulin resistance (89). As such, it is possible that, despite differences in tissue secretion, resistin still affects insulin sensitivity in humans. Of note, despite being discovered two decades ago, the regulation, mechanism, and receptor of resistin remain unknown.

Due to its initial characterization in chronic conditions such as obesity and type 2 diabetes, little attention has been focused toward the potential acute role for resistin. However, recent studies on the acute stress response in humans have demonstrated a correlation between circulating resistin and trauma or critical illness, with higher levels of resistin associated with worse outcomes (90–97). Our data corroborate these studies by demonstrating a stress-dependent, rapid release of resistin, as we see significant increases in circulating resistin within our 30-min HS model. Furthermore, our data suggest a novel lipolysis-dependent regulation of acute resistin release.

In this study, we sought to confirm and further elucidate the mechanism of acute resistin release from adipocytes and its dependence on TAG lipolysis. Using a mouse adipocyte cell line, we stimulated lipolysis with catecholamines to promote resistin release and pharmacologically inhibited lipolysis to block release. As acute stress frequently prompts oxidative stress within tissues which has been linked to impairments in insulin signaling, we investigated the effect of blocking ROS using antioxidants and the potential effect on resistin release. As humans are known to develop a strong acute stress response during cardiovascular events and surgery, and mouse studies have demonstrated that lipolysis plays an important role in regulating metabolism and recovery during these events, we investigated *in vivo* whether cardiovascular stress stimulates lipolysis-dependent, acute release of resistin. We specifically investigated in the context of heart failure and myocardial infarction. As both of these cardiovascular stressors are common in patients with obesity and given the strong link between resistin and obesity, we further investigated the effect of diet-induced obesity on the time course of resistin release after myocardial infarction. Our *in vitro* and *in vivo* studies to elucidate the mechanism regulating release as well as the profile of release during cardiovascular stress could provide insight into the role of resistin in the development of insulin resistance.

## 6.3 RESULTS

### 6.3.1 Adipocytes Acutely Release Resistin in a Lipolysis-Dependent Manner

Numerous clinical studies observed correlations between circulating resistin levels and the development of stress-induced metabolic dysfunction and morbidity (91–97). Our acute stress studies corroborate a strong relationship between resistin and stress-induced insulin resistance. Furthermore, our *in vivo* data support a lipolysis-mediated

mechanism of acute resistin release. To more definitively test this mechanism, we assessed the release of resistin in response to catecholamine-stimulated lipolysis *in vitro*. Differentiated 3T3-L1 adipocytes were treated with vehicle or ISO to stimulate β-adrenergic receptors and subsequent lipolysis (52). Media was collected at 0, 30, and 120 min after stimulation, and lipolysis was confirmed by the release of the products glycerol and NEFA **(Figure 6-1A)**. When measured by ELISA, the amount of resistin released into the media was significantly increased after 120 min of ISO-stimulated lipolysis, compared to media of vehicle-treated cells that did not undergo significant lipolysis **(Figure 6-1B)**. This significant increase in media resistin levels was visualized and corroborated by immunoblot **(Figure 6-1C)**. Resistin release into the media lagged the release of lipolytic products, which were already significantly elevated at 30 min. This observation, combined with the robust release of resistin in response to ISO treatment, further substantiates our hypothesis of a lipolysis-dependent mechanism of release.

To determine whether lipolysis is necessary for the acute release of resistin, we pretreated the 3T3-L1 adipocytes with the ATGL inhibitor atglistatin before treatment with either vehicle, ISO, or FSK to stimulate lipolysis. Media was collected at 0, 120, and 240 min. We again assessed induction of lipolysis by measuring the release of glycerol and NEFA **(Figure 6-2A)**. Both lipolytic products were significantly increased in the media after 120 min of stimulation with ISO or FSK compared to vehicle. Atglistatin treatment substantially blunted lipolysis, though levels of lipolysis in the presence of atglistatin were still higher than for vehicle-treated cells. When measured by ELISA, the amount of resistin released into the media was significantly increased after 120 min and was substantially increased compared to media of vehicle- or atglistatin-treated cells after

240 min **(Figure 6-2B)**. While the level of resistin in the media did significantly increase over time in vehicle- and atglistatin-treated cells, this is likely due to the incomplete suppression of lipolysis. When visualized by immunoblot, the increased levels of resistin in the media with ISO and FSK at 120 and 240 min measured by ELISA was corroborated **(Figure 6-2C)**. Additionally, atglistatin noticeably blunted the level of resistin in the media when visualized by immunoblot. Taken together, this data suggests that adrenergic-stimulation is sufficient to induce acute release of resistin, and lipolysis is necessary for that release.

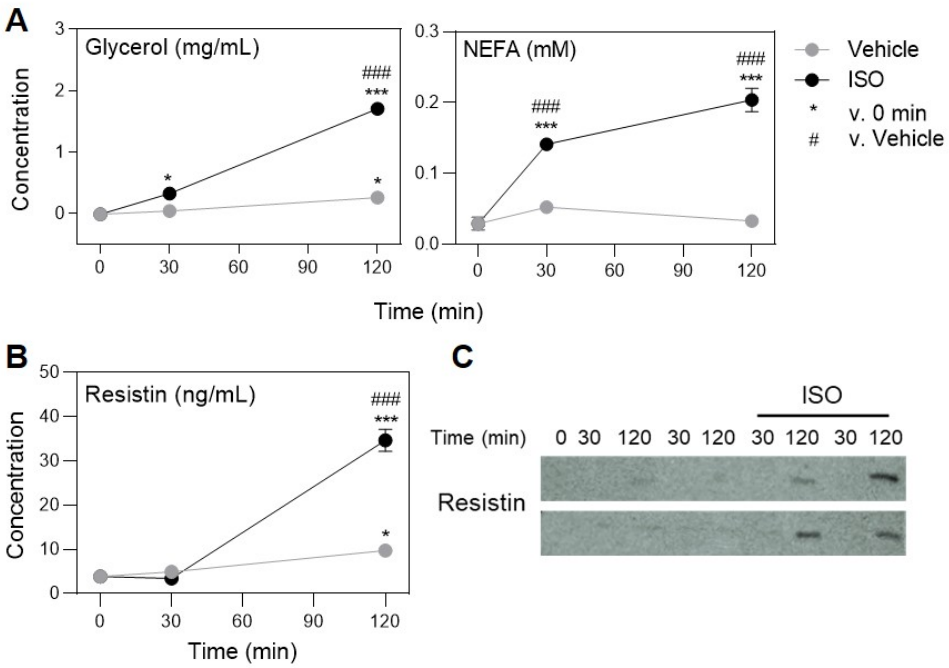


**Figure 6-1: Catecholamines stimulate lipolysis and acute release of resistin**

**Figure 6-1 Legend**

**A.** Glycerol and NEFA levels in the media of 3T3-L1 adipocytes treated with 1 μM isoproterenol (ISO) in low-glucose DMEM supplemented with 2% FA-free BSA. Media was collected after 0, 30, and 120 min of treatment. Glycerol and NEFA were measured in the media using their respective kits.

**B.** Resistin levels determined by ELISA in the media of 3T3-L1 adipocytes treated as in A.

**C.** Representative immunoblots of the media of 3T3-L1 adipocytes treated as in A.

$N$ = 3-7. Data are shown as mean ± SEM. *$P$ < 0.05 and ***$P$ < 0.001, as indicated. Statistical analyses were performed using two-way ANOVA. All comparisons differing by one variable were made and adjusted for with ANOVA, and all significant comparisons are denoted as such.

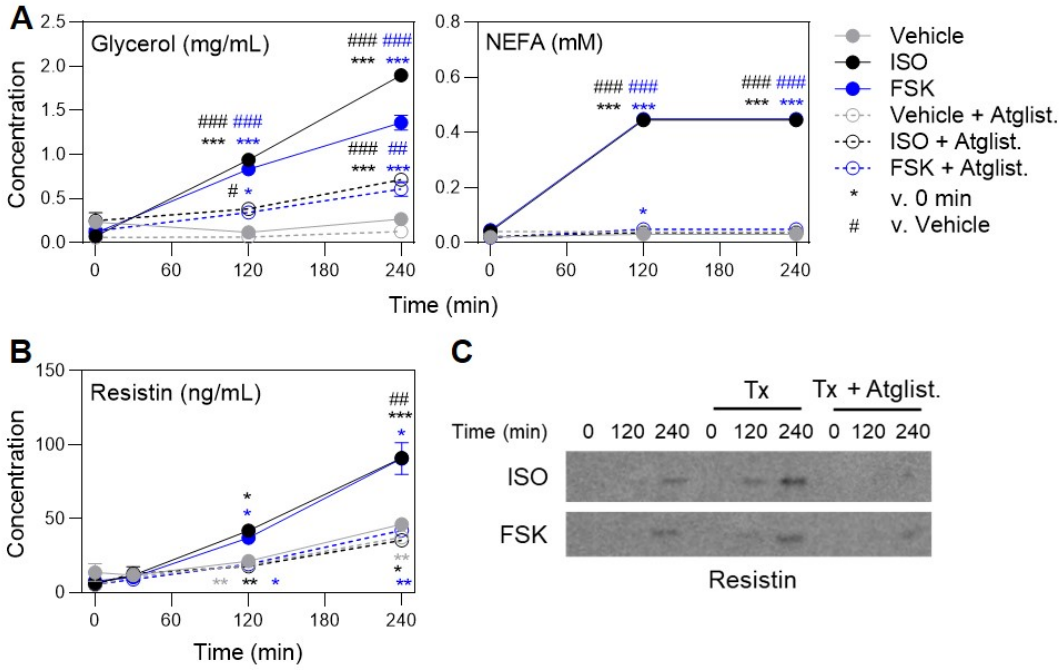


**Figure 6-2: Lipolysis is necessary for adrenergic-stimulated release of resistin**

**Figure 6-2 Legend**

**A.** Glycerol and NEFA levels in the media of 3T3-L1 adipocytes were pretreated with 10 μM atglistatin for 1 h before treatment with 1 μM isoproterenol (ISO) or 10 μM forskolin (FSK) in low-glucose DMEM supplemented with 2% fetal bovine serum. Media was collected after 0, 30, 120, and 240 min of treatment. Glycerol and NEFA were measured in the media using their respective kits.

**B.** Resistin levels determined by ELISA in the media of 3T3-L1 adipocytes treated as in A.

**C.** Representative immunoblots of the media of 3T3-L1 adipocytes treated as in A.

$N = 3$. Data are shown as mean ± SEM. $*P < 0.05$, $**P < 0.01$, and $***P < 0.001$, as indicated. Statistical analyses were performed using two-way ANOVA. All comparisons differing by one variable were made and adjusted for with ANOVA, and all significant comparisons are denoted as such.

### 6.3.2 ROS are Necessary for Lipolysis-Dependent Release of Resistin

Based on our data demonstrating the necessity of lipolysis for resistin release, we hypothesized that a product of lipolysis may be acting as a signaling molecule, such as an oxidized lipid. Our previous HPLC-MS/MS analysis of cellular media demonstrated that oxFA are rapidly released during catecholamine-stimulated lipolysis. Therefore, we next tested whether production of oxidized lipids by ROS is necessary for lipolysis-mediated release of resistin. To reduce ROS levels, we pretreated 3T3-L1 adipocytes with the antioxidant EUK overnight before stimulation with ISO. Media was collected at 0, 15, and 45 min. We confirmed induction of lipolysis by measuring release of glycerol and NEFA **(Figure 6-3A)**. Again, ISO induced lipolysis, and EUK did not affect this induction. When we analyzed by immunoblot, we observed that the level of resistin in the media increased over time with ISO stimulation of lipolysis **(Figure 6-3B)**. However, pretreatment with EUK prevented adrenergic-induced release of resistin. Due to the length of EUK incubation, we were curious if expression of resistin mRNA was affected. When measured by qPCR, we found a decrease in resistin mRNA expression after overnight incubation with EUK, with levels of resistin mRNA expression in EUK-treated cells at approximately 25% of vehicle-treated cells **(Figure 6-3C)**. ISO stimulation was not observed to have an effect on resistin mRNA expression. This is likely due to the short treatment timeframe. Taken together, these results suggest a critical role for ROS in the lipolysis-dependent mechanism of acute resistin release.

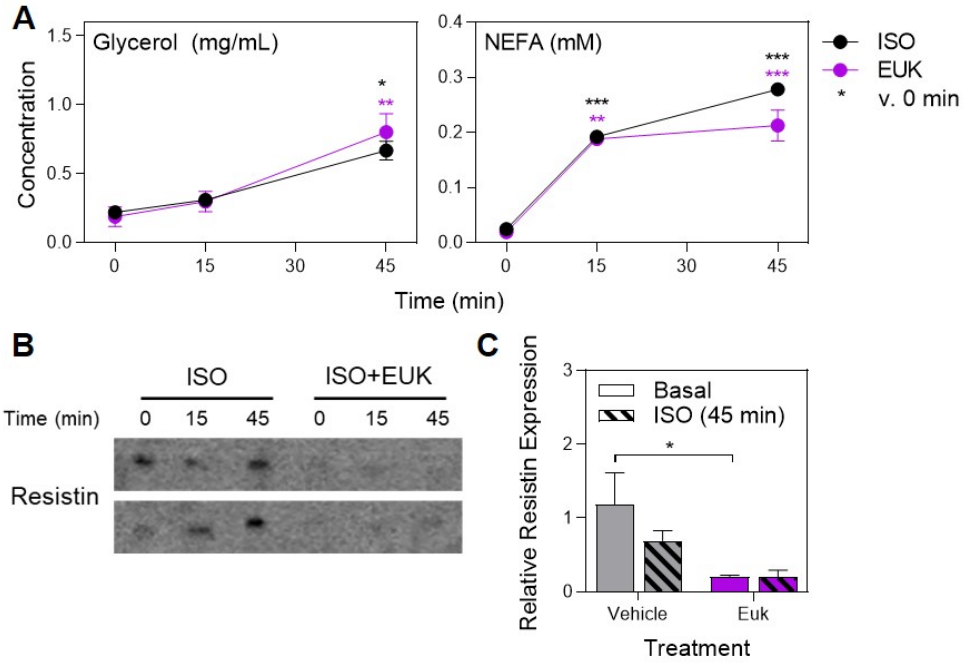


**Figure 6-3: Antioxidants reduce resistin expression and lipolysis-dependent release**

**Figure 6-3 Legend**

**A.** Glycerol and NEFA levels in the media of 3T3-L1 adipocytes were pretreated with 100 μM EUK overnight before treatment with 1 μM isoproterenol (ISO) in low-glucose DMEM supplemented with 0.5% FA-free BSA. Media was collected after 0, 15, and 45 min of treatment. Glycerol and NEFA were measured in the media using their respective kits.

**B.** Representative immunoblots of the media of 3T3-L1 adipocytes treated as in A.

**C.** Relative resistin mRNA expression measured by qPCR in 3T3-L1 adipocytes treated as in A.

$N$ = 3-4. Data are shown as mean ± SEM. *$P$ < 0.05, **$P$ < 0.01, and ***$P$ < 0.001, as indicated. Statistical analyses were performed using two-way ANOVA. All comparisons differing by one variable were made and adjusted for with ANOVA, and all significant comparisons are denoted as such.

### 6.3.3 Resistin Circulating and mRNA Expression Levels are Dynamic over the Course of Cardiovascular Stress

In humans, the development of acute stress-induced hyperglycemia and insulin resistance has been well-documented in morbidities associated with cardiovascular disease, including myocardial infarction, heart failure, and thoracic surgery (2, 4, 202). We were able to replicate the acute stress metabolic phenotype using a HS mouse model and showed that the development of these disturbances was dependent on lipolysis. Furthermore, we demonstrated that resistin was released in a stress- and lipolysis-dependent manner, which we corroborated with *in vitro* studies. Therefore, we wanted to further study the acute release of resistin in the context of cardiovascular disease. To this end, we employed two different mouse models to study this phenomenon in instances of heart failure and myocardial infarction.

To examine the release of resistin during heart failure, we used a mouse model of pressure overload-induced heart failure **(Figure 6-4A)**. Specifically, cardiomyocyte-specific deletion of *Mapk14* to create loss p38 MAPKα was induced with tamoxifen (iCMp38KO mice). Mice were then infused with AngII via an osmotic pump for 48 h. At the end of the infusion period, iCMp38KO mice had lower ejection fraction than their WT counterparts (iCMp38KO: 20.5 ± 4.9%, WT: 52.8 ± 7.3%), indicating the development of heart failure. Based on our previous studies, we hypothesized that the development of heart failure would induce the acute release of resistin. Surprisingly, in this model of heart failure, we observed the exact opposite. Basally, our iCMp38KO mice had lower levels of circulating resistin than WT mice **(Figure 6-4B)**. Furthermore, 48 h exposure to AngII to induce pressure overload resulted in a decrease in circulating resistin levels in both WT and iCMp38KO mice. One possible explanation for this

unexpected result is that AngII has been shown to decrease levels of adipocyte lipolysis (203). In our previous acute stress studies, we demonstrated that despite the presence of HS, blocking lipolysis was sufficient to blunt the release of resistin. Thus, it is possible in our heart failure model that, despite the presence of increased cardiac stress with AngII infusion, lipolysis is sufficiently inhibited by AngII to decrease the level of circulating resistin. To test the effect of lipolysis inhibition on resistin release in this model, we pharmacologically inhibited lipolysis by incorporating atglistatin into the food starting two days before infusion **(Figure 6-4A)**. With lipolysis inhibited, resistin levels tended to be further decreased in WT mice, as we would expect based on our previous *in vivo* and *in vitro* studies **(Figure 6-4B)**. We did not observe a significant change in iCMp38KO mice with inhibition of lipolysis. This may be because circulating resistin was already at a low level with AngII infusion that further reduction could not be reliably observed. When we examined resistin mRNA expression in the gonadal fat of mice in our model, we observed that, despite lower levels in circulation, resistin mRNA expression was higher in iCMp38KO mice compared to WT **(Figure 6-4C)**. While it may seem contrary, a disconnect between circulating resistin and mRNA expression levels has been repeatedly observed in the literature (86). In both genotypes, AngII and atglistatin treatment had no effect on resistin mRNA expression. Taken together, these data corroborate our previous studies supporting a lipolysis-dependent mechanism of resistin release. However, further investigations are needed to determine the time course and potential role of resistin in the development of pressure overload-induced heart failure.

We next sought to examine the release of resistin in the context of myocardial infarction. As both cardiovascular disease and resistin levels have strong links to obesity,

we investigated how HFD-feeding would affect the resistin release profile over the course of myocardial infarction and subsequent recovery. To model diet-induced obesity, mice were place on HFD for 10 weeks **(Figure 6-5A)**. We noticed that HFD-fed mice accumulated fat around their cardiac tissue, a phenomenon not observed in the chow-fed counterparts. Therefore, we first investigated the expression of resistin mRNA in various adipose depots in HFD-fed mice **(Figure 6-5B)**. As expected, resistin mRNA was expressed the highest in gonadal fat, which is almost entirely composed of WAT, and was expressed at very low levels in brown adipose tissue (204). We also found that resistin mRNA was expressed in the cardiac fat at roughly 50% of the level in gonadal fat.

To compare resistin release between lean and obese mice during myocardial infarction, we employed the LAD artery ligation model **(Figure 6-5A)**. Briefly, mice were anesthetized with isoflurane and intubated before surgery. Myocardial ischemia was produced by tightening a suture around the LAD artery for 45 min. The suture was then removed to allow reperfusion. Recovery was monitored for up to 16 days post-surgery. We measured resistin in serum basally, during surgery, and over the course of recovery **(Figure 6-5C)**. Corroborating previous literature, basal circulating resistin tended to be elevated in HFD-fed compared to chow-fed mice. Based on our previous HS studies, we would expect circulating resistin to increase in response to stress. As expected, resistin levels were elevated during surgery and myocardial ischemia in chow-fed mice. Of note, resistin levels in HFD-fed mice remained at roughly basal levels during surgery and myocardial ischemia and did not exhibit a further stress-induced increase. Resistin levels decreased in both groups over the first two days of recovery, with HFD-fed mice

exhibiting a slower rate of decrease and overall slightly higher resistin levels than their chow-fed counterparts. Interestingly, at day 8, chow-fed mice exhibited a large spike in circulating resistin and much higher levels than HFD-fed mice, in which circulating resistin remained comparable to day 2 levels. On day 16, circulating resistin began to increase in HFD-fed mice and remained elevated in chow-fed mice. Overall, chow-fed mice exhibited much larger variation in circulating resistin levels over the course of surgery and recovery, whereas levels in HFD-fed mice were much more stable and did not rise significantly above basal levels.

We next investigated the effect of diet and myocardial infarction on resistin mRNA expression. When we examined cardiac fat taken from the same HFD-fed mouse during surgery and recovery, we found a significant decrease in the level of resistin mRNA expression on day 8 **(Figure 6-5D)**. These data mirror the changes observed in circulating resistin levels. However, we did note that mice generally lost weight during recovery after myocardial infarction, resulting in reduced adipose tissue mass. This combined with removal of some of the cardiac fat during surgery likely contributed to our observation that the samples collected at day 8 were noticeably smaller than the samples collected during surgery. Therefore, we cannot rule out the possibility that sample quality affected our resistin mRNA expression analysis. Additional studies where fat is collected from separate mice at each timepoint are required to confirm these results. When we examined resistin mRNA expression differences in gonadal fat in chow- and HFD-fed mice, we found that chow-fed mice exhibited higher levels of resistin mRNA expression **(Figure 6-5E)**. Similar to previous studies and our observation in iCMp38KO mice, the expression level of resistin mRNA exhibits the opposite pattern that is seen in circulating

resistin levels, with HFD-mice exhibiting higher basal circulating levels of resistin but with lower basal mRNA expression levels. On day 8 post-surgery, resistin mRNA expression was unchanged from basal levels in chow-fed mice. Expression levels of resistin mRNA in HFD-fed mice on day 8 trended towards increased, despite day 8 circulating levels being significantly lower compared to basal levels. Despite not observing significant changes in resistin mRNA expression between pre- and post-surgery, it is still possible that expression levels change over the course of myocardial ischemia and recovery. Additional studies with tissue collected at multiple time points are needed to assess how dynamic resistin mRNA expression is in myocardial infarction and whether mRNA expression level changes correlate with changes in levels of circulating resistin. Taken together, these data put forward resistin as a dynamic circulating factor that could affect recovery after myocardial infarction. Furthermore, distinct differences in circulating resistin profiles could contribute to variations in recovery between lean and obese individuals. If so, our previous data would suggest that levels could be manipulated by inhibiting lipolysis. Additional studies are needed to assess the potential role of lipolysis on circulating resistin and recovery in the context of myocardial infarction.

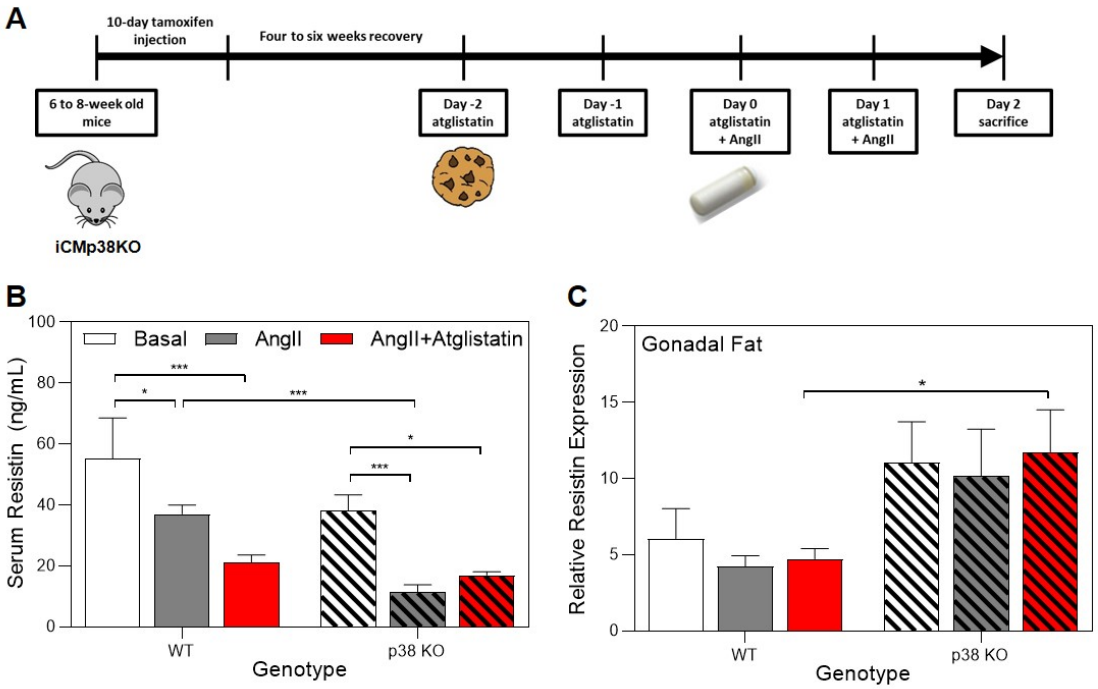


**Figure 6-4: Inhibiting lipolysis reduces circulating resistin during heart failure**

**Figure 6-4 Legend**

**A.** Illustration of the pressure overload-induced model of heart failure. Cardiomyocyte-specific loss of p38 MAPKα was generated by tamoxifen injection. Lipolysis was inhibited by administering 0.4 mg atglistatin/g food starting two days prior to pressure overload induction. Pressure overload was induced by 1.5 mg/kg/day AngII infusion by subcutaneous mini-osmotic pumps for 48 h.

**B.** Resistin levels determined by ELISA in the serum of WT or iCMp38KO mice treated as in A.

**C.** Relative resistin mRNA expression measured by qPCR in gonadal fat of WT or iCMp38KO mice treated as in A.

$N$ = 5-18. Data are shown as mean ± SEM. *$P$ < 0.05 and ***$P$ < 0.001, as indicated. Statistical analyses were performed using two-way ANOVA. All comparisons differing by one variable were made and adjusted for with ANOVA, and all significant comparisons are denoted as such.

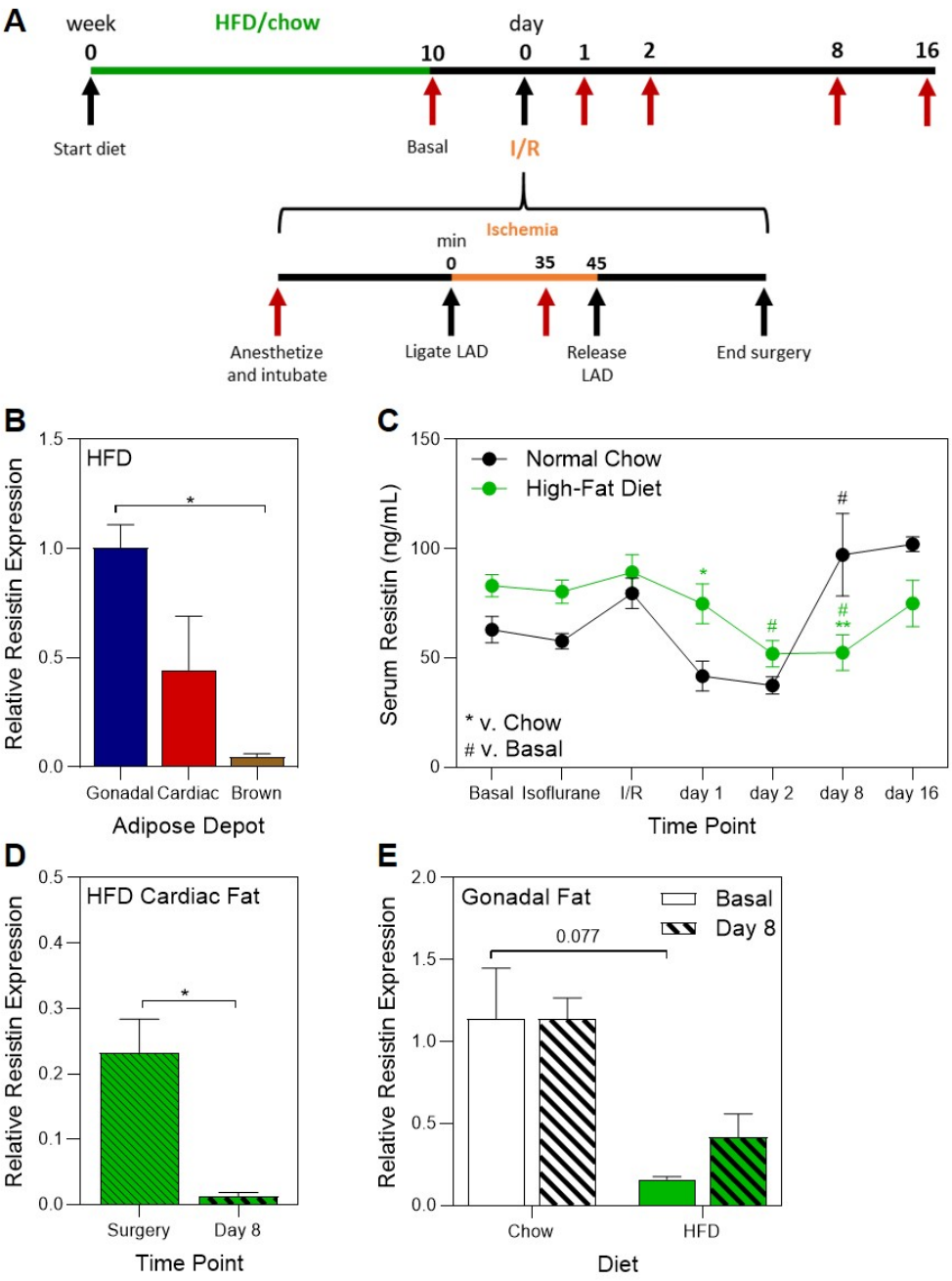


**Figure 6-5: Lean and obese mice exhibit unique resistin release and mRNA expression profiles during myocardial infarction**

**Figure 6-5 Legend**

**A.** Illustration of the LAD artery ligation model of myocardial infarction. WT mice were fed chow or HFD for 10 weeks. Mice were subjected to LAD artery ligation for 45 min. During surgery, a small portion of the cardiac fat was removed from HFD-fed mice. All other tissues were harvested at basal, day 8 post-surgery, or day 16 post-surgery. Blood was collected at all time points indicated with a red arrow.

**B.** Relative resistin mRNA expression measured by qPCR in gonadal, cardiac, and brown fat harvested from HFD at the basal timepoint.

**C.** Resistin levels determined by ELISA in the serum of chow- and HFD-fed mice treated as in A.

**D.** Relative resistin mRNA expression measured by qPCR in cardiac fat from HFD treated as in A.

**E.** Relative resistin mRNA expression measured by qPCR in gonadal fat from chow- or HFD-fed mice treated as in A.

$N$ = 3-21. Data are shown as mean ± SEM. *$P$ < 0.05 and **$P$ < 0.01, as indicated. Statistical analyses were performed in B using one-way ANOVA, C and E using two-way ANOVA, and D using an unpaired t test. All comparisons differing by one variable were made and adjusted for with ANOVA, and all significant comparisons are denoted as such.

## 6.4 DISCUSSION AND CONCLUSIONS

In this study, we investigated *in vitro* the mechanism of acute resistin release from adipocytes and its dependence on TAG lipolysis. We showed that catecholamine stimulation of mouse adipocytes resulted in lipolysis as well as resistin release. When lipolysis was inhibited, the release of resistin blunted. Interestingly, we observed that pretreatment with antioxidants also prevented the release of resistin, even in the presence of lipolysis. This indicates that an oxidized lipid, such as an oxFA which we demonstrated are released by adipocyte lipolysis, may be acting as a signaling molecule activating resistin release. Further studies are needed to more definitively determine if oxidized lipids are playing a role and if so which species are acting as a signaling molecule.

As humans are known to develop a strong acute stress response during cardiovascular events and surgery, and mouse studies have demonstrated that lipolysis plays an important role in regulating metabolism and recovery during these events, we investigated *in vivo* whether cardiovascular stress stimulates lipolysis-dependent, acute release of resistin. In a mouse model of pressure overload-induced heart failure, we demonstrated that inhibiting lipolysis with atglistatin reduced circulating levels of resistin in WT mice. Atglistatin did not affect resistin levels in iCMp38KO mice which may be because circulating resistin was already at a low level that further reduction could not be reliably observed. Surprisingly, inducing pressure overload cardiac stress with AngII resulted in a decrease in circulating resistin in both WT and iCMp38KO mice. While this may seem contrary to our HS and myocardial infarction data, blood was only sampled in this model after 48 h of AngII infusion. It is possible that, similar to our myocardial

infarction results, resistin spikes rapidly after onset of cardiac stress and then decreases during initial recovery and remodeling. By only measuring one time point, we cannot definitively conclude that resistin does not increase in response to pressure overload. Another possible explanation is that AngII has previously been shown to inhibit lipolysis through decreased local blood flow (203). Based on our previous *in vivo* and *in vitro* data which support a lipolysis-dependent mechanism, inhibition of lipolysis by AngII could inhibit resistin release. A more thorough time course in this model or evaluations of pressure-overload heart failure using a model that does not require AngII infusion, such as the transverse aortic constriction model, are required to better assess the role of resistin in heart failure.

When we investigated resistin in the context of myocardial infarction, we found that circulating resistin levels spiked during surgery and ischemia, which we would expect based on our HS studies. Recovery from myocardial infarction is generally recognized to occur in three phases: inflammation (day 0-4), healing (day 4-14), and remodeling (day 14+) (9). Resistin levels were decreased below baseline during the inflammation phase and exhibited a second spike during the healing phase with levels remaining elevated into the remodeling phase before the experiment was terminated. This observation opens up the interesting possibility that resistin plays varying roles in the initial response to acute stress but also during cardiac remodeling. Further work is needed to investigate the role of resistin during these phases and what signaling mechanisms are controlling the release of resistin during these periods. Our data suggest that changing lipolytic activity could be responsible. Future studies should measure glycerol levels in circulation to determine whether resistin levels correlate to lipolytic activity. In addition,

it would be of interest to investigate whether inhibiting lipolysis affects circulating resistin levels and what effect this has on cardiac function after myocardial infarction.

Because cardiovascular disease and resistin are both correlated with obesity, we investigated the effect of diet-induced obesity on resistin release during myocardial infarction. As expected, obese mice had higher basal levels of circulating resistin. Interestingly, obese mice did not exhibit a spike with myocardial ischemia, as was observed for lean mice. One possible explanation for this observation is that obese animals and humans are known to have higher basal levels of lipolysis (51). In addition, obese individuals exhibit marked resistance to adrenergic stimulation of lipolysis (205). Based on our data supporting a lipolysis-dependent mechanism of release, these differences in lipolytic activity would explain why obese individuals exhibit higher basal levels but no stress-induced increase in resistin. Over the course of recovery, obese mice exhibited a decrease in resistin levels to below basal during the inflammation phase, as was seen in lean mice. During this phase, resistin levels were significantly higher in obese mice compared to lean mice. This changed during the healing and remodeling phases of recovery, during which lean mice exhibited a spiking of resistin levels above that observed in obese mice. Between day 2 and 8, resistin levels in obese mice were stable and below basal levels and only began to increase at day 16. Overall, resistin levels in obese mice were more resistant to change and less dynamic than in lean mice. Further studies are needed to determine if this difference in resistin release profile correlates to differences in cardiac function after myocardial infarction between lean and obese individuals.

In summary, our *in vitro* studies demonstrate that acute release of resistin is induced by and dependent on adrenergic-stimulated lipolysis. Our antioxidant data suggest a potential signaling function for oxidized lipids in this pathway. Our *in vivo* studies demonstrate that resistin is released acutely in response to cardiovascular stress and is a dynamic factor that could contribute to metabolic disturbances during recovery. In our heart failure studies, we corroborate our hypothesis that resistin release is lipolysis-dependent. Our myocardial infarction studies show that circulating resistin spikes in response to myocardial ischemia, decreases during the inflammatory phase of recovery, and increases again during the healing and remodeling phases. Diet-induced obesity changes this profile, with no spike observed during ischemia and more stable values over the course of recovery. Our *in vitro* studies to elucidate this mechanism as well as our *in vivo* studies to investigate the profile of resistin release during cardiovascular stress could provide insight into the role of resistin in the development of acute and chronic insulin resistance and open up further investigation into a potential therapeutic target.

## ACKNOWLEDGEMENTS

I would like to thank the other members of the Harris and Gödecke labs for their continued support. This research was funded by NIH Cardiovascular Research Training Grant T32 HL0007284-41 (K.W.A.), American Heart Association Predoctoral Fellowship 17PRE33660609 (K.W.A.), NIH NRSA Predoctoral Fellowship 1F31DK121482-01A1 (K.W.A.), German Research Foundation IRTG1902 (V.O. and L.K.), German Research Foundation CRC1116TPA06 (A.G.), Dr. Sigrid-Worch-Pöhler Foundation (A.G.), and NIH R01 1R01DK101946 (T.E.H.).

## AUTHOR CONTRIBUTIONS

The studies were designed by Katelyn Ahern, Hannah Chung, Dr. Axel Gödecke, Dr. Thurl Harris, Arad Jain, Dr. Lisa Kalfhues, Dr. Vici Oenarto, Zachary Palas, and Dr. André Spychala. Experimental work was performed by Katelyn Ahern, Hannah Chung, Arad Jain, Dr. Lisa Kalfhues, Jesse Lynch, Dr. Vici Oenarto, Zachary Palas, and Dr. André Spychala. Data analysis was performed by Katelyn Ahern, Hannah Chung, Arad Jain, Dr. Lisa Kalfhues, Dr. Vici Oenarto, Zachary Palas, and Dr. André Spychala. Funding was provided by Katelyn Ahern, Dr. Axel Gödecke, Dr. Thurl Harris, Dr. Lisa Kalfhues, and Dr. Vici Oenarto.

# 7 CONCLUSIONS AND FUTURE DIRECTIONS

## 7.1 SUMMARY

The present dissertation outlines the contributions of adipocyte lipolysis to acute stress-induced metabolic disturbances through the release of two signaling molecules: oxFA and resistin. To study the potential role of oxFA, we developed a novel HPLC-MS/MS method to measure full-length oxidation products of LA and AA. Using this method, we demonstrated levels of oxFA increased in response to adipocyte lipolysis both *in vitro* and *in vivo*. Building upon our previous work, we showed that ROS production is critical for lipolysis-dependent inhibition of the mTOR complexes and provided preliminary data that an oxFA is responsible. We demonstrated *in vivo* that resistin is released in a stress- and lipolysis-dependent manner. When we further investigated this mechanism *in vitro*, we observed a significant, lipolysis-dependent release of resistin from adipocytes into the media. In addition, treatment with an antioxidant prevented lipolysis-dependent secretion, suggesting a role for oxFA signaling in the acute release of resistin.

Because both oxidized lipids and resistin are typically linked to chronic metabolic impairments, we also studied their action in the context of obesity. We demonstrated oxFA levels were increased with HFD. In addition, oxFA exposure increased inflammatory gene expression, a hallmark of ATM in obesity. When we investigated resistin in myocardial infarction, we found that obese mice had higher basal levels of resistin and more stable resistin levels during ischemia and recovery compared to lean controls. Based on these studies, we propose that oxFA and resistin are acutely released in response to stress-stimulated lipolysis. By elucidating this mechanism, our work could

provide insight into the role of adipose tissue in the development of acute and chronic insulin resistance.

## 7.2 CONCLUSIONS AND SIGNIFICANCE

The work presented here addresses important unanswered questions regarding mechanisms of anabolic and catabolic signaling crosstalk and fills significant gaps in our understanding of how insulin resistance develops during acute stress. It is well-accepted that severe trauma activates the acute stress response, resulting in systemic insulin resistance and hyperglycemia (1). While hyperglycemia has been shown to be an independent risk factor for increased mortality and morbidity after surgery, the only treatment currently available is intensive insulin therapy (2–4). Unfortunately, insulin therapy is only effective in some patients, requires careful monitoring, and increases the risk of hypoglycemic incidents (1). In addition, this treatment does not correct the underlying insulin resistance. By shedding light on the crosstalk underlying the development of stress-induced insulin resistance, this work provides new avenues for investigation and potential therapeutic targets for more effective and safer maintenance of euglycemia in the ICU.

Adipose tissue has long been recognized for its role in energy storage and as a regulator of energy homeostasis, but in recent years, the importance of adipose tissue as an endocrine organ has been increasingly appreciated (151). For example, adipose-derived factors such as cytokines, adipokines, and lipid intermediates have been demonstrated to impair insulin-stimulated glucose disposal (151). One such adipokine is resistin which has been shown to be increased in obesity in mice and obesity and type 2 diabetes in humans (84, 148). Due to its initial characterization in chronic conditions,

little attention has been focused toward the potential acute role for resistin. However, recent studies on the acute stress response in humans have demonstrated a correlation between circulating resistin and trauma or critical illness, with higher levels of resistin associated with worse outcomes (90–97). In our acute stress studies, we see significant increases in circulating resistin within a 30-min timeframe. Our studies demonstrate for the first time that acute resistin release correlates with the development of transient insulin resistance and hyperglycemia, such as during trauma and surgery.

Furthermore, our data suggest a novel lipolysis-dependent regulation of acute resistin release. In our *in vivo* studies, resistin showed a robust induction with HS, which was attenuated with lipolysis inhibition. Corroborating this observation, epinephrine infusion during hyperinsulinemic-euglycemic clamps increased circulating resistin levels with inhibition of lipolysis abrogating this response. In addition, circulating resistin levels were positively correlated with net lipolysis as shown by glycerol levels. Through our *in vitro* studies, we confirmed that catecholamine stimulation of mouse adipocytes resulted in lipolysis as well as resistin release. When lipolysis was inhibited, the release of resistin blunted. These data suggest a previously unknown mechanism regulating the release of resistin. Considering that resistin has gained interest as a potential therapeutic target, this new mechanism provides previously unconsidered mechanisms for manipulating endogenous levels of resistin for the treatment of acute and chronic pathologies.

Another means by which adipose tissue can influence whole-body metabolism is through lipid signaling molecules, such as oxFA. In order to study these species, we developed a targeted method that is able to identify and absolutely quantify multiple full-length oxFA species independent of regioisomer. The ability to faithfully quantify

individual oxFA species, regardless of regioisomer, was an unmet need in the oxidized lipids field. We have demonstrated our method to be highly sensitive, without requiring time-consuming and destructive derivitization steps, due to the utilization of sodium adducts to take advantage of positive-ion ionization and DiffE QIM to quantify based on regioisomer-independent, high intensity, pseudo-molecular transitions. The implementation of DiffE QIM also circumvents the difficulty of fragmentation since it does not rely on characteristic fragmentation. To our knowledge, this is the first study implementing DiffE QIM to measure oxFA, and based on our success measuring full-length oxFA, this could likely be applied to other oxFA species for regioisomer-independent quantification.

Using this method, we demonstrated levels of oxFA increased in response to adipocyte lipolysis both *in vitro* and *in vivo*. In addition, our previous work demonstrated a critical role for adipocyte lipolysis in the development of impairments in insulin signaling through dissociation of the mTOR complexes. However, traditional lipolytic products were found to have no effect on mTOR complex activity. This led us to hypothesize that oxFA may be responsible for acute insulin resistance. The production of ROS was found to be critical for mTOR complex inhibition with antioxidants rescuing complex integrity and increased oxidative stress decreasing mTOR complex activity. Taken together, these data show that oxidized lipolytic products facilitate mTOR complex inhibition through complex dissociation and serve as one mechanism of catecholamine-induced insulin resistance. This represents a novel means of mTOR complex regulation and a previously undiscovered signaling pathway for oxidized lipids. By elucidating this mechanism, we have provided further insight into the complex

crosstalk between catabolic and anabolic signaling. This work has implications, not only for acute stress-induced insulin resistance, but also for chronic conditions such as obesity.

Because both oxidized lipids and resistin are typically linked to chronic metabolic impairments, we also studied their action in the context of obesity. When we examined oxFA, we demonstrated oxFA levels were increased with HFD. When the effect on macrophages was tested *in vitro*, these full-length oxPL induced macrophage phenotypes characteristic of obesity, including increased proinflammatory gene expression (45). In addition, it had yet to be studied whether the oxidized moiety of the oxPL alone was capable of inducing the same macrophage phenotypic changes. Through our studies, we demonstrated oxFA exposure increased inflammatory gene expression, a hallmark of ATM in obesity. These results indicate that the oxFA moiety is responsible for the effects of oxPL exposure on macrophage phenotype and puts forward oxFA as a critical species for study in obese adipose tissue. When we investigated resistin in the context of obesity and myocardial infarction, we found that obese mice had higher basal levels of resistin and more stable resistin levels during ischemia and recovery compared to lean controls. This data puts forward resistin as a dynamic circulating factor that could affect recovery after myocardial infarction. Furthermore, distinct differences in circulating resistin profiles could contribute to variations in recovery between lean and obese individuals. If so, our previous data would suggest that levels could be manipulated by inhibiting lipolysis.

## 7.3 FUTURE DIRECTIONS

Our studies show that adrenergic action and subsequent adipocyte lipolysis are necessary for the development of stress-induced disturbances in glucose homeostasis and

peripheral insulin resistance. One limitation of our studies is the focus on catecholamine effects in a short acute stress timeframe. While catecholamines play an important role during the initial response to acute stress, other hormones play significant roles in the days to weeks following injury, including glucagon, cortisol, and inflammatory cytokines. It is important to note that while these hormones are induced at different times and have tissue-specific effects, all of these hormones may act similarly as they all oppose insulin action and induce adipocyte lipolysis (116). However, in order to evaluate the lipolytic pathway as a therapeutic target, future studies are needed to determine the signaling role of additional hormones and the effect of lipolysis during more prolonged illness.

In our *in vivo* studies, we made the initially surprising observation that the increase in glycerol observed with HS was not accompanied by an increase in circulating NEFA levels. This disconnect between circulating glycerol and NEFA levels observed during HS has previously been ascribed to vasoconstriction in WAT (135, 136). Thus, while adipocyte lipolysis is required for the induction of insulin resistance and impaired glucose uptake during acute stress, our studies suggest this could be uncoupled from an elevation in circulating NEFA. However, an important caveat to examining static levels of NEFA in circulation is that this could miss an increase in NEFA flux from adipocytes into tissues. Until studies examining lipid flux under these conditions have been performed, we cannot rule out the possibility that release of NEFA from adipose into circulation has been missed due to compensating changes in uptake or oxidation.

Because we did not see an increase in NEFA in our HS studies, we focused on other possible signaling molecules connecting insulin resistance and lipolysis, such as oxFA. In

order to study oxFA, we developed a novel HPLS-MS/MS method to quantify these species. We focused on full-length oxidation products because of previous work demonstrating that these species of oxPL increase in obesity and promote an inflammatory macrophage polarization (45). Indeed, using our method, we demonstrated that full-length oxFA increase with HFD feeding. However, our method was limited in the number of species measured. We measured three full-length species for each LA and AA, however there are many more in the oxidized lipidome that still need to be investigated. Furthermore, our method did not measure any truncated species. Previous work demonstrated that both full-length and truncated oxPL species increase during obesity, but full-length species disproportionately increase (45). While we see increases in full-length oxFA in obese mice, we cannot account for how truncated oxFA change or the proportion of full-length to truncated species. Future studies will need to add more oxFA species to our method for quantification to make that determination.

In response to surgery and HS, our data demonstrated that levels of oxFA increased in response to adipocyte lipolysis both *in vitro* and *in vivo*. Adipocytes have vast stores of TAG in the form of lipid droplets, and we and others have found that, even under basal conditions, there is a considerable quantity of oxidized esterified acyl chains on TAG (198). It is possible during lipolysis that these oxidized acyl chains are hydrolyzed and released into the cell as oxFA. However, we cannot rule out the possibility that these oxFA are produced by oxidation after hydrolysis. While it is in fact likely that both oxFA production mechanisms contribute to the increase observed after lipolysis, more studies are needed to determine the level of contribution from each pathway. Of note, we measured increased oxFA in extracellular media and in circulation. Our data does not

delineate whether these oxFA are produced in the cell, such as from hydrolysis of oxidized TAG, and exported, or if the NEFA are exported from the cell and become oxidized in circulation. Again, further studies are needed to determine the potential method of export and degree of contribution from each oxFA production mechanism.

In addition, our previous work led us to hypothesize that oxFA may be responsible for acute insulin resistance. Preliminary data suggest that the lipid responsible for mTOR complex inhibition is a product of oxLA. Further studies are needed to confirm that an oxLA species is responsible and which species have mTOR complex inhibition activity. Currently, our data does not provide a mechanism for how oxFA species dissociate the mTOR complexes. Previous studies have shown that phosphatidic acid binds directly to the rapamycin-FKBP12 binding domain of mTOR and positively regulates activity (71, 199). It is hypothesized that phosphatidic acid activates mTOR complexes through strengthening the association of the complex, and that the mTOR complexes dissociate in the absence of phosphatidic acid. Therefore, it is possible that the oxFA competes with phosphatidic acid for binding to mTOR, thus resulting in complex dissociation. Further studies are needed to test this potential mechanism.

In addition to the release of oxFA, catecholamines and lipolysis were shown to affect the secretion profile of adipokines from adipose tissue. Of note, resistin was released in a stress- and lipolysis-dependent manner and has previously been linked to the development of chronic insulin resistance in obesity (84, 86, 148). Interestingly, we observed that pretreatment with antioxidants prevented the release of resistin, even in the presence of lipolysis. This indicates that an oxidized lipid may be acting as a signaling molecule activating resistin release. Further studies are needed to more definitively

determine if oxidized lipids are playing a role and if so which species are acting as a signaling molecule.

When we investigated resistin in the context of myocardial infarction, we found that circulating resistin levels spiked during ischemia, decreased below baseline during the initial recovery, and exhibited a second spike during late recovery. This observation opens up the interesting possibility that resistin plays varying roles in the initial response to acute stress but also during cardiac remodeling. Further work is needed to investigate the role of resistin during these phases and what signaling mechanisms are controlling the release of resistin during these periods. Our data suggest that changing lipolytic activity could be responsible. Future studies should measure glycerol levels in circulation to determine whether resistin levels correlate to lipolytic activity. In addition, it would be of interest to investigate whether inhibiting lipolysis affects circulating resistin levels and what effect this has on cardiac function after myocardial infarction.

Because cardiovascular disease and resistin are both correlated with obesity, we investigated the effect of diet-induced obesity on resistin release during myocardial infarction. We found that obese mice had higher basal levels of resistin and more stable resistin levels during ischemia and recovery compared to lean controls. Further studies are needed to determine if this difference in resistin release profile correlates to differences in cardiac function after myocardial infarction between lean and obese individuals. One possible explanation for this observation is that obese animals and humans are known to have higher basal levels of lipolysis (51). In addition, individuals with obesity exhibit marked resistance to adrenergic stimulation of lipolysis (205). Based on our data supporting a lipolysis-dependent mechanism of resistin release, these

differences in lipolytic activity would explain why individuals with obesity exhibit higher basal levels of resistin but no stress-induced increase in resistin. However, lipolysis data, such as glycerol levels, would be required to confirm this posited correlation.

# 8 APPENDIX: CHARACTERIZATION OF ADIPOSE-DERIVED SIGNALING MOLECULES IN COVID-19 PATIENTS

## 8.1 ABSTRACT

Acute hyperglycemia and systemic insulin resistance often develop during severe illness. This stress response leads to increased post-operative complications and mortality. Of critical public health importance, hyperglycemia has been found to develop in patients affected by COVID-19 and is linked to poor patient prognosis. Our previous work has demonstrated a central role for lipolysis and adipokines in the development of stress-induced metabolic derangements. However, it has yet to be studied how these adipose-derived signaling molecules, such as adipokines and lipids, are affected during COVID-19 specifically. To examine whether these signaling molecules are playing a unique role in COVID-19, we collected blood samples during the first 72 h from patients admitted to the University of Virginia Medical Center ICU. COVID-19 patients exhibited decreased adiponectin levels and increased PAI-1 levels compared to other ICU patients, suggesting that they may have more severe insulin resistance. Resistin levels were found to spike at 24 h, while NEFA levels tended to increase over the duration of hospital stay. Corroborating our hypothesis that acute resistin release is lipolysis dependent, we observed a significant, positive correlation between relative resistin and NEFA levels in our COVID-19 patients. The data presented here provide interesting observations regarding a potential role for adipose tissue-derived signaling molecules in stress-related metabolic derangements in COVID-19 patients

## 8.2 INTRODUCTION

Severe trauma activates an acute stress response which results in systemic insulin resistance and hyperglycemia, even in patients without prior history of diabetes (1–4, 47, 115, 117, 118, 206). While a variety of trauma and critical illness can stimulate the acute stress response, severe infections have been well-documented to cause metabolic impairments in humans (47, 117, 118, 206). Of concern, hyperglycemia has been shown to be an independent risk factor for increased mortality and morbidity. As a result, the maintenance of euglycemia is a major therapeutic target in the ICU after injury or critical illness (5–7). However, intensive insulin therapy is only effective in some patients and requires careful monitoring and individualization, as it increases hypoglycemic incidents which often negate the positive effects of tight glucose control (1, 117, 118). Furthermore, this treatment does not correct the underlying insulin resistance, the mechanism of which remains unknown.

COVID-19 is caused by the Severe Acute Respiratory Syndrome Coronavirus-2 (SARS-CoV-2) and has affected 54.5 million people worldwide and resulted in 1.3 million deaths since it was first reported in December 2019. Due to its infectious nature and the lack of a vaccine, cases and deaths continue to rise daily. Similar to previous coronavirus infections such as SARS-CoV-1 and Middle-East Respiratory Syndrome Coronavirus (MERS-CoV), the presence of diabetes has been identified as an independent risk factor associated with mortality in COVID-19 patients (207–209). More specifically, poorly controlled hyperglycemia has been linked to more severe prognoses in people hospitalized for COVID-19 (209–213). As with other instances of acute stress, the association between hyperglycemia and worse outcomes has also been found in

individuals with no history of diabetes (209–213). As such, glycemic control in COVID-19 patients is a critical therapeutic avenue, especially considering the disease's high mortality rate and lack of specific treatment. In addition, further investigation is needed to determine the degree of stress-induced insulin resistance present in COVID-19 patients which may contribute to the severity of hyperglycemia.

Even though stress-induced insulin resistance depends on insulin action in various tissues, multiple studies have supported adipose tissue as a central player in controlling peripheral insulin signaling. For example, we previously demonstrated that decreased rictor expression in adipose tissue led to hyperglycemia and systemic insulin resistance (50). This indicates that impaired insulin action in adipose tissue alone is sufficient to drive hyperglycemia and whole-body insulin resistance. In addition, recent work from our laboratory has shown that adipocyte lipolysis is necessary for the onset of hyperglycemia and systemic insulin resistance during acute stress (52, 214). In particular, this work highlighted a potential role for the adipokine resistin in the development of stress-induced metabolic disturbances. Our work using a mouse model of acute stress suggested that acute release of resistin is dependent on adipocyte lipolysis. Further investigation is needed to see if this mechanism is at work in human patients affected by severe trauma or illness.

Due to increasing recognition of adipose tissue as an endocrine organ, there has been much interest in investigating the unique roles of adipokines during severe illness (90, 91). For example, adipokines such as resistin and PAI-1 have been linked to insulin resistance, while the adipokine adiponectin has been shown to increase insulin sensitivity (75–79, 82, 84, 87). While the correlations of these adipokines to prognosis has been

studied in other instances of severe infections and sepsis, these adipokines have yet to be studied in the setting of COVID-19 (90, 91). As such, we designed a clinical study to examine whether adipose tissue-derived signaling molecules such as adipokines and lipids are playing a unique role in COVID-19 compared to other causes of respiratory failure. Our work will not only contribute to the metabolic characterization of this novel and deadly virus, but may also provide new therapeutic targets to alleviate hyperglycemia and improve patient outcomes.

## 8.3 METHODS

NEFA levels in serum were measured using the HR series NEFA-HR detection kit (Wako Diagnostics) following manufacturer's protocol (32). Human adipokine (adiponectin, PAI-1, and resistin) levels in plasma were measured using the Milliplex Human Adipokine Magnetic Bead Panel 1 kit (Millipore Sigma) following manufacturer's protocol. Plasma samples were prepared at a 1:400 dilution. If analytes were found to be above the linear range, samples were run again with a 1:40,000 dilution.

Data are presented as mean ± SEM. Statistical analyses were performed using two-way ANOVA or Pearson correlation. For all ANOVA analyses, all meaningful comparisons (differing by one variable) were performed and adjusted for. All statistically significant comparisons are denoted in the figures. The numbers for each group are reported in the figure legend. GraphPad Prism software was used for statistical analysis.

## 8.4 RESULTS

As adipose tissue is increasingly appreciated as an endocrine organ, there has been much interest in investigating the unique roles of adipokines during severe illness

(90, 91). To further examine whether adipose tissue and adipokines are playing a unique role in COVID-19, we collected blood samples from patients admitted to the University of Virginia Medical Center ICU. Patients were sorted into groups based on primary diagnosis: COVID-19, viral pneumonia, bacterial pneumonia, non-infectious respiratory failure, and critical illness without respiratory failure. Samples were collected at admission in addition to 24 and 48 h into their hospital stay. Circulating adiponectin, PAI-1, resistin, and NEFA levels were measured at each time point.

Adiponectin levels have been consistently linked to improved insulin sensitivity (145, 146). In our ICU patients, we found adiponectin levels to be decreased in COVID-19 patients in comparison to other forms of infectious respiratory failure (viral and bacterial pneumonia) **(Figure 8-1A)**. In addition, circulating PAI-1 has been linked to impaired insulin sensitivity, and we observed increased levels of PAI-1 in COVID-19 patients compared to other diagnoses **(Figure 8-1A)** (76, 82). When the relative change in these adipokines was examined for each patient over the course of 72 h, the fold change in adiponectin in COVID-19 patients did not noticeably differ from other forms of respiratory failure **(Figure 8-1B)**. However, PAI-1 levels exhibited a marked increase at 24 h in COVID-19 patients **(Figure 8-1B)**. These results indicate that COVID-19 patients may exhibit significant stress-induced insulin resistance, corroborating previous results (209–213).

Numerous clinical studies observed correlations between circulating resistin levels and the development of stress-induced metabolic dysfunction and morbidity (91–97). Our acute stress studies corroborate a strong relationship between resistin and stress-induced insulin resistance. In our ICU patients, we found the concentration of circulating

resistin to not be markedly different between diagnoses **(Figure 8-1A)**. However, when the relative levels of resistin were examined, COVID-19 patients exhibited a noticeable spike at 24 h **(Figure 8-1B)**. Circulating NEFA levels were also not largely different between diagnoses, but did show a trend towards increasing over the course of hospital stay in COVID-19 patients **(Figure 8-1A)**. This trend was further corroborated by examining the relative change in NEFA levels over the course of the hospital stay **(Figure 8-1B)**. Our acute stress and *in vitro* studies demonstrated a link between lipolysis and resistin release. As such, we were interested to assess whether there was any correlation between adiponectin, resistin, and NEFA in our ICU patients. We observed no significant correlation between absolute or relative levels of adiponectin and resistin in the ICU or COVID-19 patient populations **(Figure 8-2A)**. We also observed no significant correlation between adiponectin and NEFA levels **(Figure 8-2B)**. Based on our previous findings, we would expect to find a positive correlation between resistin and NEFA levels. However, when we looked at our total ICU patient population, we did not observe any significant correlation between absolute or relative levels of resistin and NEFA **(Figure 8-2C)**. When we specifically examined the COVID-19 patients, we observed a significant, positive correlation between relative levels of resistin and NEFA, corroborating our hypothesis that acute resistin release is lipolysis dependent.

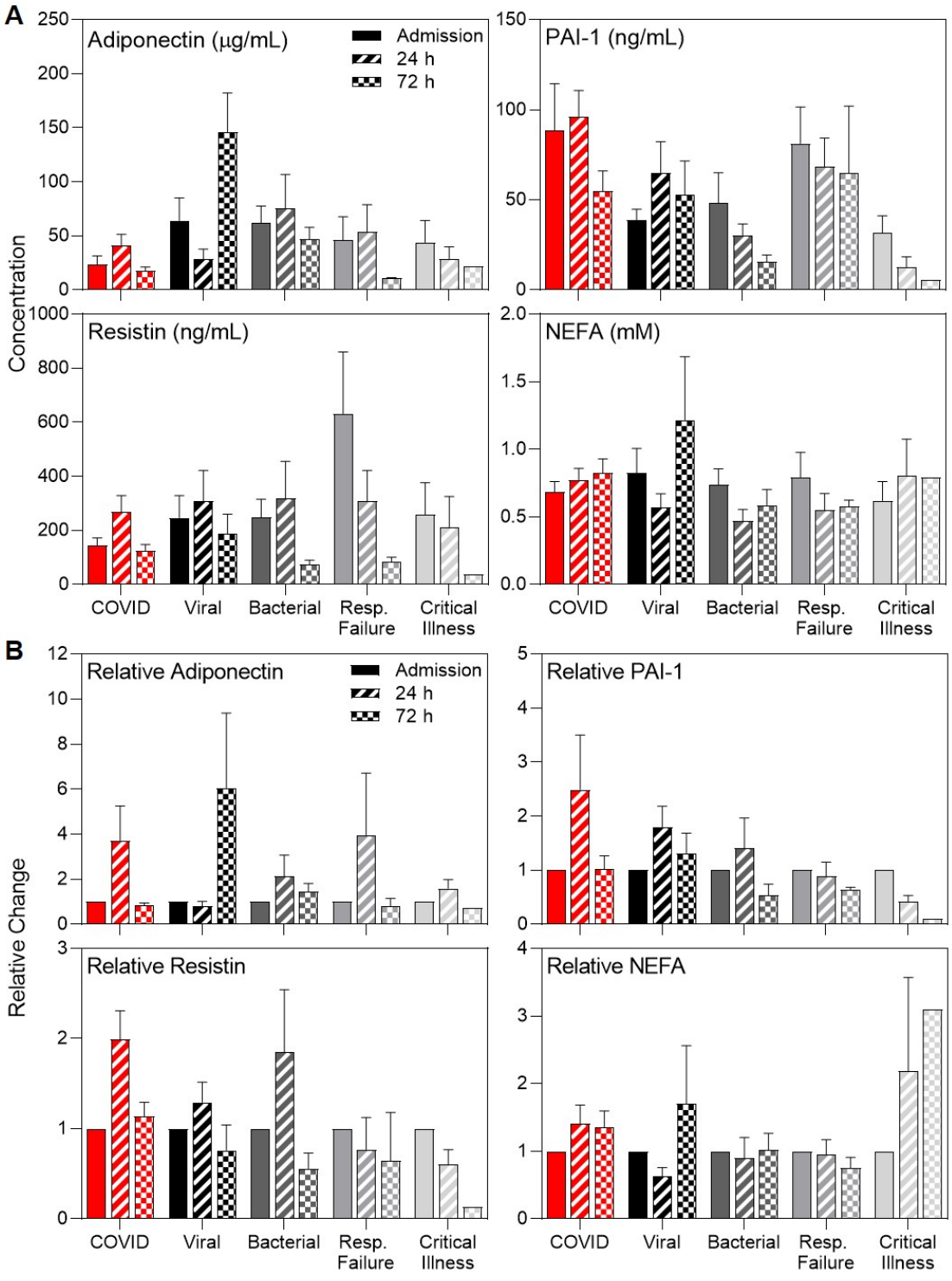


**Figure 8-1: Circulating levels of adipose-derived signaling molecules in ICU patients**

**Figure 8-1 Legend**

**A.** Circulating concentration of adipose-derived signaling molecules in ICU patients. Adiponectin, PAI-1, and resistin levels in plasma were measured by Luminex. NEFA levels in serum were measured by colorimetric assay.

**B.** Relative circulating concentration of adipose-derived signaling molecules in ICU patients. Analytes were measured as in A. Values reflect change from admission levels for each patient.

*N* = 1-12. Data are shown as mean ± SEM. Statistical analyses were performed using two-way ANOVA. All comparisons differing by one variable were made and adjusted for with ANOVA, and all significant comparisons are denoted as such.

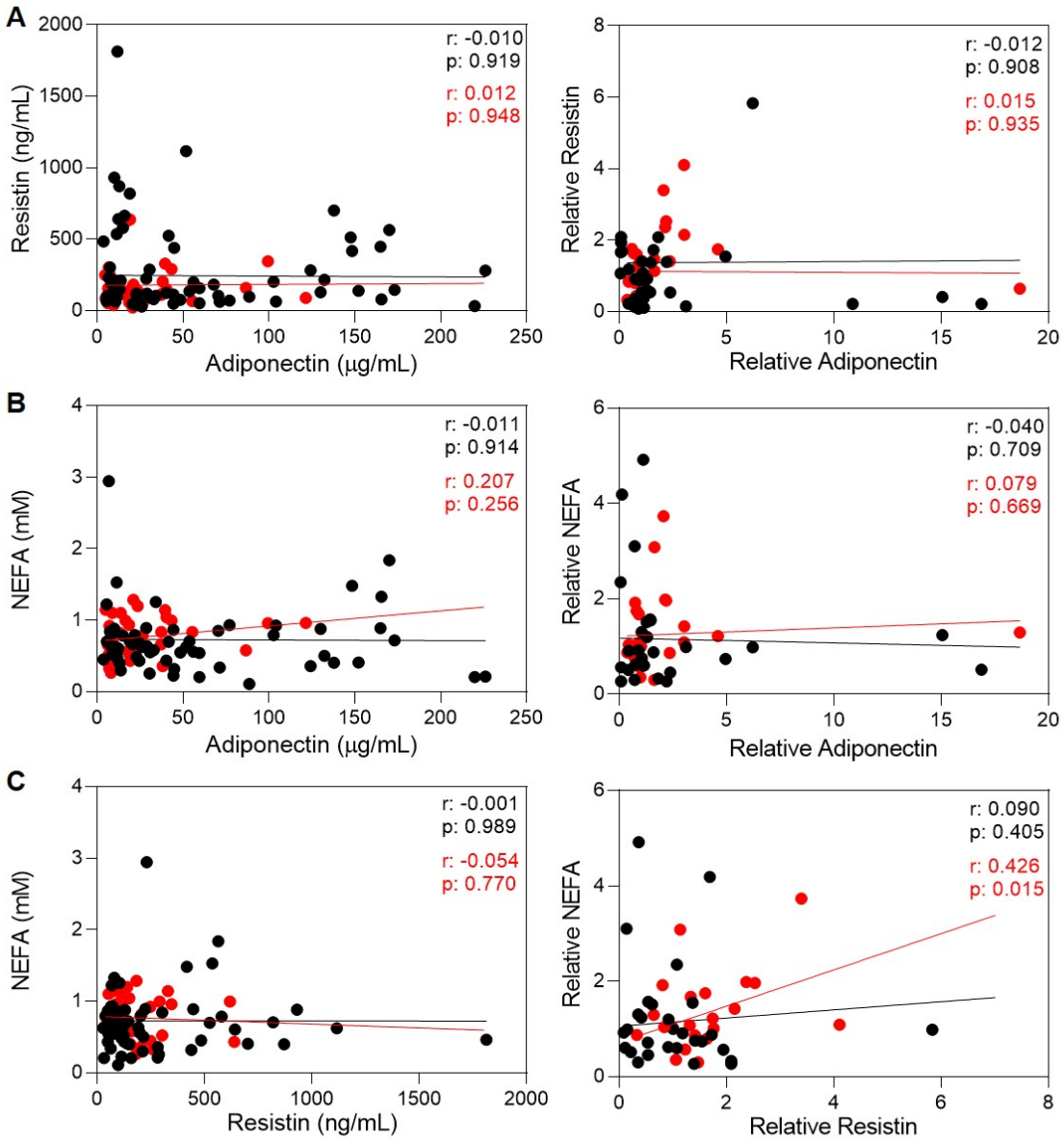


**Figure 8-2: Correlations between adipose-derived signaling molecules in ICU patients**

**Figure 8-2 Legend**

**A.** Correlation between absolute and relative circulating adiponectin and resistin levels in ICU patients. Absolute adiponectin and resistin levels in plasma were measured by Luminex. Relative values reflect change from admission levels for each patient.

**B.** Correlation between absolute and relative circulating adiponectin and NEFA levels in ICU patients. Absolute adiponectin levels were measured as in A. Absolute NEFA levels in serum were measured by colorimetric assay. Relative values reflect change from admission levels for each patient.

**C.** Correlation between absolute and relative circulating resistin and NEFA levels in ICU patients. Absolute resistin levels were measured as in A. Absolute NEFA levels were measured as in B. Relative values reflect change from admission levels for each patient.

$N$ = 95-100. Statistical analyses were performed using Pearson correlation. Red circles indicate values from COVID-19 patients. The red line indicates correlation exclusively for COVID-19 samples. Black circles indicate values from all other diagnoses. The black line indicates correlation for all samples.

## 8.5 DISCUSSION AND CONCLUSIONS

Acute hyperglycemia and systemic insulin resistance often develop during severe illness. This stress response leads to increased post-operative complications and mortality. Of critical public health importance, hyperglycemia has been found to develop in patients affected by COVID-19 and is linked to poor patient prognosis. As such, glycemic control in COVID-19 patients is a critical therapeutic avenue, especially considering the disease's high mortality rate and lack of specific treatment.

Our previous work has demonstrated a central role for lipolysis and adipokines in the development of stress-induced metabolic derangements. However, it had yet to be studied how these adipose-derived signaling molecules are affected during COVID-19 specifically. To examine this, we collected blood samples from patients admitted to the ICU. We found that COVID-19 patients exhibited decreased adiponectin levels and increased PAI-1 levels compared to other ICU patients, suggesting that they may have more severe stress-induced insulin resistance which likely contributes to the onset of hyperglycemia. However, we cannot rule out the possibility that low adiponectin and high PAI-1 levels may indicate a susceptibility to respiratory distress and hospitalization with COVID-19 infection. Our previous work specifically implicated lipolysis-dependent resistin release in the development of stress-related metabolic derangements. When we tested our COVID-19 patients, we found that resistin levels spiked at 24 h, while NEFA levels tended to increase over the duration of hospital stay. Further corroborating our hypothesis that acute resistin release is lipolysis dependent, we observed a significant, positive correlation between relative resistin and NEFA levels in our COVID-19 patients.

While the data presented here provide interesting observations regarding a potential role for adipose tissue-derived signaling molecules in stress-related metabolic derangements in COVID-19 patients, it is important to note that this represents preliminary analysis. Adipokine levels are known to be affected by factors such as body mass index (BMI), insulin administration, and diabetic status, among others (91). While we performed analysis normalizing the adipokines of each patient to their admission levels to account for innate differences, further and more sophisticated statistical analysis is required to properly control for these variables. In addition, previous studies have noted that adipokine levels serve as an independent risk factor for patient prognosis in instances of severe infection (90, 91). Further analysis is needed to determine if this relationship hold trues for COVID-19 patients within our cohort.

## ACKNOWLEDGEMENTS

I would like to thank the other members of the Harris lab for their continued support. This research was funded by NIH Cardiovascular Research Training Grant T32 HL0007284-41 (K.W.A.), NIH NRSA Predoctoral Fellowship 1F31DK121482-01A1 (K.W.A.), and NIH R01 1R01DK101946 (T.E.H.).

## AUTHOR CONTRIBUTIONS

The studies were designed by Katelyn Ahern, Stefan Hargett, Dr. Thurl Harris, Dr. William Horton, Dr. Alexandra Kadl, Dr. Sean Kearns. Experimental work was performed by Katelyn Ahern, Stefan Hargett, Dr. Thurl Harris. Data analysis was performed by Katelyn Ahern. Funding was provided by Katelyn Ahern and Dr. Thurl Harris.

# 9 PUBLICATIONS

## 9.1 PUBLICATIONS RESULTING FROM THIS WORK

1. Serbulea V, Upchurch CM, **Ahern KW**, Bories G, Voigt P, DeWeese DE, Meher AK, Harris TE, Leitinger N. Macrophages sensing oxidized DAMPs reprogram their metabolism to support redox homeostasis and inflammation through a TLR2-Syk-ceramide dependent mechanism. *Mol Metab*. 2017 Nov 7. doi: 10.1016/j.molmet.2017.11.002
2. Oenarto V, **Ahern KW**, Kadl A, Keller SR, Raje V, Harris TE. Adipocyte lipolysis drives acute stress-induced metabolic dysfunction. [Abstract] *Shock*. 2018 Jun. doi: 10.1097/SHK.0000000000001158
3. **Ahern K**, Mullins G, Raje V, Granade M, Harris T. Oxidized neutral lipid lipolysis regulates insulin signaling during acute stress. [Abstract] *Free Rad Biol Med*. 2018 Nov 20. doi: 10.1016/j.freeradbiomed.2018.10.174
4. Raje V, Howell NL, Martinez BA, **Ahern KW**, Oenarto V, Granade ME, Kim JW, Keller SR, Kadl A, Harris TE. Adipocyte lipolysis is necessary for acute-stress induced insulin resistance. [Abstract] *Shock*. 2019 Jun. doi: 10.1097/SHK.0000000000001374
5. **Ahern KW**, Serbulea V, Wingrove CL, Palas ZT, Leitinger N, Harris TE. Regioisomer-independent quantification of fatty acid oxidation products by HPLC-ESI-MS/MS analysis of sodium adducts. *Sci Rep*. 2019 Aug 1. doi: 10.1038/s41598-019-47693-5
6. Raje V, **Ahern KW**, Howell NL, Martinez BA, Oenarto V, Granade ME, Kim JW, Tundup S, Bottermann K, Gödecke A, Keller SR, Kadl A, Bland ML, Harris TE. Adipocyte lipolysis drives acute stress-induced insulin resistance and hyperglycemia. *Sci Rep*. 2020 November 1.

## 9.2 ADDITIONAL PUBLICATIONS

1. Hunt EA, Moutsiopoulou A, Ioannou S, **Ahern K**, Woodward K, Dikici E, Daunert S, Deo SK. Truncated variants of *Gaussia* luciferase with tyrosine linker for site-specific bioconjugate applications. *Sci Rep*. 2016 Jun 8. doi: 10.1038/srep26814
2. Oenarto V, Nederlof R, **Ahern K**, Harris T, Gödecke A. Adipose tissue lipolysis mediates lipid accumulation in pressure overloaded heart, leading to neutrophil infiltration and a decline in cardiac function. [Abstract] *Acta Physiol*. 2019 Sep 27. doi: 10.1111/apha.13384

# 10 REFERENCES


1. L. Li, J. L. Messina, Acute insulin resistance following injury. *Trends Endocrinol. Metab.* **20**, 429–435 (2009).

2. O. Ljungqvist, Insulin resistance and outcomes in surgery. *J. Clin. Endocrinol. Metab.* **95**, 4217–4219 (2010).

3. T. Doenst, *et al.*, Hyperglycemia during cardiopulmonary bypass is an independent risk factor for mortality in patients undergoing cardiac surgery. *J. Thorac. Cardiovasc. Surg.* **130**, 1144.e1-1144.e8 (2005).

4. H. Sato, *et al.*, The association of preoperative glycemic control, intraoperative insulin sensitivity, and outcomes after cardiac surgery. *J. Clin. Endocrinol. Metab.* **95**, 4338–4344 (2010).

5. L. Zhai, S. W. Ballinger, J. L. Messina, Role of reactive oxygen species in injury-induced insulin resistance. *Mol. Endocrinol.* **25**, 492–502 (2011).

6. G. Van Den Berghe, *et al.*, Intensive insulin therapy in critically ill patients. *N. Engl. J. Med.* **345**, 1359–1367 (2001).

7. M. E. McDonnell, G. E. Umpierrez, Insulin therapy for the management of hyperglycemia in hospitalized patients. *Endocrinol Metab Clin North Am* **41**, 175–201 (2012).

8. A. Schomig, Catecholamines in myocardial ischemia. Systemic and cardiac release. *Circulation* **82**, 13–22 (1990).

9. C. Riehle, J. Bauersachs, Key inflammatory mechanisms underlying heart failure. *Herz* **44**, 96–106 (2019).

10. S. D. Prabhu, N. G. Frangogiannis, The biological basis for cardiac repair after myocardial infarction. *Circ. Res.* **119**, 91–112 (2016).

11. J. K. Kjekshus, O. D. Mjos, Effect of inhibition of lipolysis on infarct size after experimental coronary artery occlusion. *J. Clin. Invest.* **52**, 1770–1778 (1973).

12. M. R. Luxton, N. E. Miller, M. F. Oliver, Antilipolytic therapy in angina pectoris Reduction of exercise-induced ST segment depression. *Heart* **38**, 1204–1208 (1976).

13. D. Levy, M. G. Larson, S. V. Ramachandran, W. B. Kannel, K. K. L. Ho, The progression from hypertension to congestive heart failure. *JAMA* **275**, 1557–1562 (1996).

14. W. B. Kannel, A. J. Belanger, Epidemiology of heart failure. *Am. Heart J.* **121**, 951–957 (1991).

15. A. H. Gradman, F. Alfayoumi, From left ventricular hypertrophy to congestive heart failure: management of hypertensive heart disease. *Prog. Cardiovasc. Dis.* **48**, 326–341 (2006).

16. C. L. Ogden, M. D. Carroll, C. D. Fryar, K. M. Flegal, Prevalence of obesity among adults and youth: United States, 2011-2014. *NCHS Data Brief*, 1–8 (2015).

17. A. A. Hedley, *et al.*, Prevalence of overweight and obesity among US children, adolescents, and adults, 1999-2002. *J. Am. Med. Assoc.* **291**, 2847–2850 (2004).

18. W. H. Organization, Autonomic neuropathy and transcutaneous oxymetry in diabetic lower extremities. *World Health Organ. Tech. Rep. Ser.* **894**, 1–268 (2000).

19. C. M. Hales, M. D. Carroll, C. D. Fryar, C. L. Ogden, Prevalence of obesity among adults and youth: United States, 2015–2016. *NCHS Data Brief*, 1–8 (2017).

20. S. Wild, G. Roglic, A. Green, R. Sicree, H. King, Estimates for the year 2000 and projections for 2030. *Diabetes Care* **27**, 1047–1053 (2004).

21. E. A. Finkelstein, J. G. Trogdon, J. W. Cohen, W. Dietz, Annual medical spending attributable to obesity: payer-and service-specific estimates. *Health Aff.* **28**, 822–831 (2009).

22. M. Mauro, V. Taylor, S. Wharton, A. M. Sharma, Barriers to obesity treatment. *Eur. J. Intern. Med.* **19**, 173–180 (2008).

23. G. A. Bray, D. H. Ryan, Drug treatment of the overweight patient. *Gastroenterology* **132**, 2239–2252 (2007).

24. R. Padwal, A. Kezouh, M. Levine, M. Etminan, Long-term persistence with orlistat and sibutramine in a population-based cohort. *Int. J. Obes.* **31**, 1567–1570 (2007).

25. J. G. Kral, E. Näslund, Surgical treatment of obesity. *Nat. Clin. Pract. Endocrinol. Metab.* **3**, 574–583 (2007).

26. M. P. Mattson, Perspective: Does brown fat protect against diseases of aging? *Ageing Res. Rev.* **9**, 69–76 (2010).

27. A. Gómez-Hernández, N. Beneit, S. Díaz-Castroverde, Ó. Escribano, Differential role of adipose tissues in obesity and related metabolic and vascular complications. *Int. J. Endocrinol.* **2016**, 1–15 (2016).

28. A. Gastaldelli, *et al.*, Metabolic effects of visceral fat accumulation in type 2 diabetes. *J. Clin. Endocrinol. Metab.* **87**, 5098–5103 (2002).

29. P. J. Coon, E. M. Rogus, D. Drinkwater, D. C. Muller, A. P. Goldberg, Role of body fat distribution in the decline in insulin sensitivity and glucose tolerance with age. *J. Clin. Endocrinol. Metab.* **75**, 1125–1132 (1992).

30. P. Björntorp, Metabolic implications of body fat distribution. *Diabetes Care* **14**, 1132–1143 (1991).

31. J. Hellmer, C. Marcus, T. Sonnenfeld, P. Arner, Mechanisms for differences in lipolysis between human subcutaneous and omental fat cells. *J. Clin. Endocrinol. Metab.* **75**, 15–20 (1992).

32. A. Green, Catecholamines inhibit insulin-stimulated glucose transport adipocytes, in the presence of adenosine deaminase. **152**, 0–3 (1983).

33. S. E. Kahn, R. L. Hull, K. M. Utzschneider, Mechanisms linking obesity to insulin resistance and type 2 diabetes. *Nature* **444**, 840–846 (2006).

34. E. D. Rosen, B. M. Spiegelman, Adipocytes as regulators of energy balance and glucose homeostasis. *Nature* **444**, 847–853 (2006).

35. S. Daemen, J. D. Schilling, The interplay between tissue niche and macrophage cellular metabolism in obesity. *Front. Immunol.* **10**, 1–16 (2020).

36. I. Harman-Boehm, *et al.*, Macrophage infiltration into omental versus subcutaneous fat across different populations: effect of regional adiposity and the comorbidities of obesity. *J. Clin. Endocrinol. Metab.* **92**, 2240–2247 (2007).

37. A. Ehrlund, *et al.*, The cell-type specific transcriptome in human adipose tissue and influence of obesity on adipocyte progenitors. *Sci. Data* **4**, 1–11 (2017).

38. R. Cancello, *et al.*, Reduction of macrophage infiltration and chemoattractant gene expression changes in white adipose tissue of morbidly obese subjects after surgery-induced weight loss. *Diabetes* **54**, 2277–2286 (2005).

39. S. P. Weisberg, *et al.*, Obesity is associated with macrophage accumulation in adipose tissue. *J. Clin. Invest.* **112**, 1796–1808 (2003).

40. S. Cinti, *et al.*, Adipocyte death defines macrophage localization and function in adipose tissue of obese mice and humans. *J. Lipid Res.* **46**, 2347–2355 (2005).

41. M. Keuper, *et al.*, An inflammatory micro-environment promotes human adipocyte apoptosis. *Mol. Cell. Endocrinol.* **339**, 105–113 (2011).

42. C. N. Lumeng, J. L. Bodzin, A. R. Saltiel, Obesity induces a phenotypic switch in adipose tissue macrophage polarization. *J. Clin. Invest.* **117**, 175–184 (2007).

43. H. Lee, I. S. Lee, R. Choue, Obesity, inflammation and diet. *Pediatr. Gastroenterol. Hepatol. Nutr.* **16**, 143–152 (2013).

44. V. Serbulea, *et al.*, Macrophages sensing oxidized DAMPs reprogram their metabolism to support redox homeostasis and inflammation through a TLR2-Syk-ceramide dependent mechanism. *Mol. Metab.* **7**, 23–34 (2017).

45. V. Serbulea, *et al.*, Macrophage phenotype and bioenergetics are controlled by oxidized phospholipids identified in lean and obese adipose tissue. *Proc. Natl. Acad. Sci.* **115**, 6254–6263 (2018).

46. S. E. Shoelson, L. Herrero, A. Naaz, Obesity, inflammation, and insulin resistance. *Gastroenterology* **132**, 2169–2180 (2007).

47. J. P. Desborough, The stress response to trauma and surgery. *Br. J. Anaesth.* **85**, 109–117 (2000).

48. J. Boucher, A. Kleinridders, C. R. Kahn, Insulin receptor signaling in normal and

insulin-resistant states. *Cold Spring Harb Perspect Biol 2014* **6**, a009191 (2014).

49. M. Laplante, D. M. Sabatini, mTOR signaling in growth control and disease. *Cell* **149**, 274–293 (2012).

50. A. Kumar, *et al.*, Fat cell-specific ablation of rictor in mice impairs insulin-regulated fat cell and whole-body glucose and lipid metabolism. *Diabetes* **59**, 1397–1406 (2010).

51. R. E. Duncan, M. Ahmadian, K. Jaworski, E. Sarkadi-Nagy, H. S. Sul, Regulation of lipolysis in adipocytes. *Annu. Rev. Nutr.* **27**, 79–101 (2007).

52. G. R. Mullins, *et al.*, Catecholamine-induced lipolysis causes mTOR complex dissociation and inhibits glucose uptake in adipocytes. *Proc. Natl. Acad. Sci.* **111**, 17450–17455 (2014).

53. M. Schweiger, *et al.*, Adipose triglyceride lipase and hormone-sensitive lipase are the major enzymes in adipose tissue triacylglycerol catabolism. *J. Biol. Chem.* **281**, 40236–40241 (2006).

54. G. Haemmerle, *et al.*, Defective lipolysis and altered energy metabolism in mice lacking adipose triglyceride lipase. *Science (80-. ).* **312**, 734–737 (2006).

55. M. Hatting, C. D. J. Tavares, K. Sharabi, A. K. Rines, P. Puigserver, Insulin regulation of gluconeogenesis. *Ann. N. Y. Acad. Sci.* **1411**, 21–35 (2018).

56. J. Wijkander, T. R. Landström, V. Manganiello, P. Belfrage, E. Degerman, Insulin-induced phosphorylation and activation of phosphodiesterase 3b in rat adipocytes: Possible role for protein kinase b but not mitogen-activated protein kinase or p70 s6 kinase. *Endocrinology* **139**, 219–227 (1998).

57. C. Carpene, *et al.*, B3-adrenergic receptors are responsible for the adrenergic inhibition of insulin-stimulated glucose transport in rat adipocytes. *Biochem. J.* **296**, 99–105 (1993).

58. E. E. Jacobs, D. R. Sanadi, Phosphorylation coupled to electron transport mediated by high potential electron carriers. *Biochim. Biophys. Acta* **38**, 12–34 (1960).

59. E. Niki, Evidence for beneficial effects of vitamin E. *Korean J. Intern. Med.* **30**, 571–579 (2015).

60. T. L. Clanton, Hypoxia-induced reactive oxygen species formation in skeletal muscle. *J. Appl. Physiol.* **102**, 2379–2388 (2007).

61. H. Nohl, L. Gille, K. Staniek, Intracellular generation of reactive oxygen species by mitochondria. *J. Clin. Endocrinol. Metab.* **15**, 51–64 (2010).

62. M. G. Rosca, *et al.*, Oxidation of fatty acids is the source of increased mitochondrial reactive oxygen species production in kidney cortical tubules in early diabetes. *Diabetes* **61**, 2074–2083 (2012).

63. C. M. Havrilla, D. L. Hachey, N. A. Porter, Coordination (ag+) ion spray - mass spectrometry of peroxidation products of cholesterol linoleate and cholesterol

arachidonate: high-performance liquid chromatography - mass spectrometry analysis of peroxide products from polyunsaturated lipid autoxidati. *J. Am. Chem. Soc.* **122**, 8042–8055 (2000).

64. L. Gao, *et al.*, Novel n-3 fatty acid oxidation products activate Nrf2 by destabilizing the association between Keap1 and Cullin3. *J. Biol. Chem.* **282**, 2529–2537 (2007).

65. V. Serbulea, D. DeWeese, N. Leitinger, The effect of oxidized phospholipids on phenotypic polarization and function of macrophages. *Free Radic. Biol. Med.* **111**, 156–168 (2017).

66. A. Ayala, M. F. Munoz, S. Argüelles, Lipid peroxidation: production, metabolism, and signaling mechanisms of malondialdehyde and 4-hydroxy-2-nonenal. *Oxid. Med. Cell. Longev.* **2014** (2014).

67. D. K. MacMillan, R. C. Murphycor, Analysis of lipid hydroperoxides and long-chain conjugated keto acids by negative ion electrospray mass spectrometry. *J. Am. Soc. Mass Spectrom.* **6**, 1190–1201 (1995).

68. J. Neuzil, *et al.*, Oxidation of parenteral lipid emulsion by ambient and phototherapy lights: potential toxicity of routine parenteral feeding. *J. Pediatr.* **126**, 785–790 (1995).

69. F. J. Schopfer, C. Cipollina, B. A. Freeman, Formation and signaling actions of electrophilic lipids. *Chem. Rev.* **111**, 5997–6021 (2011).

70. S. S. Davies, L. Guo, Lipid peroxidation generates biologically active phospholipids including oxidatively N-modified phospholipids. *Chem. Phys. Lipids* **181**, 1–33 (2014).

71. A. Toschi, *et al.*, Regulation of mTORC1 and mTORC2 Complex Assembly by Phosphatidic Acid: Competition with Rapamycin. *Mol. Cell. Biol.* **29**, 1411–1420 (2009).

72. Y. Minokoshi, C. R. Kahn, B. B. Kahn, Tissue-specific ablation of the GLUT4 glucose transporter or the insulin receptor challenges assumptions about insulin action and glucose homeostasis. *J. Biol. Chem.* **278**, 33609–33612 (2003).

73. E. Tozzo, B. B. Kahn, P. F. Pilch, K. V. Kandror, Glut4 is targeted to specific vesicles in adipocytes of transgenic mice overexpressing Glut4 selectively in adipose tissue. *J. Biol. Chem.* **271**, 10490–10494 (1996).

74. N. Ouchi, J. L. Parker, J. J. Lugus, K. Walsh, Adipokines in inflammation and metabolic disease. *Nat. Rev. Immunol.* **11**, 85–97 (2011).

75. K. Makki, P. Froguel, I. Wolowczuk, Adipose tissue in obesity-related inflammation and insulin resistance: cells, cytokines, and chemokines. *ISRN Inflamm.* **2013**, 1–12 (2013).

76. M. Coelho, T. Oliveira, R. Fernandes, Biochemistry of adipose tissue: An endocrine organ. *Arch. Med. Sci.* **9**, 191–200 (2013).

77. Y. Arita, *et al.*, Paradoxical decrease of an adipose-specific protein, adiponectin, in obesity. *Biochem. Biophys. Res. Commun.* **425**, 560–564 (2012).

78. P. Almeda-Valdes, *et al.*, Total and high molecular weight adiponectin have similar utility for the identification of insulin resistance. *Cardiovasc. Diabetol.* **9**, 1–10 (2010).

79. S. Galic, J. S. Oakhill, G. R. Steinberg, Adipose tissue as an endocrine organ. *Mol. Cell. Endocrinol.* **316**, 129–139 (2010).

80. M. Itoh, T. Suganami, R. Hachiya, Y. Ogawa, Adipose tissue remodeling as homeostatic inflammation. *Int. J. Inflam.* **2011**, 1–8 (2011).

81. A. M. Van Den Hoek, *et al.*, Leptin deficiency per se dictates body composition and insulin action in ob/ob mice. *J. Neuroendocrinol.* **20**, 120–127 (2008).

82. M. L. G. Correia, W. G. Haynes, A role for plasminogen activator inhibitor-1 in obesity: From pie to PAI? *Arterioscler. Thromb. Vasc. Biol.* **26**, 2183–2185 (2006).

83. I. Mertens, L. F. Van Gaal, Visceral fat as a determinant of fibrinolysis and hemostasis. *Semin. Vasc. Med.* **5**, 48–55 (2005).

84. C. M. Steppan, *et al.*, The hormone resistin links obesity to diabetes. *Nature* **409**, 307–312 (2001).

85. P. G. Mcternan, C. M. Kusminski, S. Kumar, Resistin. *Curr. Opin. Lipidol.* **17**, 170–175 (2006).

86. K. Barnes, J. Miner, Role of resistin in insulin sensitivity in rodents and humans. *Curr. Protein Pept. Sci.* **10**, 96–107 (2009).

87. Q. Hu, H. Tan, D. M. Irwin, Evolution of the vertebrate resistin gene family. *PLoS One* **10**, 1–16 (2015).

88. R. Z. Yang, *et al.*, Comparative studies of resistin expression and phylogenomics in human and mouse. *Biochem. Biophys. Res. Commun.* **310**, 927–935 (2003).

89. C. de Luca, J. M. Olefsky, Inflammation and insulin resistance. *FEBS Lett.* **582**, 97–105 (2008).

90. I. Karampela, G. S. Christodoulatos, M. Dalamaga, The role of adipose tissue and adipokines in sepsis: inflammatory and metabolic considerations, and the obesity paradox. *Curr. Obes. Rep.* **8**, 434–457 (2019).

91. T. Hajri, M. Gharib, S. Kaul, M. S. Karpeh, Association between adipokines and critical illness outcomes. *J. Trauma Acute Care Surg.* **83**, 507–519 (2017).

92. J. Sundén-Cullberg, *et al.*, Pronounced elevation of resistin correlates with severity of disease in severe sepsis and septic shock. *Crit. Care Med.* **35**, 1536–1542 (2007).

93. S. P. J. Macdonald, *et al.*, Sustained elevation of resistin, NGAL and IL-8 are

associated with severe sepsis/septic shock in the emergency department. *PLoS One* **9**, 110678 (2014).

94. A. Koch, O. A. Gressner, E. Sanson, F. Tacke, C. Trautwein, Serum resistin levels in critically ill patients are associated with inflammation, organ dysfunction and metabolism and may predict survival of non-septic patients. *Crit. Care* **13**, 1–9 (2009).

95. X. Q. Dong, Y. Y. Hu, W. H. Yu, Z. Y. Zhang, High concentrations of resistin in the peripheral blood of patients with acute basal ganglia hemorrhage are associated with poor outcome. *J. Crit. Care* **25**, 243–247 (2010).

96. X. Q. Dong, *et al.*, Resistin is associated with mortality in patients with traumatic brain injury. *Crit. Care* **14**, 190–194 (2010).

97. A. Erturk, *et al.*, Serum resistin levels may be new prognostic factor of crimean-congo hemorrhagic fever. *Int. J. Clin. Exp. Med.* **7**, 3536–3542 (2014).

98. A. Bonavia, L. Miller, J. A. Kellum, K. Singbartl, Hemoadsorption corrects hyperresistinemia and restores anti-bacterial neutrophil function. *Intensive Care Med. Exp.* **5**, 36–48 (2017).

99. J. C. Jang, *et al.*, Human resistin protects against endotoxic shock by blocking LPS–TLR4 interaction. *Proc. Natl. Acad. Sci. U. S. A.* **114**, E10399–E10408 (2017).

100. A. D. Watson, *et al.*, Structural identification by mass spectrometry of oxidized phospholipids in minimally oxidized low density lipoprotein that induce monocyte/endothelial interactions and evidence for their presence in vivo. *J. Biol. Chem.* **272**, 13597–13607 (1997).

101. N. Maeda, *et al.*, Adaptation to fasting by glycerol transport through aquaporin 7 in adipose tissue. *Proc. Natl. Acad. Sci. U. S. A.* **101**, 17801–17806 (2004).

102. D. S. Sohal, *et al.*, Temporally regulated and tissue-specific gene manipulations in the adult and embryonic heart using a tamoxifen-inducible Cre protein. *Circ. Res.* **89**, 20–25 (2001).

103. M. Kuroda, R. C. Honnor, S. W. Cushman, C. Londos, I. A. Simpson, Regulation of insulin-stimulated glucose transport in the isolated rat adipocyte. cAMP-independent effects of lipolytic and antilipolytic agents. *J. Biol. Chem.* **262**, 245–253 (1987).

104. S. Boroda, *et al.*, The phosphatidic acid – binding , polybasic domain is responsible for the differences in the phosphoregulation of lipins 1 and 3. *J. Biol. Chem.* **292**, 20481–20493 (2017).

105. H. G. Joost, A. D. Habberfield, I. A. Simpson, A. Laurenza, K. B. Seamon, Activation of adenylate cyclase and inhibition of glucose transport in rat adipocytes by forskolin analogues: structural determinants for distinct sites of action. *Mol. Pharmacol.* **33**, 449–453 (1988).

106. J. E. Ayala, *et al.*, Hyperinsulinemic-euglycemic clamps in conscious, unrestrained mice. *J. Vis. Exp.*, e3188 (2011).

107. A. Heinen, *et al.*, IGF1 treatment improves cardiac remodeling after infarction by targeting myeloid cells. *Mol. Ther.* **27**, 46–58 (2019).

108. C. Hellmuth, M. Weber, B. Koletzko, W. Peissner, Nonesterified fatty acid determination for functional lipidomics: Comprehensive ultrahigh performance liquid chromatography-tandem mass spectrometry quantitation, qualification, and parameter prediction. *Anal. Chem.* **84**, 1483–1490 (2012).

109. T. Delatour, P. Mottier, E. Gremaud, Limits of suspicion, recognition and confirmation as concepts that account for the confirmation transitions at the detection limit for quantification by liquid chromatography-tandem mass spectrometry. *J. Chromatogr. A* **1169**, 103–110 (2007).

110. U. Harder, B. Koletzko, W. Peissner, Quantification of 22 plasma amino acids combining derivatization and ion-pair LC-MS/MS. *J. Chromatogr. B Anal. Technol. Biomed. Life Sci.* **879**, 495–504 (2011).

111. European Council, Legislation. *Off. J. Eur. Communities* **45**, 1–39 (2002).

112. I. Ferrer, J. A. Zweigenbaum, E. M. Thurman, Analysis of 70 Environmental Protection Agency priority pharmaceuticals in water by EPA Method 1694. *J. Chromatogr. A* **1217**, 5674–5686 (2010).

113. Agilent Technologies, *Agilent MassHunter workstation software* (2010).

114. F. André, *et al.*, Trends in the identification of organic residues and contaminants: EC regulations under revision. *TrAC - Trends Anal. Chem.* **20**, 435–445 (2001).

115. I. H. Chaudry, M. S. Mohammed, A. E. Baue, Insulin resistance in experimental shock. *J. Am. Med. Assoc.* **109**, 412–415 (1974).

116. E. Duggan, K. Carlson, G. Umpierresz, Metabolic consequences of surgical stress. *Anesthesiology* **126**, 547–560 (2017).

117. A. Lipshutz, M. Gropper, Perioperative glycemic control. *Anesthesiology* **110**, 408–421 (2009).

118. I. Vanhorebeek, J. Gunst, G. Van den Berghe, Critical care management of stress-induced hyperglycemia. *Curr. Diab. Rep.* **18**, 1–12 (2018).

119. H. Nojima, *et al.*, The mammalian target of rapamycin (mTOR) partner, raptor, binds the mTOR substrates p70 S6 kinase and 4E-BP1 through their TOR signaling (TOS) motif. *J. Biol. Chem.* **278**, 15461–15464 (2003).

120. E. Jacinto, *et al.*, SIN1/MIP1 maintains rictor-mTOR complex integrity and regulates Akt phosphorylation and substrate specificity. *Cell* **127**, 125–137 (2006).

121. C. A. Chu, *et al.*, Comparison of the direct and indirect effects of epinephrine on hepatic glucose production. *J. Clin. Invest.* **99**, 1044–1056 (1997).

122. S. D. Mittelman, R. N. Bergman, Inhibition of lipolysis causes suppression of endogenous glucose production independent of changes in insulin. *Am. J. Physiol. - Endocrinol. Metab.* **279**, 630–637 (2000).

123. R. J. Perry, *et al.*, Hepatic acetyl CoA links adipose tissue inflammation to hepatic insulin resistance and type 2 diabetes. *Cell* **160**, 745–758 (2015).

124. P. M. Titchenell, *et al.*, Direct hepatocyte insulin signaling is required for lipogenesis but is dispensable for the suppression of glucose production. *Cell Metab.* **23**, 1154–1166 (2016).

125. R. Zechner, *et al.*, FAT SIGNALS - Lipases and lipolysis in lipid metabolism and signaling. *Cell Metab.* **15**, 279–291 (2012).

126. Y. Ma, P. Wang, J. F. Kuebler, I. H. Chaudry, J. L. Messina, Hemorrhage induces the rapid development of hepatic insulin resistance. *Am. J. Physiol. Gastrointest. Liver Physiol.* **284**, G107–G115 (2003).

127. R. W. Stevenson, *et al.*, Dose-related effects of epinephrine on glucose production in conscious dogs. *Am. J. Physiol. - Endocrinol. Metab.* **260**, 363–370 (1991).

128. O. P. McGuinness, *et al.*, Impact of chronic stress hormone infusion on hepatic carbohydrate metabolism in the conscious dog. *Am. J. Physiol. - Endocrinol. Metab.* **265**, 314–322 (1993).

129. N. Mayer, *et al.*, Development of small-molecule inhibitors targeting adipose triglyceride lipase. *Nat. Chem. Biol.* **9**, 785–787 (2013).

130. S. W. Coppack, D. L. Chinkes, J. M. Miles, B. W. Patterson, S. Klein, A multicompartmental model of in vivo adipose tissue glycerol kinetics and capillary permeability in lean and obese humans. *Diabetes* **54**, 1934–1941 (2005).

131. S. Rosell, E. Belfrage, Blood circulation in adipose tissue. *Physiol Rev* **59**, 1078–1104 (1979).

132. E. Belfrage, P. Hjemdahl, B. B. Fredholm, Metabolic effects of blood flow restriction in adipose tissue. *Acta Physiol. Scand.* **105**, 222–227 (1979).

133. A. G. Kovách, *et al.*, Blood flow, oxygen consumption, and free fatty acid release in subcutaneous adipose tissue during hemorrhagic shock in control and phenoxybenzamine-treated dogs. *Circ. Res.* **26**, 733–741 (1970).

134. A. M. Rofe, D. H. Williamson, Mechanism for the “anti-lipolytic” action of vasopressin in the starved rat. *Biochem. J.* **212**, 899–902 (1983).

135. A. G. Kovach, Blood flow and release of free fatty acids in the omentum, mesentery, and subcutaneous adipose tissue of the dog in haemorrhagic shock. *Acta Physiol. Hung.* **45**, 79–87 (1974).

136. A. G. Kovach, *et al.*, Blood flow, oxygen consumption, and free fatty acid release in subcutaneous adipose tissue during hemorrhagic shock in control and phenoxybenzamine-treated dogs. *Circ Res* **26**, 733–741 (1970).

137. V. L. Williams, R. E. Martin, J. L. Franklin, R. W. Hardy, J. L. Messina, Injury-induced insulin resistance in adipose tissue. *Biochem. Biophys. Res. Commun.* **421**, 442–448 (2012).

138. L. Thompson, H. Kim, Y. Ma, N. Kokorina, J. Messina, Acute, muscle-type specific insulin resistance following injury. *Mol. Med.* **14**, 715–723 (2008).

139. M. Schweiger, *et al.*, Pharmacological inhibition of adipose triglyceride lipase corrects high-fat diet-induced insulin resistance and hepatosteatosis in mice. *Nat. Commun.* **8**, 1–14 (2017).

140. A. K. Dhalla, Y. W. Mei, P. J. Voshol, L. Belardinelli, G. M. Reaven, A1 adenosine receptor partial agonist lowers plasma FFA and improves insulin resistance induced by high-fat diet in rodents. *Am. J. Physiol. - Endocrinol. Metab.* **292**, 1358–1363 (2007).

141. P. M. Staehr, *et al.*, Reduction of free fatty acids, safety, and pharmacokinetics of oral GS-9667, an a1 adenosine receptor partial agonist. *J. Clin. Pharmacol.* **53**, 385–392 (2013).

142. D. C. Deibert, R. A. Defronzo, Epinephrine-induced insulin resistance in man. *J. Clin. Invest.* **65**, 717–721 (1980).

143. J. M. Berg, J. L. Tymoczko, L. Stryer, "Glucose can be synthesized from noncarbohydrate precursors" in *Biochemistry 5th Edition*, (2002), p. Section 16.3.

144. T. Hibuse, *et al.*, Aquaporin 7 deficiency is associated with development of obesity through activation of adipose glycerol kinase. *Proc. Natl. Acad. Sci. U. S. A.* **102**, 10993–10998 (2005).

145. R. J. Perry, *et al.*, Leptin mediates a glucose-fatty acid cycle to maintain glucose homeostasis in starvation. *Cell* **172**, 234-248.e17 (2018).

146. A. H. Berg, T. P. Combs, X. Du, M. Brownlee, P. E. Scherer, The adipocyte-secreted protein Acrp30 enhances hepatic insulin action. *Nat. Med.* **7**, 947–953 (2001).

147. E. D. Muse, T. K. T. Lam, P. E. Scherer, L. Rossetti, Hypothalamic resistin induces hepatic insulin resistance. *J. Clin. Invest.* **117**, 1670–1678 (2007).

148. M. W. Rajala, *et al.*, Regulation of resistin expression and circulating levels in obesity, diabetes, and fasting. *Diabetes* **53**, 1671–1679 (2004).

149. F. Jahoor, S. Klein, R. Wolfe, Mechanism of regulation of glucose production by lipolysis in humans. *Am. Physiol. Soc.* **262**, 353–358 (1992).

150. D. T. Watts, Arterial blood epinephrine levels during hemorrhagic hypotension in dogs. *Am. J. Physiol.* **184**, 271–274 (1956).

151. M. C. Petersen, G. I. Shulman, Mechanisms of insulin action and insulin resistance. *Physiol. Rev.* **98**, 2133–2223 (2018).

152. N. S. Dhalla, R. M. Temsah, T. Netticadan, Role of oxidative stress in

cardiovascular diseases. *J. Hypertens.* **18**, 655–73 (2000).

153. C. J. Wruck, *et al.*, Role of oxidative stress in rheumatoid arthritis: Insights from the Nrf2-knockout mice. *Ann. Rheum. Dis.* **70**, 844–850 (2011).

154. P. Manna, S. K. Jain, Obesity, oxidative stress, adipose tissue dysfunction, and the associated health risks: causes and therapeutic strategies. *Metab. Syndr. Relat. Disord.* **13**, 423–444 (2015).

155. E. J. Henriksen, M. K. Diamond-Stanic, E. M. Marchionne, Oxidative stress and the etiology of insulin resistance and type 2 diabetes. *Free Radic. Biol. Med.* **51**, 993–999 (2011).

156. Z. Yang, V. E. Laubach, B. A. French, I. L. Kron, Acute hyperglycemia enhances oxidative stress and exacerbates myocardial infarction by activating NADPH oxidase during reperfusion. *J. Thorac. Cardiovasc. Surg.* **137**, 723–729 (2009).

157. R. Harkewicz, E. A. Dennis, Applications of mass spectrometry to lipids and membranes. *Annu. Rev. Biochem.* **80**, 301–325 (2011).

158. O. Quehenberger, *et al.*, Lipidomics reveals a remarkable diversity of lipids in human plasma. *J. Lipid Res.* **51**, 3299–3305 (2010).

159. C. Schneider, P. Schreier, M. Herderich, Analysis of lipoxygenase-derived fatty acid hydroperoxides by electrospray ionization tandem mass spectrometry. *Lipids* **32**, 331–336 (1997).

160. J. G. Bollinger, G. Rohan, M. Sadilek, M. H. Gelb, LC/ESI-MS/MS detection of FAs by charge reversal derivatization with more than four orders of magnitude improvement in sensitivity. *J. Lipid Res.* **54**, 3523–3530 (2013).

161. J. G. Bollinger, *et al.*, Improved sensitivity mass spectrometric detection of eicosanoids by charge reversal derivatization. *Anal. Chem.* **82**, 6790–6796 (2010).

162. M. N. Clifford, V. Lopez, L. Poquet, G. Williamson, N. Kuhnert, A systematic study of carboxylic acids in negative ion mode electrospray ionisation mass spectrometry providing a structural model for ion suppression. *Rapid Commun. Mass Spectrom.*, 2014–2018 (2007).

163. J. Bylund, J. Ericsson, E. H. Oliw, Analysis of cytochrome P450 metabolites of arachidonic and linoleic acids by liquid chromatography-mass spectrometry with ion trap MS. *Anal. Biochem.* **265**, 55–68 (1998).

164. J. L. Kerwin, J. J. Torvik, Identification of monohydroxy fatty acids by electrospray mass spectrometry and tandem mass spectrometry. *Anal. Biochem.* **237**, 56–64 (1996).

165. J. Ito, S. Mizuochi, K. Nakagawa, S. Kato, T. Miyazawa, Tandem mass spectrometry analysis of linoleic and arachidonic acid hydroperoxides via promotion of alkali metal adduct formation. *Anal. Chem.* **87**, 4980–4987 (2015).

166. B. S. Levison, *et al.*, Quantification of fatty acid oxidation products using on-line

high performace liquid chromatography tandem mass spectrometry. *Free Radic. Biol. Med.* **59**, 2–13 (2013).

167. K. A. Lagerborg, J. D. Watrous, S. Cheng, M. Jain, High-throughput measure of bioactive lipids using non-targeted mass spectrometry. *Metab. Signal. Methods Protoc.* **1862**, 17–35 (2018).

168. C. Dufour, M. Loonis, Regio- and stereoselective oxidation of linoleic acid bound to serum albumin: identification by ESI-mass spectrometry and NMR of the oxidation products. *Chem. Phys. Lipids* **138**, 60–68 (2005).

169. H. J. Helbock, P. a Motchnik, B. N. Ames, Toxic hydroperoxides in intravenous lipid emulsions used in preterm infants. *Pediatrics* **91**, 83–7 (1993).

170. W. S. Powell, J. Rokach, Biosynthesis, biological effects, and receptors of hydroxyeicosatetraenoic acids (HETEs) and oxoeicosatetraenoic acids (oxo-ETEs) derived from arachidonic acid. *Biochim. Biophys. Acta - Mol. Cell Biol. Lipids* **1851**, 340–355 (2015).

171. J. Ito, *et al.*, A novel chiral stationary phase LC-MS/MS method to evaluate oxidation mechanisms of edible oils. *Sci. Rep.* **7**, 1–10 (2017).

172. D. A. Zehethofer, N; Pinto, D.M.; Volmer, Plasma free fatty acid profiling in a fish oil human intervention study using ultra-performance liquid chromatography/electrospray ionization tandem mass spectrometry. *Rapid Commun. Mass Spectrom.* **22**, 2161–2175 (2008).

173. E. Davoli, M. L. Gross, Charge remote fragmentation of fatty acids cationized with alkaline earth metal ions. *J. Am. Soc. Mass Spectrom.* **1**, 320–324 (1990).

174. C. Cheng, D. Giblin, M. L. Gross, Structural determination of oxofatty acids by charge-remote fragmentations. *J. Am. Soc. Mass Spectrom.* **9**, 216–224 (1998).

175. J. S. Crockett, M. L. Gross, W. W. Christie, R. T. Holman, Collisional activation of a series of homoconjugated octadecadienoic acids with fast atom bombardment and tandem mass spectrometry. *J. Am. Soc. Mass Spectrom.* **1**, 183–191 (1990).

176. F. Hsu, J. Turk, Distinction among isomeric unsaturated fatty acids as lithiated adducts by electrospray ionization mass spectrometry using low energy collisionally activated dissociation on a triple stage quadrupole instrument. *J Am Soc Mass Spectrom* **0305** (1999).

177. F. Hsu, J. Turk, Structural characterization of triacylglycerols as lithiated adducts by electrospray ionization mass spectrometry using low-energy collisionally activated dissociation on a triple stage quadrupole instrument. *J. Am. Soc. Mass Spectrom.* **10**, 600–612 (1999).

178. A. Haemers, H. Van den Heuvel, L. Nizigiyimana, M. Claeys, I. Vedernikova, Charge-remote and charge-proximate fragmentation processes in alkali-cationized fatty acid esters upon high-energy collisional activation. A new mechanistic proposal. *J. Mass Spectrom.* **33**, 631–643 (2002).

179. J. Adams, M. L. Gross, Energy requirements for remote charge site ion decompositions and structural information from collisional activation of alkali metal cationized fatty alcohols. *J. Am. Chem. Soc.* **108**, 6915–6921 (1986).

180. J. Adams, M. L. Gross, Charge-remote fragmentations of closed-shell ions. A thermolytic analogy. *J. Am. Chem. Soc.* **111**, 435–440 (2005).

181. T. M. Annesley, Methanol-associated matrix effects in electrospray ionization tandem mass spectrometry. *Clin. Chem.* **53**, 1827–1834 (2007).

182. K. L. Napoli, More on methanol-associated matrix effects in electrospray ionization mass spectrometry. *Clin. Chem.* **55**, 1249–1250 (2009).

183. J. M. Hevko, R. C. Murphy, Electrospray ionization and tandem mass spectrometry of cysteinyl eicosanoids: leukotriene C4and FOG7. *J. Am. Soc. Mass Spectrom.* **12**, 763–771 (2001).

184. C. Hellmuth, B. Koletzko, W. Peissner, Aqueous normal phase chromatography improves quantification and qualification of homocysteine, cysteine and methionine by liquid chromatography-tandem mass spectrometry. *J. Chromatogr. B Anal. Technol. Biomed. Life Sci.* **879**, 83–89 (2011).

185. H. Nygren, T. Seppänen-laakso, S. Castillo, "Liquid chromatography-mass spectrometry-based lipidomics for studies of body fluids and tissues" in *Methods in Molecular Biology*, (2011), pp. 247–257.

186. S. H. Lee, C. Pettinella, I. A. Blair, LC/ESI/MS analysis of saturated and unsaturated fatty acids in rat intestinal epithelial cells. *Curr. Drug Metab.* **7**, 929–937 (2006).

187. R. Yang, L. A. Barouch, Leptin signaling and obesity: cardiovascular consequences. *Circ. Res.* **101**, 545–559 (2007).

188. K. Landin, P. Lonnroth, M. Krotkiewski, G. Holm, U. Smith, Increased insulin resistance and fat cell lipolysis in obese but not lean women with a high waist/hip ratio. *Eur. J. Clin. Invest.* **20**, 530–535 (1990).

189. I. Hornstein, J. A. Alford, L. E. Elliott, P. F. Crowe, Determination of free fatty acids in fat. *Anal. Chem.* **32**, 540–542 (1960).

190. M. A. Abdul-Ghani, *et al.*, Mitochondrial reactive oxygen species generation in obese non-diabetic and type 2 diabetic participants. *Diabetologia* **52**, 574–582 (2009).

191. C. Bonnard, *et al.*, Mitochondrial dysfunction results from oxidative stress in the skeletal muscle of diet-induced insulin-resistant mice. *J. Clin. Invest.* **118**, 789–800 (2008).

192. N. Houstis, E. D. Rosen, E. S. Lander, Reactive oxygen species have a causal role in multiple forms of insulin resistance. *Nature* **440**, 944–948 (2006).

193. N. Kumashiro, *et al.*, Impact of oxidative stress and peroxisome proliferator-

activated receptor y coactivator-1a in hepatic insulin resistance. *Diabetes* **57**, 2083–2091 (2008).

194. J. Abilés, *et al.*, Oxidative stress is increased in critically ill patients according to antioxidant vitamins intake, independent of severity: a cohort study. *Crit. Care* **10**, 1–9 (2006).

195. C. N. Lumeng, J. B. Delproposto, D. J. Westcott, A. R. Saltiel, Phenotypic switching of adipose tissue macrophages with obesity is generated by spatiotemporal differences in macrophage subtypes. *Diabetes* **57**, 3239–3246 (2008).

196. H. Ochi, I. Morita, S. Murota, Roles of glutathione and glutathione peroxidase in the protection against endothelial cell injury induced by 15-hydroperoxyeicosatetraenoic acid. *Arch. Biochem. Biophys.* **294**, 407–411 (1992).

197. D. Puzzo, *et al.*, CL316,243, a β3-adrenergic receptor agonist, induces muscle hypertrophy and increased strength. *Sci. Rep.* **5**, 1–9 (2016).

198. D. Mohammadyani, *et al.*, Molecular speciation and dynamics of oxidized triacylglycerols in lipid droplets: mass spectrometry and coarse-grained simulations. *Free Radic. Biol. Med.* **76**, 53–60 (2014).

199. V. Veverka, *et al.*, Structural characterization of the interaction of mTOR with phosphatidic acid and a novel class of inhibitor: Compelling evidence for a central role of the FRB domain in small molecule-mediated regulation of mTOR. *Oncogene* **27**, 585–595 (2008).

200. I. Shimizu, *et al.*, P53-induced adipose tissue inflammation is critically involved in the development of insulin resistance in heart failure. *Cell Metab.* **15**, 51–64 (2012).

201. J. Salatzki, *et al.*, Adipose tissue ATGL modifies the cardiac lipidome in pressure-overload-induced left ventricular failure. *PLoS Genet.* **14**, 1–24 (2018).

202. O. Gruzdeva, *et al.*, Insulin resistance and inflammation markers in myocardial infarction. *J. Inflamm. Res.* **6**, 83–90 (2013).

203. G. H. Goossens, E. E. Blaak, W. H. M. Saris, M. A. Van Baak, Angiotensin II-induced effects on adipose and skeletal muscle tissue blood flow and lipolysis in normal-weight and obese subjects. *J. Clin. Endocrinol. Metab.* **89**, 2690–2696 (2004).

204. P. Oliver, C. Pico, F. Serra, A. Palou, Resistin expression in different adipose tissue depots during rat development. *Mol. Cell. Biochem.* **252**, 397–400 (2003).

205. S. Reynisdottir, K. Ellerfeldt, H. Wahrenberg, H. Lithell, P. Arner, Multiple lipolysis defects in the insulin resistance (metabolic) syndrome. *J. Clin. Invest.* **93**, 2590–2599 (1994).

206. M. E. McDonnell, G. E. Umpierrez, Insulin therapy for the management of hyperglycemia in hospitalized patients. *Endocrinol. Metab. Clin. North Am.* **41**,

175–201 (2012).

207. J. K. Yang, *et al.*, Plasma glucose levels and diabetes are independent predictors for mortality and morbidity in patients with SARS. *Diabet. Med.* **23**, 623–628 (2006).

208. B. M. Alraddadi, *et al.*, Risk factors for primary middle east respiratory syndrome coronavirus illness in humans, Saudi Arabia, 2014. *Emerg. Infect. Dis.* **22**, 49–55 (2016).

209. B. Bode, *et al.*, Glycemic characteristics and clinical outcomes of COVID-19 patients hospitalized in the United States. *J. Diabetes Sci. Technol.* **14**, 813–821 (2020).

210. C. Sardu, *et al.*, Outcomes in patients with hyperglycemia affected by COVID-19: Can we do more on glycemic control? *Diabetes Care* **43**, 1408–1415 (2020).

211. A. Coppelli, *et al.*, Hyperglycemia at hospital admission is associated with severity of the prognosis in patients hospitalized for COVID-19: The Pisa COVID-19 study. *Diabetes Care* **43**, 2345–2348 (2020).

212. R. Gianchandani, *et al.*, Managing hyperglycemia in the COVID-19 inflammatory storm. *Diabetes* **69**, 2048–2053 (2020).

213. A. K. Singh, R. Singh, Hyperglycemia without diabetes and new-onset diabetes are both associated with poorer outcomes in COVID-19. *Diabetes Res. Clin. Pract.* **167**, 108382 (2020).

214. V. Raje, *et al.*, Adipocyte lipolysis drives acute stress-induced insulin resistance. *Sci. Rep.* **10**, 1–13 (2020).